UNIVERSITA' DEGLI STUDI DI PADOVA

Dipartimento di Biologia

SCUOLA DI DOTTORATO DI RICERCA IN BIOSCIENZE E BIOTECNOLOGIE
INDIRIZZO: GENETICA E BIOLOGIA MOLECOLARE DELLO SVLUPPO
XXIV CICLO

TESI DI DOTTORATO

IDENTIFICATION OF NOVEL LOCI AND GENES INVOLVED IN ARRHYTHMOGENIC RIGHT VENTRICULAR CARDIOMYOPATHY

Direttore della Scuola: Ch.mo Prof. Giuseppe Zanotti
Coordinatore d'indirizzo: Ch.mo Prof. Paolo Bonaldo
Supervisore: Ch.mo Prof. Maria Luisa Mostacciuolo

Dottoranda: Dott.ssa Ilena Egle Astrid Li Mura

31 gennaio 2012

Table of Contents

SUMMARY

Introduction. Arrhythmogenic right ventricular cardiomyopathy (ARVC) is an inherited cardiac disease characterized by fibrofatty replacement of myocardial tissue and high incidence of serious ventricular tachyarrhythmias. It significantly increases the risk of sudden cardiac death, in particular in young people and athletes. To date, fourteen loci have been mapped and ten disease-genes have been identified, five of which encoding desmosomal proteins: desmoplakin (DSP), plakophilin-2 (PKP2), desmoglein-2 (DSG2), desmocollin-2 (DSC2), and plakoglobin (JUP).

Since causative mutations in ARVC genes have been detected in about 50% of probands, additional and still unknown disease-genes could be involved.

Aim of the study. The study described in the present thesis aimed at determining the spectrum and prevalence of desmosomal mutations in a cohort of 80 Italian unrelated index cases. Moreover, the identification of novel disease loci and genes in three families with recurrence of ARVC was attempted by integrating different approaches, including genome-wide linkage study, Copy Number Variations (CNVs) analysis, and exome-sequencing.

Methods. Mutation screening of five desmosomal ARVC genes (*PKP2, DSP, DSG2*, *DSC2*, and *JUP*) was performed by Denaturing High-Performance Liquid Chromatography (DHPLC) and direct sequencing in a cohort of 80 Italian unrelated index cases. Whenever possible, genetic analysis was extended to available family members to evaluate the segregation of each mutation identified in the index case.

In order to map novel loci and, possibly, to identify novel genes, a genome wide scan, using High−density SNP arrays (Illumina HumanCNV370-Duo BeadChip), was performed in three independent families with recurrence of ARVC, showing no mutations in any of the desmosomal genes. An affected-only linkage study was conducted in each family to identify critical genomic regions segregating with the disease phenotype and, then, to select candidate genes for mutation screening. Moreover, the presence of large genomic deletions or duplications (>1 Kb), shared by all affected individuals within each family, was evaluated by Copy Number Variations (CNVs) analysis.

In addition, in Family #2 and in Family #3 a combined strategy of linkage analysis and

exome sequencing was adopted to identify novel ARVC genes.

Results. Mutation screening of five desmosomal ARVC genes in 80 Italian probands identified single point mutations in 32.5% of cases and multiple mutations in 12.5%. No mutations were identified in the remaining 55% of probands.

A total of 46 variants were identified in this study and in six cases the same variation occurred in different patients. The genes most frequently involved were *PKP2*, *DSP* and *DSG2,* accounting respectively for 34.8%, 30.4%, and 26.1% of the total mutations, whereas *DSC2* and *JUP* variants account for 4.3%. Genetic analysis extended to available family members confirmed the high heterogeneity in the clinical expression of ARVC mutations even among relatives, whose phenotype ranged from a complete lack of symptoms and/or clinical manifestations to a severe form of disease.

Among the index cases negative for point mutations in desmosomal genes, three belong to independent families with recurrence of ARVC.

Assuming a further genetic heterogeneity in these families, a genome-wide scan was performed in order to identify novel loci and genes.

In Family #1, linkage analysis gave a maximum parametric LOD score of 1.17, not statistically significant, in 11 chromosomal regions, one of them included *PKP2* locus. The subsequent CNVs analysis identified a hemizygous deletion of 122.5 Kb on chromosome 12p11.21, encompassing the entire *PKP2* gene and shared by all affected family members. It was not present in any of available public CNVs databases and was confirmed by quantitative real-time PCR.

In Family #2, a significant evidence of linkage to a single region on chromosome 19p13.3 was obtained, with a maximum parametric LOD score of 3.85. All clinically affected individuals shared a region of about 2 Mb, including 44 genes and 2 ORFs. Non parametric Homozygosity Haplotype (HH) analysis confirmed linkage results. These data provided evidence for the existence of a novel ARVC locus (ARVC15) on chromosome 19p13.3. CNVs analysis excluded the presence of rare genomic rearrangements shared by all affected subjects. Among genes mapped to the critical interval and expressed in myocardium, *Protein-Tyrosine Phosphatase Receptor-type Sigma* (*PTPRS*) was selected as candidate gene for mutation screening, because of its possible role in cell to cell adhesion. Direct sequencing of coding and UTRs regions of *PTPRS* gene in the proband did not reveal any causative mutation. Therefore, exome sequencing was performed in two affected subjects of this family to attempt the identification of the causal mutation. Of 147 novel detected variants shared by both

subjects, none involved genes mapped on 19p13.3 critical interval. The subsequent evaluation of sequence coverage depth in this region revealed a poor uniformity and a low read depth (<15X) for several exons of different genes.

Finally, in Family #3, linkage analysis gave a maximum multipoint LOD score of 0.90, inconsistent with linkage, for 17 chromosomal regions. Moreover, CNVs analysis did not detect any structural variation shared by all affected family members. The subsequent exome-sequencing of two affected family members identified 12 novel functional variants (missense, nonsense, frame-shift insertions and/or deletions, and splice-site affecting changes) shared by both subjects and located in different regions previously identified by linkage analysis. Of 10 variants confirmed by Sanger sequencing, six co-segregated with the disease phenotype within the family.

Discussion. ARVC is a recognized cause of sudden cardiac death, which may be prevented by timely detection and intervention. When properly interpreted, genetic testing allows diagnosis confirmation, early identification of asymptomatic carriers, and interpretation of borderline clinical phenotypes.

In the present study, genetic screening of five desmosomal ARVC genes in 80 Italian probands identified causative mutations in 45% of cases, mainly involving the “big3” genes *PKP2, DSP*, and *DSG2*, according to data reported in literature. The relatively high incidence of multiple mutations, detected in 12.5% of index cases, indicated that this condition is quite frequent among ARVC patients. Genetic analysis of family members confirmed the high heterogeneity in the clinical expression of ARVC mutations even among relatives; modifier genes are likely to account for much of the broad spectrum of disease expression and await elucidation. Mutation screening of desmosomal genes failed to detect causative mutations in more than 50% of index cases, suggesting that additional and still unknown genes could be involved. However, possibility of misdiagnosis in some cases, presence of mutations in sequences not analyzed, as promoter and UTRs regions, and/or large genomic deletions/duplications, not detectable by DHPLC and direct sequencing, cannot be excluded. Assuming a further genetic heterogeneity, a genome-wide scan was performed in three large ARVC families, showing no mutations in any of the desmosomal genes.

In Family #1, a heterozygous *PKP2* deletion segregating with the pathogenic phenotype was identified by CNVs analysis, highlighting the importance of complementing the conventional mutation screening in ARVC genes with other approaches able to detect possible structural variations. Moreover, a genome-wide CNV analysis of multiplex

families could be useful for identifying large deletions/duplications in novel disease genes. The presence of a low-copy repeat (LCRs) adjacent to the deletion breakpoint suggested that this segmental duplication can cause genomic instability and either mediate or stimulate nonrecurrent CNV formation.

In Family #2, exome-sequencing failed to detect the causal variant underlying the pathogenic phenotype, because of several technical and analytical limitations of this approach. However, genome-wide linkage results provided strong evidence for a novel ARVC locus on chromosome 19p13.3, highlighting the soundness of this strategy for identifying susceptibility regions in large, highly informative families and providing the basis for the identification of a novel disease gene.

In Family #3, exome-sequencing identified *COL20A1* gene as putative candidate gene for ARVC. Genetic screening of *COL20A1* in a large cohort of ARVC patients, negative for mutation in the known genes, could elucidate its effective involvement in the genetic determination of the disease.

Identification of novel ARVC genes is of great importance for understanding the molecular pathogenesis of this disease, as well as for increasing the power of genetic screening and developing successful targeted therapies.

RIASSUNTO

Introduzione. La Cardiomiopatia Aritmogena del Ventricolo Destro (ARVC) è una malattia ereditaria del muscolo cardiaco caratterizzata dalla progressiva perdita e sostituzione fibro-adiposa dei cardiomiociti che costituiscono la parete libera del ventricolo destro. La disomogeneità del tessuto cardiaco altera la normale conduzione dell'impulso elettrico, determinando l'insorgenza di aritmie che occasionalmente portano a fibrillazione ventricolare e morte improvvisa per arresto cardiaco, soprattutto nei giovani e negli atleti.

Attualmente, sono noti 14 loci indipendentemente implicati nella trasmissione della malattia; per 10 di questi è stato identificato il gene che, se mutato, determina l'insorgere della malattia. Cinque dei geni ARVC codificano per proteine costituenti il desmosoma cardiaco: Placofilina-2 (PKP2), Desmoplachina (DSP), Desmogleina-2 (DSG2), Desmocollina-2 (DSC2) e Placoblobina (JUP). L'identificazione di mutazioni solo nel 50% dei casi ARVC suggerisce il coinvolgimento di altri geni, non ancora noti.

Scopo dello studio. Lo studio descritto nella presente tesi mira a valutare la prevalenza e lo spettro di mutazioni nei cinque geni ARVC desmosomali in un gruppo di 80 casi indice Italiani, non imparentati tra loro. Inoltre, in tre grandi famiglie con ricorrenza di casi ARVC e in cui non sono state identificate mutazioni nei geni desmosomali, è stata effettuata un'analisi *genome-wide* integrando diversi approcci, quali studio di linkage, analisi di *Copy Number Variations* (CNVs) e sequenziamento dell' esoma, allo scopo di identificare nuovi loci e geni malattia.

Metodi. Lo *screening* per la ricerca di mutazioni nei cinque geni ARVC desmosomali ha coinvolto 80 casi indice ed è stato effettuato tramite analisi DHPLC (*Denaturing High-Performance Liquid Chromatography*) e sequenziamento diretto del DNA. In alcuni casi è stato possibile estendere l'analisi genetica anche ai familiari dei casi indice, allo scopo di valutare la segregazione delle mutazioni identificate nel probando.

I soggetti appartenenti a ciascuna delle tre famiglie selezionate per l'analisi *genome-wide* sono stati genotipizzati utilizzando un pannello di marcatori ad alta densità che include più di 370.000 polimorfismi di singolo nucleotide (SNPs) (Illumina HumanCNV370-Duo BeadChip). In ciascuna famiglia è stata effettuata un'analisi di *linkage* allo scopo di identificare regioni genomiche che segregano con la malattia e

dentro le quali selezionare dei geni candidati per lo *screening* di mutazioni. Inoltre, la presenza di grandi delezioni o duplicazioni nel genoma (superiori a 1Kb), condivise da tutti i soggetti affetti di ciascuna famiglia, è stata valutata tramite analisi di *Copy Number Variations.*

Nella Famiglia #2 e nella #3 l'identificazione del gene malattia è stata tentata integrando i risultati dello studio di linkage con i dati ottenuti dal sequenziamento dell'esoma di due soggetti affetti.

Risultati. L'analisi delle sequenze codificanti dei geni *PKP2*, *DSP*, *DSG2*, *DSC2* e *JUP* in 80 casi indice Italiani ha permesso di identificare mutazioni singole nel 32.5% dei casi e mutazioni multiple nel 12.5%. Il 55% dei probandi non è risultato portatore di alcuna mutazione nei geni desmosomali. In totale sono state identificate 46 mutazioni, di cui 6 presenti in più di un probando. La maggior parte delle mutazioni ha coinvolto i geni *PKP2*, *DSP*, *DSG2,* in cui sono state identificate rispettivamente il 34.8%, 30.4%, e 26.1% del totale delle varianti, mentre le mutazioni nei geni *DSC2* e *JUP* hanno rappresentato solo il 4.3% del totale. L' analisi genetica dei familiari dei casi indice ha confermato la penetranza incompleta e l'elevata eterogeneità di espressione fenotipica delle mutazioni ARVC, anche all'interno della stessa famiglia. Tra i casi indice in cui non sono state identificate mutazioni nei geni desmosomali, tre appartengono a famiglie indipendenti con ricorrenza di casi ARVC. In ognuna di queste famiglie è stata effettuata un'analisi *genome-wide* allo scopo di identificare nuovi loci e geni malattia.

Nella Famiglia #1, l'analisi di *linkage* ha fornito un valore massimo di *LOD score* parametrico pari a 1.17, non statisticamente significativo, per marcatori associati a 11 diverse regioni cromosomiche, di cui una comprendente il locus del gene desmosomale *PKP2*. La successiva analisi di CNVs su tutto il genoma ha identificato una delezione di 122.5 Kb sul cromosoma 12p11.21, presente in eterozigosi in tutti i soggetti affetti e confermata mediante *real-time* PCR quantitativa. Tale delezione comporta la perdita di tutti i 14 esoni del gene *PKP2* e non è riportata nei *databases* di CNVs attualmente disponibili.

Nella Famiglia #2, l'analisi di *linkage* ha fornito un valore massimo di *LOD score* parametrico pari a 3.85, statisticamente significativo, per marcatori associati al cromosoma

19p13.3. L'analisi di segregazione dell'aplotipo di marcatori in questa regione ha permesso di identificare un aplotipo a rischio, condiviso da tutti i soggetti affetti. Due eventi di ricombinazione in soggetti affetti hanno definito una regione genomica critica,

di circa 2 Mb, in cui attualmente sono mappati 44 geni e 2 ORFs. Una successiva analisi di tipo non parametrico, chiamata *Homozygosity Haplotype (HH) analysis,* ha confermato tale dato.

I risultati ottenuti forniscono una significativa evidenza dell'esistenza di un nuovo locus ARVC (ARVC15) sul cromosoma 19p13.3. La successiva analisi di CNVs ha escluso la presenza di grandi delezioni/duplicazioni, condivise da tutti i soggetti affetti, in questa e in altre regioni del genoma. Tra i geni mappati sul cromosoma 19p13.3, il gene *PTPRS* (*Protein-Tyrosine Phosphatase Receptor-type Sigma)* è stato scelto come candidato per lo *screening* di mutazioni, tenendo conto del suo ruolo nel regolare la stabilità dei complessi giunzionali cardiaci. Tuttavia, l'analisi delle sequenze codificanti e delle regioni regolative UTRs del gene *PTPRS* non ha evidenziato la presenza di alcuna mutazione nel DNA del probando. Alla luce dei risultati ottenuti, l'identificazione del gene responsabile della trasmissione della malattia in questa famiglia è stata tentata tramite il sequenziamento dell'esoma di due soggetti affetti. Questo approccio ha permesso di identificare 147 varianti condivise da entrambi i soggetti, ma nessuna di questa coinvolge un gene localizzato nella regione critica sul cromosoma 19p13.3. La successiva analisi della copertura di sequenziamento di questa regione ha evidenziato una copertura poco uniforme e inferiore al 15X per diversi esoni di geni differenti.

Infine, nella Famiglia #3 l'analisi di *linkage* ha fornito un valore massimo di *LOD score* parametrico pari a 0.90, non statisticamente significativo, per marcatori associati a 17 diverse regioni cromosomiche. La successiva analisi di CNVs ha escluso la presenza di variazioni strutturali nel genoma, condivise da tutti i soggetti affetti. Di conseguenza, anche in questa famiglia è stato effettuato il sequenziamento dell'esoma di due soggetti affetti, allo scopo di identificare la mutazione responsabile della malattia. Focalizzandosi sulle mutazioni di tipo missenso, nonsenso, *frame-shift,* e nei siti di *splicing,* sono state identificate 12 varianti condivise da entrambi i soggetti, di cui due non sono state confermate mediante sequenziamento Sanger. Delle rimanenti 10 varianti comuni a entrambi i soggetti affetti, 6 co-segregano con la malattia all'interno della famiglia.

Discussione. L' ARVC è una causa frequente di morte improvvisa tra i giovani e gli atleti sotto i 35 anni di età. Se interpretato in maniera corretta, l'analisi genetica dei geni coinvolti nella malattia può permettere di chiarire la diagnosi dei casi indice e identificare tempestivamente i familiari portatori della stessa mutazione che sono verosimilmente a rischio di sviluppare la malattia. Lo *screening* di mutazioni dei geni ARVC desmosomali in un gruppo di 80 probandi italiani ha permesso di identificare

mutazioni nel 45% dei casi, confermando il prevalente coinvolgimento dei tre geni *PKP2, DSP* e *DSG2.* L'alta incidenza di mutazioni multiple, identificate nel 12.5% dei casi, suggerisce che tale condizione è relativamente frequente tra i pazienti ARVC. L'analisi genetica dei familiari dei probandi ha confermato la penetranza incompleta e l'espressività variabile della malattia, anche all'interno della stessa famiglia. L'assenza di mutazioni in più del 50% dei casi suggerisce il coinvolgimento di altri geni nella determinazione genetica dell'ARVC. In quest' ottica, un'analisi *genome-wide* è stata effettuata in tre famiglie con ricorrenza di casi ARVC e in cui non sono state identificate mutazioni nei geni desmosomali, allo scopo di identificare nuovi loci e geni malattia. Nella Famiglia #1, l'identificazione di una delezione in eterozigosi del gene *PKP2,* condivisa da tutti i soggetti affetti, sottolinea l'importanza di associare alle metodiche tradizionali utilizzate per lo *screening* di mutazioni puntiformi approcci che permettano di identificare eventuali variazioni strutturali presenti nel genoma. Inoltre, un'analisi di CNVs su tutto il genoma potrebbe individuare delezioni o duplicazioni in nuovi geni malattia. La presenza di una duplicazione segmentale, adiacente al limite telomerico del locus *PKP2*, potrebbe favorire la formazione di CNVs in questa regione.

Nella Famiglia #2, il sequenziamento dell'esoma di due soggetti affetti non ha permesso di identificare la mutazione responsabile della malattia; tuttavia, l'analisi di linkage ha fornito una significativa evidenza dell'esistenza di un nuovo locus ARVC sul cromosoma 19p13.3, fornendo le basi per l'identificazione di nuovi geni.

Infine, nella Famiglia #3, il sequenziamento dell'esoma di due soggetti affetti ha identificato il gene *COL20A1* come un possibile candidato per l'ARVC. Lo screening di *COL20A1* nei pazienti ARVC che non presentano mutazioni nei geni noti potrà chiarire il suo contributo alla determinazione genetica della malattia.

1. INTRODUCTION

1.1 Arrhythmogenic Right Ventricular Cardiomyopathy (ARVC)

Clinical and pathological profile

Arrhythmogenic Right Ventricular Cardiomyopathy (ARVC; Mendelian Inheritance in Man database code MIM107970) is a genetically determined heart muscle disorder and a major cause of sudden death, secondary to fatal ventricular arrhythmias, in particular in young people and athletes (Thiene *et al*., 1988).

The prevalence of the disease in the general population has been estimated to vary from 1 in 1,000 to 1 in 5,000 individuals (Corrado *et al*., 2006) and men are more frequently affected than women, with an approximate ratio of 3:1 (Bauce *et al*., 2008). However, the exact prevalence could be higher than the estimated, as milder cases are frequently not diagnosed and non classic subtypes are commonly misattributed to dilated cardiomyopathy.

The histopathological hallmark of ARVC consists of diffuse or segmental loss of cardiomyocytes, myocardial degeneration, and replacement by fibrofatty scar tissue, predominantly in the right ventricle (Figure 1.1a). The presence of fibroadiposis in myocardium interferes with electrical impulse conduction, leading to delay (late potentials, epsilon waves, parietal right bundle branch block) and re-entrant ventricular arrhythmias (Thiene *et al*., 2007).

The degenerative process is progressive, starting from the subepicardial areas, with small clusters of surviving myocytes interspersed within the fibrofatty tissue, and ultimately reaching the endocardium as to result in transmural lesions. The so-called “triangle of dysplasia”, including the inferior, apical, and infundibular walls, is primarily involved .

As the disorder progresses, the histological substrate becomes more prominent, while the early “concealed” phase of ARVC is characterized by a predisposition to ventricular arrhythmias and sudden cardiac death, in the context of well-preserved morphology, histology, and ventricular function. Disease progression leads to structural abnormalities ranging from focal areas of severe muscle thinning, that may transilluminate on macroscopic examination (Figure 1.1b), ventricular aneurysms, regional wall motion

abnormalities, and increased trabeculation, up to global ventricular dilation and dysfunction (Thiene and Basso, 2001).

The acquired nature of myocardial atrophy, occurring after birth as a consequence of cumulative myocyte loss, differentiates ARVC from congenital heart diseases, as Uhl's anomaly (Gerlis *et al*., 1993). This idea has led to the current term “cardiomyopathy” to replace the original designation of “dysplasia” (Marcus *et al*., 1982).

The disease name reflects its right ventricular preponderance; however, most recently, clinicogenetic characterization of affected families allowed to recognize non classic left-dominant and biventricular subtypes, supporting adoption of the broader term “Arrhythmogenic Cardiomyopathy” (Sen-Chowdhry *et al*., 2007).

In classic right-dominant pattern of disease expression four clinical phases have been observed (Thiene *et al*., 1990). During the early subclinical phase patients are asymptomatic and subtle structural abnormalities mask a significant risk of sudden cardiac death, mostly during intense physical exercise. The second phase is characterised by an overt electrical disorder, with palpitations, syncope, and symptomatic ventricular arrhythmias of left bundle branch block morphology, reflecting its right ventricular origin. Arrhythmias range from isolated premature ventricular complexes to sustained ventricular tachycardia and fibrillation, leading to cardiac arrest. Moreover, structural abnormalities, confined to the right ventricle, become more evident and discernible by imaging. In the third phase, the progressive myocyte loss results in right ventricular failure, with relatively preserved left ventricular function. The progressive left ventricular involvement leads to the final stage of bi-ventricular pump failure and related complications. In such conditions, disease phenotype resembles dilated cardiomyopathy and contractile dysfunction may be severe enough to require cardiac transplantation.

Left-dominant arrhythmogenic cardiomyopathy is characterized by early and predominant left ventricular manifestations, in the setting of preserved global right ventricular function; while the biventricular variant is defined by parallel involvement of both ventricles.

Coexistence of the three phenotypic profiles in the ARVC population, even within the same family, highlights their interrelation in the same spectrum of disease expression, that can be represented as a continuum at extremes of which lie the right- and left-dominant subtypes (Sen-Chowdhry *et al*., 2008).

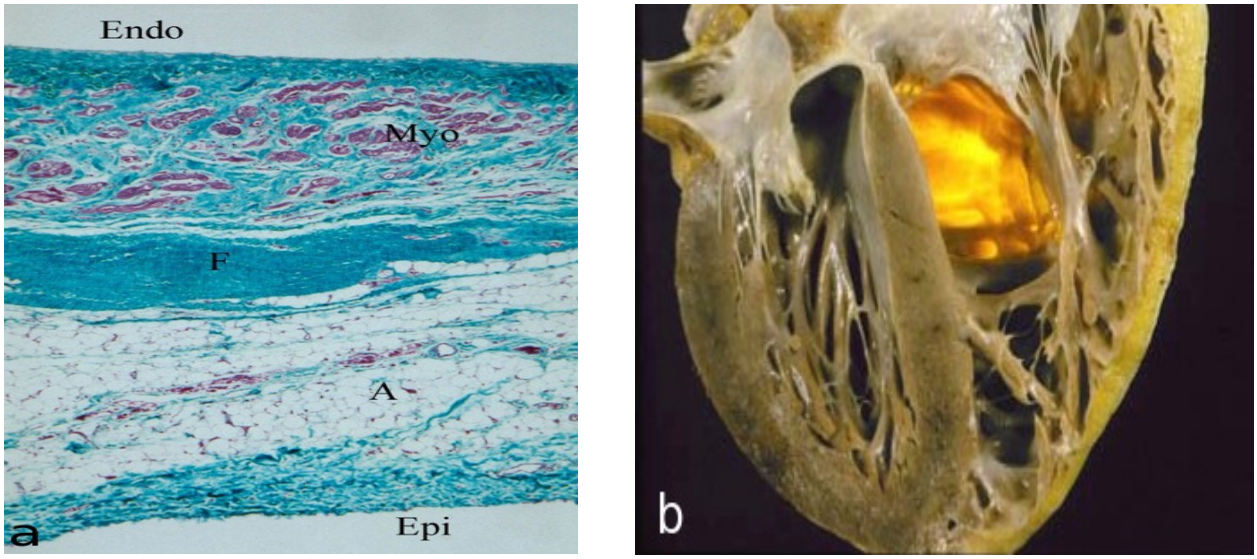

Figure 1.1: Typical histologic and morphologic features of ARVC.

a. Trichrome staining reveals areas of fibrosis (F) and adipose tissue (A) in the epicardial (Epi) and mid-myocardial zones, with islands of surviving myocytes near the endocardium (Endo) (From Indik and Marcus, 2003, with permission). **b**. Four chamber view cut of an autoptic heart specimen shows the transmural fatty replacement of the right ventricular free wall and the translucent infundibulum (From Thiene *et al*., 1998, with permission).

Diagnosis and treatment

ARVC, as progressive disease evolving over time, shows an age-related penetrance and becomes clinically overt from the second to the fourth decade of life (Nava *et al*., 1989; Daliento *et al*., 1995). Childhood presentation of the disorder is rare but documented, particularly in digenic subjects.

Clinical manifestations are variable and often subtle during early disease stages. The most common presenting symptoms are palpitations, dizziness, syncope, and sudden ventricular fibrillatory arrest, frequently related to physical exercise. Sudden cardiac death may also be the first manifestation of disease.

In vivo diagnosis relies on demonstration of structural, functional, and electrophysiological alterations, due to the underlying histological changes, and existence of family disease.

Comprehensive noninvasive assessment of patients with suspected ARVC is done by clinical and family history, physical examination, chest radiography, 12-lead ECG, signal-averaged ECG, Holter monitoring, 24-hour ambulatory ECG, maximal exercise testing to induce arrhythmia, and two-dimensionals echocardiography (Nava *et al*.,

2000).

Electrophysiologic studies allow to detect repolarisation abnormalities and delayed depolarisations (late potentials) resulting from slowed ventricular activation, which provides the substrate for re-entrant arrhythmias. Echocardiography is a widely used imaging technique for evaluating the disease onset and progression during follow-up of affected patients and relatives. Functional and structural changes in the right ventricle, as outflow tract dilatation, wall motion abnormalities, trabecular derangement, and sacculation, are detectable by this approach (Yoerger *et al*., 2005).

Selected patients might require further evaluation by cardiac magnetic resonance (MRI) with late enhancement and invasive tests, such as contrast angiography, endomyocardial biopsy, and three-dimensional electroanatomic mapping. MRI with gadolinium enhancement has the potential to detect intramyocardial fibrosis which can precede functional abnormalities during early disease stages, allowing identification of concealed cases (Tandri *et al*., 2005).

Angiography is usually considered the imaging gold standard for diagnosis of ARVC. Angiographic evidence of ventricular aneurysms and akinetic or dyskinetic areas in the triangle of dysplasia has a high diagnostic specificity (>90%) (Marcus *et al*., 2007).

Endomyocardial biopsy may be useful to confirm diagnosis by indicating fibrofatty replacement and excluding phenocopies, as myocarditis and sarcoidosis. However, the ventricular septum is usually spared and samples acquisition from the ventricular free wall carries an increased risk of perforation (Angelini *et al*., 1996). A potential role of endomyocardial biopsy even for early diagnosis is suggested by preliminary data indicating that changes in intercalated disk proteins are detectable with immunohistochemical staining of myocardial tissue from affected subjects (Basso *et al*., 2009).

Three-dimensional electroanatomical mapping reveals low-voltage areas, corresponding to fibrofatty myocardial replacement, and may facilitate differential diagnosis with inflammatory cardiomyopathy and idiopathic right ventricular outflow tract tachycardia (Corrado *et al*., 2005).

Due to the non specific nature of clinical features of ARVC and the heterogenous pattern of disease expression, a Task Force of international experts set forth guidelines to standardize diagnosis in 1994 (McKenna *et al*.,1994). Structural, histological, electrocardiographic, arrhythmic, and familial features of the disorder were incorporated into major or minor criteria, according to the specificity of their association with ARVC.

Based on Task Force guidelines, definite diagnosis is established when two major or one major plus two minor or four minor criteria from different categories are fulfilled. These criteria are highly specific and reduce the diagnostic ambiguity in probands, allowing differential diagnosis with dilated cardiomyopathy and idiopathic right ventricular outflow tract tachycardia. However, in 1994 left-dominant and biventricular variants were not recognized and clinical experience with right-dominant disease was mainly based on symptomatic probands and sudden cardiac death victims, resulting in significant underreporting of early and familial forms, as well as non classic subtypes. Modifications of the Task Force guidelines have been proposed to facilitate clinical diagnosis in first-degree relatives with mild or incomplete expression of the disease, during familial screening of index cases with confirmed ARVC (Hamid *et al*., 2002). Very recently, the original criteria have been revised by Marcus and colleagues to account for advances in genetics of ARVC, as well as in diagnosis techniques, and to enhance overall diagnostic sensitivity, maintaining the specificity (Marcus *et al*., 2010). The new criteria (Table 1.1) incorporate quantitative criteria for properly classify the various degree of right ventricular dilatation or dysfunction and fibrofatty myocardial replacement; moreover, abnormalities are defined on the basis of comparison with normal subject data.

However, consensus guidelines for recognition of non classic subtypes of arrhythmogenic cardiomyopathy are still awaited.

At present, no curative therapy of ARVC is available and the most important management strategy is prevention of sudden cardiac death. Treatment of affected subjects includes lifestyle modifications, antiarrhtythmic drugs, β-blockers therapy, radiofrequency catheter ablation, defibrillator implantation and heart transplantation. Patients should avoid competitive sport activities, since acute volume overload and stretching of the right ventricle, during effort, may trigger life-threatening arrhythmias, increasing by five-fold the risk of sudden death. Nevertheless, excessive mechanical stress can worsen the underlying myocardial lesion, accelerating disease progression (Corrado *et al*., 2003). Pharmacological therapy with β-blockers and/or class III antiarrhythmic drugs, as sotalol and amiodarone, is effective in treatment of patients with haemodynamically stable arrhythmias, as inducible and noninducible ventricular tachycardia (Wichter *et al*., 2005). Cardioverter-defibrillator implantation (ICD) is indicated as secondary prevention after prior cardiac arrest and in subjects with unexplained syncope or drug-refractory arrhythmias, to provide life-saving

antitachycardia pacing and defibrillation shocks as needed (Corrado *et al*., 2003). In cases of drug-refractory and incessant ventricular tachicardia or frequent ICD discharges, radiofrequency catheter ablation is used to eliminate re-entrant circuits that are critical to perpetuation of arrhythmias; however, relapses are frequent, due to the disease progression (Dalal *et al*., 2007).

Heart transplantation remains the final therapeutic option for patients with refractory congestive heart failure and untreatable recurrent arrhythmias (Lacroix *et al*., 2005).

Table 1.1. Modified criteria for diagnosis of ARVC (Marcus *et al*., 2010)

	Major criteria	Minor criteria
I. Global or regional dysfunction/ structural alterations*	*By 2D echo:* • Regional RV akinesia, dyskinesia, or aneurysm • *and* 1 of the following (end diastole): ◦ PLAX RVOT ≥32 mm (corrected for body size [PLAX/BSA] ≥19 mm/m^2) ◦ PSAX RVOT ≥36 mm (corrected for body size [PSAX/BSA] ≥21 mm/m^2) ◦ *or* fractional area change ≤33% *By MRI:* • Regional RV akinesia, dyskinesia, or dyssynchronous RV contraction • *and* 1 of the following: ◦ Ratio of RV end-diastolic volume to BSA ▪ ≥110 mL/ m^2 (male) ▪ ≥100 mL/ m^2 (female) ◦ *or* RV ejection fraction ≤40% *By RV angiography:* • Regional RV akinesia, dyskinesia, or aneurysm	*By 2D echo:* • Regional RV akinesia or dyskinesia • *and* 1 of the following (end diastole): ◦ PLAX RVOT ≥29 to <32 mm (corrected for body size [PLAX/BSA] ≥16 to <19 mm/m^2) ◦ PSAX RVOT ≥32 to <36 mm (corrected for body size [PSAX/BSA] ≥18 to <21 mm/m^2) ◦ *or* fractional area change >33% to ≤40% *By MRI:* • Regional RV akinesia, dyskinesia, or dyssynchronous RV contraction • *and* 1 of the following: ◦ Ratio of RV end-diastolic volume to BSA ▪ ≥100 to <110 mL/ m^2 (male) ▪ ≥90 to <100 mL/ m^2 (female) ◦ *or* RV ejection fraction >40 to ≤45%
II. Tissue characterization of walls	• Residual myocytes <60% by morphometric analysis (or <50% if estimated), with fibrous replacement of the RV free wall myocardium in ≥1 sample, with or without fatty replacement of tissue on endomyocardial biopsy	• Residual myocytes 60-75% by morphometric analysis (or 50-65% if estimated), with fibrous replacement of the RV free wall myocardium in ≥1 sample, with or without fatty replacement of tissue on endomyocardial biopsy
III. Repolarization abnormalities	• Inverted T-waves in right precordial leads (V1, V2, and V3) or beyond in individuals >14 years of age (in the absence of complete RBBB QRS ≥120 ms)	• Inverted T-waves in leads V1 and V2 in individuals >14 years of age (in the absence of complete RBBB) or in V4, V5, or V6 • Inverted T-waves in leads V1, V2, V3, and V4 in individuals >14 years of age in the presence of complete RBBB
IV. Depolarization/conduction abnormalities	• Epsilon wave (reproducible low-amplitude signals between end of QRS complex to onset of the T-wave) in right precordial leads (V1 to V3)	• Late potentials by SAECG in ≥1 of 3 parameters in the absence of a QRS duration of ≥110 ms on the standard ECG • Filtered QRS duration (fQRS) ≥114 ms • Duration of terminal QRS <40 µV (low-amplitude signal duration) ≥38 ms • Root-mean-square voltage of terminal 40 ms ≤20 µV • Terminal activation duration of QRS ≥55 ms measured from the nadir of the S wave to the end of the QRS, including R', in V1, V2, or V3, in the absence of complete RBBB

Table 1.1 continued

	Major criteria	Minor criteria
V. Arrhythmias	• Non-sustained or sustained ventricular tachycardia of left bundle-branch morphology with superior axis (negative or indeterminate QRS in leads II, III, and aVF and positive in lead aVL)	• Non-sustained or sustained ventricular tachycardia of RV outflow configuration, left bundle-branch block morphology with inferior axis (positive QRS in leads II, III, and aVF and negative in lead aVL) or of unknown axis • >500 VES per 24 h (Holter)
VI. Family history	• ARVC confirmed in a first-degree relative who meets current Task Forse criteria • ARVC confirmed pathologically at autopsy or surgery in a first-degree relative • Identification of a pathogenic mutation[a] categorized as associated or probably associated with ARVC in the patient under evaluation	• History of ARVC in a first-degree in whom it is not possible or practical to determine whether the family member meets current Task Force criteria • Premature sudden death (<35 years of age) due to suspected ARVC in a first-degree relative • ARVC confirmed pathologically or by current Task Force Criteria in second-degree relative

* Morphological changes in I as detected by echocardiography, angiography, cardiac magnetic resonance imaging or radionuclide scintigraphy

[a] A pathogenic mutation is a DNA alteration associated with ARVC that alters or is expected to alter the encoded protein, is absent or rare in a large control population, and either alters or is predicted to alter the protein structure or function or has demonstrated linkage to the disease phenotype in a conclusive pedigree

RV: right ventricle, VES: ventricular extrasystole, VT: ventricular tachycardia, RBBB: right bundle branch block, ECG: electrocardiogram; LV: left ventricle, PLAX: parasternal long-axis view, RVOT: RV outflow tract, BSA: body surface area, PSAX: parasternal short-axis view, aVF augmented voltage unipolar left foot lead, aVL: augmented voltage unipolar left arm lead

Definite diagnosis: two major, or one major and two minor, or four minor criteria from different categories

Borderline diagnosis: one major and one minor or three minor criteria from different categories

Possible diagnosis: one major or two minor criteria from different categories

Molecular Genetics

ARVC is familial in nearly 50% of cases (Hamid *et al*., 2002), although reduced and age-related penetrance, along with variable phenotypic expression, may lead, in clinical practice, to underestimate the prevalence of familial disease, especially in small and nuclear pedigrees.

The disorder is usually inherited as an autosomal dominant trait (Nava *et al*., 1989); however, also recessive forms have been described. ARVC shows a high degree of genetic heterogeneity. Since identification of the first ARVC locus in 1994 (Rampazzo *et al*., 1994), fourteen loci have been mapped, by linkage analysis and/or direct

sequencing of candidate genes (Table 1.2). Among the known ARVC genes, five (*DSP*, *PKP2*, *DSG2*, *DSC2*, and *JUP*) encode for different components of the cardiac desmosome at the intercalated disk, thereby defining ARVC primarily as a "disease of the desmosome" and the intercalated disk as a major player in molecular pathogenesis of the disorder.

Locus	Inheritance	Chromosome	Gene	Reference
ARVC1	AD	14q23-q24	*TGFβ3*	Rampazzo *et al.*, 1994 Beffagna *et al.*, 2005
ARVC2	AD	1q42-q43	*RyR2*	Rampazzo *et al.*, 1995 Tiso *et al.*, 2001
ARVC3	AD	14q12-q22	-	Severini *et al.*, 1996
ARVC4	AD	2q32.1-q32.2	-	Rampazzo *et al.*, 1997
ARVC5	AD	3p23	*TMEM43*	Ahmad *et al.*, 1998 Merner *et al.*, 2008
ARVC6	AD	10p12-p14	-	Li *et al.*, 2000
ARVC7	AD	10q22.3	-	Melberg *et al.*, 1999
ARVC8	AD/AR	6p24	*DSP*	Rampazzo *et al.*, 2002 Alcalai *et al.*, 2003
ARVC9	AD/AR	12p11	*PKP2*	Gerull *et al.*, 2004 Awad *et al.*, 2006
ARVC10	AD	18q12	*DSG2*	Pilichou *et al.*, 2006
ARVC11	AD/AR	18q12	*DSC2*	Syrris *et al.*, 2006 Simpson *et al.*, 2009
ARVC12/Naxos	AD/AR	17q21	*JUP*	Asimaki *et al.*, 2007 McKoy *et al.*, 2000
ARVC13	AD	2q35	*DES*	Klauke *et al.*, 2010
ARVC14	AD	2q31	*TTN*	Taylor *et al.*, 2011

AD: Autosomal Dominant; AR: Autosomal Recessive; TGFβ3: Transforming Growth Factor β3; RyR2: Cardiac Ryanodine Receptor 2; TMEM43: Transmembrane protein 43; DSP: Desmoplakin; PKP2: Plakophilin 2; DSC2: Desmocollin 2; DSG2: Desmoglein 2;JUP: Plakoglobin; DES: Desmin; TNT: Titin

Table 1.2. Known ARVC loci and genes identified so far

The Cardiac Intercalated Disk

The structural and functional integrity of the heart is maintained through the proper organization of different junctional complexes at specialized cell-cell contacts, called intercalated disks, providing mechanical and electrochemical coupling between cardiomyocytes. The original description of the cardiac intercalated disk has identified three separate structures, discernible by electron microscopy: gap junctions, adherens junctions of the *fascia adhaerens* type, and desmosomes (Forbes and Sperelakis, 1985).

Gap junctions form intercellular channels that enable cell-cell communication and transfer of depolarizing current, by mediating direct diffusion of small molecules and ions between cardiac myocytes. Accordingly, propagation velocity of action potentials and three-dimensional temporal/spatial pattern of electrical activation in the myocardium depend on number and spatial distribution of gap junctions. Each channel consists of two exameric structures, called connexons, resulting from oligomerization of the transmembrane protein connexin (Cx). In the heart, the most abundant connexin isotype is Cx43. Connexons dock across the extracellular space, forming a permeable, low-resistance, pore (Saffitz *et al*., 2004).

Since membrane regions containing these channels are rigid and susceptible to fragmentation under shear stress, *fascia adhaerens* junctions and desmosomes stabilize the sarcolemmas of interconnected cells, ensuring mechanical coupling between adjacent cells, through a series of intermolecular interactions involving several transmembrane, cytoplasmic, and cytoskeletal components.

In the classical model for *fascia adhaerens* junctions, the extracellular domains of trasmembrane proteins N-cadherins tightly bind to each other, while the cytoplasmic ends are indirectly associated to actin cytoskeleton, by β-catenin and plakoglobin. Both these intracellular linker proteins bind to α-catenin, which is in direct contact with actin. Other interactions occur between α-catenin and either vinculin and α-actinin (Gates and Peifer 2005).

The other class of adhesive junctions, desmosomes, tether intermediate filaments to the plasma membrane of adjacent cells, providing further support to the structural and functional tissue integrity.

Desmosomal structure is highly conserved throughout vertebrate evolution and consists of proteins belonging to three different families: desmosomal cadherins, armadillo proteins, and plakins. The primary site of adhesion lies in the extracellular domains of transmembrane desmosomal cadherins, desmogleins and desmocollins, that directly mediate intercellular connection by homophilic and heterophilic interactions. On the intracellular side, several proteins constitute an electron-dense plaque, which can be further subdivided into outer dense plaque (ODP) and inner dense plaque (IDP), based on increased distance from the plasma membrane. In the outer dense plaque, the cytoplasmic tails of desmosomal cadherins bind to the armadillo proteins pakoglobin and plakophilin, which in turn interact with desmoplakin, a member of the plakin family.

The association between desmoplakin and intermediate filaments forms the inner dense

plaque, anchoring the cytoskeletal network to the desmosome. Lateral interactions among proteins in the junctional plaque further stabilizes the structure of the complex (Delva *et al*., 2009).

Traditionally, the molecular composition of adherens junctions and desmosomes in the cardiac intercalated disks was considered mutually exclusive, with the exception of plakoglobin as common component.

However, more recently, a comprehensive immunoelectron microscopy study demonstrated that, in normal heart muscle, all the known cardiac desmosomal proteins are not restricted to desmosome-like junctions, but can also be identified in adhesive structures with a morphology originally described as *fascia adhaerens* (Franke *et al*., 2006). Subsequently, Borrmann and colleagues showed that typical components of adherens junctions, including N-cadherin, α-catenin, and β-catenin, colocalize with desmosomal proteins at the cardiac intercalated disks (Borrmann *et al*., 2006). Moreover, extensive studies, using yeast two-hybrid approach and co-immunoprecipitation, provided molecular evidence that desmosomal protein plakophilin-2 interacts specifically with αT-catenin, a member of α-catenin family that is predominantly expressed in heart tissue. In addition, immunoelectron microscopy identified colocalization of αT-catenin not only with other components of cadherin/catenin complex, as αE-catenin, β-catenin and N-cadherin, but also with the desmosomal protein plakophilin-2, desmoglein-2, and desmoplakin, at the *fascia adhaerens*-like junctions (Goossens *et al*., 2007; Janssens *et al.*, 2001).

Overall, these observations suggested that the predominant type of adhesive junction present at cell-cell contacts in the myocardium is a hybrid structure combining typical desmosomal and *fascia adhaerens* elements and forming, together with desmosomes, an *area composita,* characterized by an unusually high molecular complexity. In the *area composita*, αT-catenin is thought to recruit desmosomal proteins to the hybrid adhering junctions, thereby acting as a specific linker protein between the cadherin-catenin complex, associated with the actin cytoskeleton, and desmosomal proteins, liked to the intermediate filaments, strengthening intercellular adhesion in the cardiac tissue. This mixed-type, reinforced junction may have evolved to ensure formation and maintenance of large gap junctions arrays in the mammalian heart, which is exposed to high mechanical stress.

Previous studies have suggested that gap junction formation requires the presence of neighboring adhesive junctions in cardiac myocytes (Kostin *et al*., 1999).

Moreover, interactions between junctional and non junctional molecules, as several components of the voltage-gated sodium channel, can be observed at the cardiac intercalated disks (Meadows and Isom 2005; Sato *et al*., 2009).
In conclusion, these evidences supports the view of the cardiac intercalated disk not as a collection of molecules with independent functions, but rather as a highly specialized unit, where the cross-talk between components of macromolecular complexes allows to achieve functional synchrony within the cardiac tissue (Delmar 2004).

Desmosomal ARVC genes

Plakoglobin (*JUP*)

The first desmosomal ARVC gene was identified in Naxos disease, an autosomal recessive cardiocutaneous syndrome, characterized by arrhythmogenic right ventricular cardiomyopathy associated with woolly hair and palmoplantar keratoderma. Affected individuals typically show hair and skin phenotype from infancy, whereas cardiac abnormalities occur later, after puberty (Protonotarios *et al.*, 1986). Following linkage mapping of the disease locus on chromosome 17q21 (Coonar *et al.*, 1998), a homozygous 2 bp deletion in *JUP* gene (c.2157_2158delTG) was identified as the causal mutation in 13 Greek families and one Turkish family with Naxos disease. This deletion leads to a frameshift producing a premature stop codon and resulting in a truncated protein at the C-terminus (McKoy *et al*., 2000). Moreover, a heterozygous *JUP* mutation was described in a German family showing autosomal dominant inheritance of ARVC without dermatological manifestations (Asimaki *et al*., 2007). Interestingly, a recent study reported two novel homozygous mutations in *JUP* gene identified in children from Argentina and Kuwait with a cutaneous phenotype characterized by skin blistering, diffuse palmoplantar keratoderma, and woolly hair, but no symptoms of cardiomyopathy. Unlike heterozygous carriers of the Naxos disease allele, subjects heterozygous for both these variants did not present with woolly hair. Along with the lack of skin blistering in Naxos patients, these observations suggested that the homozygous *JUP* mutations identified in this study result in a distinct phenotype; nevertheless it can not be excluded that cardiomyopathy will develop in early adulthood (Cabral *et al*., 2010).

Plakoglobin (γ-catenin) protein belongs to the armadillo family whose members are characterized by a central domain containing a variable number of imperfect 42-aa repeats (*arm* repeats). X-ray crystallography studies of the β-catenin *arm*-repeat region showed that a typical armadillo repeat consists of three α helices forming a right-handed superhelix. The superhelical structure of the complete *arm*-repeat domain results in a long positively charged groove that is the binding site for several ligands, including cadherins (Huber *et al*., 1997).

Plakoglobin is highly homologous to β-catenin and both consist of 12 *arm* repeats, as well as globular domains with ~100 residues at the N- and C-terminus. Interaction between plakoglobin and the conserved region of desmoglein and desmocollin, known as the intracellular catenin-binding site, represents an early step in desmosome assembly (Witcher *et al*., 1996). The central armadillo domain of plakogloblin also binds to the N-terminus of desmoplakin, which tethers intermediate filaments to the desmosomal plaque. Moreover, observation that a deletion of the plakoglobin C-terminal domain leads to formation of large tandemly linked desmosomes, in cultured cells, suggests a possible role of plakoglobin in regulating desmosome size and lateral association between other desmosomal components (Palka and Green, 1997).

In addition to a structural function in cell-cell adhesion junctions, plakoglobin also participates in intracellular signal transduction. Several studies indicates that plakoglobin has a role in the Wnt/β-catenin signalling, an evolutionarily conserved pathway that is directly implicated in the regulation of cell fate, proliferation, and apoptosis. Plakoglobin is closely related to β-catenin, the effector for canonical Wnt signalling, and both interact with many of the same molecules (Zhurinsky *et al*., 2000). The cytoplasmic concentration of plakoglobin and β-catenin is tightly regulated by multiple factors, including their recruitment to intercellular adhesion junctions and the availability of secreted Wnt ligands. Under basal conditions, both armadillo proteins are mainly located in junctional complexes. In the absence of a Wnt signal, free catenins are targeted for ubiquitin-proteasome-dependent degradation by a multimolecular complex consisting of adenomatous polyposis coli (APC) protein, axin, and glycogen synthase kinase 3β (GSK3β), which phosphorylates β-catenin and plakoglobin. The ubiquitin lygase β-TrCP recognizes the phosphoserin residues in the N-terminal domain of catenins, enabling their ubiquitination and degradation by the proteasome. Activation of Wnt signalling, by binding of Wnt to Frizzled receptor, results in suppression of GSK3β complex activity, by Disheveled protein, leading to

accumulation of catenins in the cytoplasm and nuclear traslocation. In the nucleus, β-catenin interacts with transcription factors of the Tcf/Lef (T cell factor/lymphocyte-enhancing factor) family and activates target gene expression by providing the transactivation domain to the Tcf/Lef complex.

Plakoglobin is also able to associate with Tcf/Lef factors and contains a transactivation domain in the C-terminus. Whether plakoblobin itself affects gene expression by binding Tcf/Lef factors or indirectly by interfering with β-catenin-mediated signalling is still controversial. Some evidences suggest that plakoglobin can inhibit trascription of Wnt/β-catenin-responsive genes, as Tcf-4 complexes containing plakoblobin do not bind to DNA (Miravet *et al*., 2002). On the other hand, recent reports have demonstrated that plakoglobin exhibits transcriptional activity when co-expressed with Tcf-4 or Lef-1, in a β-catenin-deficient cell line; therefore it is able to directly activate the Wnt signalling cascade (Maeda *et al*., 2004).

Moreover, it was proposed that plakoglobin may modulate the Wnt pathway also by interfering with the β-catenin turnover and/or localization at adhesion junctions, leading, in each case, to elevated nuclear β-catenin (Miller and Moon 1997; Garrod and Chidgey 2008).

In addition, other data provide support for a role of plakoglobin in β-catenin-independent pathways, regulating the transcription of plakoglobin-specific target genes (Green 2007).

Desmoplakin (*DSP*)

The first disease gene associated with autosomal dominant ARVC showing typical right ventricular phenotype was desmoplakin. A linkage study in an Italian ARVC family allowed to map the disease locus on chromosome 6p24. Subsequent DNA sequencing of all *DSP* exons in affected family members revealed a missense mutation which modifies a putative phosphorylation site in the N-terminal domain binding plakoglobin (Rampazzo *et al.,* 2002).

Moreover, mutations in *DSP* gene have been shown to underlie some cases of different cutaneous and/or cardiac disorders, including an autosomal recessive form of ARVC associated with wooly hair and keratoderma (Alcalai *et al*., 2003); an autosomal dominant skin disease without cardiac abnormalities (striate palmoplantar keratoderma II) (Armstrong *et al*., 1999); and an autosomal recessive condition, called Carvajal

syndrome, characterized by biventricular dilated cardiomyopathy, wooly hair and keratoderma (Norgett *et al*., 2000).

Desmoplakin protein is a crucial component of the desmosomal plaque, playing a role in lateral clustering of cadherins and in linking intermediate filaments to the junctional complex. The primary structure of desmoplakin is tripartite with globular N- and C-terminal domains flanking a central α-helical rod region that allows dimerization through a coiled coil interaction. The N-terminal plakin domain, consisting of two pairs of spectrin repeats separated by a Src-homology-3 domain, is essential for targeting to the desmosomal plaque by interaction with plakoglobin and plakophilin (Jefferson *et al*., 2007).

The C-terminal tail associates with intermediate filaments and contains three plakin-repeat domains (PRDs), named A, B and C, which are connected by variable length linker sequences. Each PRD comprises 4.5 tandem repeats of a 38-residue motif and forms a globular structure with a basic groove representing the intermediate filament binding site (Choi *et al.*, 2002). Phosphorylation of serine residue in the glycine-serine-arginine rich domain (GSR) may regulate the ability of desmoplakin to interact with intermediate filaments (Stappenbeck *et al*., 1993).

Two isoforms of desmoplakin (DSPI and DSPII) are generated by alternative splicing and differ in the length of the central rod domain (Virata *et al*., 1998); isoform I is the only one expressed in cardiomyocytes (Angst *et al*., 1990).

Plakophilin-2 (*PKP2*)

Plakophilin-2 was selected as candidate ARVC gene following observation that a homozygous deletion caused a lethal cardiac defect in mice (Grossmann *et al*., 2004).

DNA sequencing of all *PKP2* exons in a cohort of 120 unrelated ARVC index cases led to identification of 25 different heterozygous mutations in 32 probands (Gerull *et al*., 2004).

Subsequent studies reported *PKP2* mutations in 7% to 52% of ARVC patients with autosomal dominant inheritance pattern (Gerull *et al.*, 2004; Van Tintelen *et al.*, 2006; Pilichou *et al.*, 2006; Dalal *et al.,* 2006; Syrris *et al.*, 2007; Awad *et al*., 2006; Heuser *et al*., 2006; Yang *et al.*, 2006; Lahtinen *et al*., 2008; Christensen *et al*., 2010; Bhuiyan *et al.*, 2009; Den Haan *et al.*, 2009; Bauce *et al.*, 2010; Fressart *et al.*, 2010).

This variability can be attributed to several factors, such as regional differences,

presence of founder mutations, and strictness in applying the Task Force diagnostic criteria.

In addition, Awad and colleagues identified a homozygous mutation in *PKP2* gene which is responsible for an autosomal recessive form of ARVC without cutaneous abnormalities (Awad *et al*., 2006).

Plakophilin-2 is an armadillo-related protein located in the outer dense desmosomal plaque and belonging to the $p120^{ctn}$ subfamily, which is distinct from the subgroup including plakoglobin and β-catenin. Three plakophilins are known (PKP1-3) and show complex tissue and differentiation specific patterns of expression. Plakophilin-2 is the only isoform expressed in cardiomyocytes, but it is also found in lymph node follicles, in simple and complex epithelia as well as in the lower layers of stratified epithelia (Hatzfeld 2006). Plakophilins contain 9 *arm* repeats with an insert between repeats 5 and 6 introducing a bend into the overall structure. The large N-terminal domain mediates interaction with every other desmosomal component, whereas no binding partners have been reported for the central armadillo domain, whose specific role remains unknown (Choi and Weis 2005). Plakophilin-2, like PKP1, exist in two isoforms, a shorter “a” variant and a longer “b” form, generated by alternative splicing and differing in addition of 44 amino acids between repeats 2 and 3 (Mertens *et al*., 1996). In desmosomes, plakophilins are likely to play a crucial role in transport of desmoplakin to plasma membrane and in lateral association of cadherins during desmosome assembly, driving formation of a highly ordered structure (Delva *et al*., 2009).

Plakophilins are also found in the nucleus. Some evidence suggests that intracellular localization may depend on recognition of phosphoserine residue 82 by 14-3-3 proteins; serine 82 PKP2 mutants that cannot bind 14-3-3 predominantly exhibit nuclear localization (Muller *et al.*, 2003). The extra-junctional function of plakophilins is not yet clear. Observation that nuclear PKP2 is associated with RNA polymerase III and RNA binding proteins provides support for a more general role in structure or regulation of transcriptional machinery (Mertens *et al*., 2001). In addition, a possible indirect role in Wnt signaling has been proposed following the evidence that PKP2 interacts with β-catenin through the N-terminal domain and expression of PKP2 in SW480 cells up-regulates β-catenin/Tcf signalling in a β-catenin dependent fashion (Chen *et al*., 2002).

Desmoglein-2 (*DSG2*) and desmocollin-2 (*DSC2*)

Using a candidate gene approach, several heterozygous causative mutations were identified in *DSG2* and *DSC2* genes in patients with autosomal dominant ARVC (Pilichou *et al*., 2006; Awad *et al*., 2006; Heuser *et al*, 2006 Syrris *et al*., 2006). More recently, Simpson and colleagues reported the first case of a homozygous *DSC2* mutation associated with the phenotypic triad of autosomal recessive ARVC, palmoplantar keratoderma and woolly hair (Simpson *et al*., 2009).

Desmoglein-2 and desmocollin-2 are transmembrane glycoproteins belonging to desmosomal cadherin family and forming the adhesive core of desmosome. In humans, seven desmosomal cadherins are known, four desmogleins (DSG1-4) and three desmocollins (DSC1-3), which exhibit tissue and differentiation specific patterns of expression. Isoform 2 of both desmoglein and desmocollin is the only one expressed in cardiac myocytes, as well as in all other tissues containing desmosomes, whereas expression of the other isoforms is restricted to stratified epithelial tissues. All desmosomal cadherin genes are clustered together in the same region of chromosome 18, suggesting that gene expression may be coordinated by shared long-range genetic elements. Desmocollins exist in two alternatively spliced forms, a longer variant “a” and a shorter form “b”, differing only in length of their C-terminal tails (Dusek *et al*., 2006).

The extracellular domains of DSGs and DSCs consist of four cadherin homology repeats (EC1-4) containing a calcium binding motif and a membrane proximal extracellular anchor. Cadherin mediated adhesion depends on calcium binding that enables the extracellular domains to assume a rigidified and functional conformation, which is a requisite for the hyper-adhesive state of desmosomes, characterized by a strong adhesive affinity (Pokutta and Weis 2007). Hyper-adhesiveness is the normal state of tissue desmosomes, which are therefore resistant to disruption by mechanical forces (Garrod *et al.*, 2007).

Desmosomal cadherins contain a single pass transmembrane region, followed by an intracellular anchor. Desmogleins and the longer variant “a” of desmocollin harbor an intracellular cadherin-like sequence (ICS) involved in interactions with other desmosomal components, principally plakoglobin. Additional specific motifs found only in desmoglein cytoplasmic tails include the intracellular proline-rich linker (IPL), repeat unit domain (RUD) containing a variable number of 29 amino acid repeats, and a glycine-rich desmoglein terminal domain (DTD). The DSG2 RUD domain consists of 6 repeating units (Garrod and Chidgey 2007).

The function of the desmoglein specific cytoplasmic region is not well defined. It seems likely that these unique motifs could be involved in desmosomal assembly and organization, by mediating interactions with plakophilins, as well as specify extra-junctional roles in embryogenesis, differentiation, cell polarity, and signal transduction (Dusek *et al*., 2006). Finding of putative protein kinase C (PKC) phosphorylation sites in the RUD repeats of all desmogleins suggests that phosphorylation within this domain and resulting conformational change may transmit a signal to the extracellular space, allowing the desmosome to lose hyper-adhesiveness and shift to a more dynamic lower-affinity state, during wound healing and embryogenesis (Garrod *et al*., 2005).

Extradesmosomal ARVC genes

Cardiac Ryanodine Receptor 2 (*RyR2*)

Cardiac Ryanodine Receptor 2 gene is involved in an autosomal dominant form of ARVC (ARVC2), characterized by juvenile sudden cardiac death and effort-induced polymorphic ventricular tachycardia. Moreover, fibro-fatty replacement of myocardial tissue is less pronounced than in the typical ARVC (Tiso *et al*., 2001).

RyR2 gene encodes the monomer of a homo-tetrameric complex known as cardiac ryanodine receptor, which is located in the smooth sarcoplasmic reticulum membrane and allows excitation-contraction coupling of cardiomyocytes, by a mechanism based on a calcium-induced calcium release. Entry of calcium ions into the cytoplasm, in response to stimulation of voltage-sensitive dihydropyrydine receptors on the outer myocardial cell membrane, activates release of larger amounts of calcium from the sarcoplasmic reticulum lumen via RyR2, resulting in myocardial contraction (Stokes and Wagenknecht 2000).

Functional studies on *RyR2* missense mutations, identified in ARVC2 patients, revealed an increased Ca^{2+} release after stimulation. This evidence suggests that a defective RyR2 receptor, unable to remain closed, leads to calcium overload following an intense adrenergic stimulation under emotional or physical stress, triggering arrhythmias (Thomas *et al*., 2004).

Loss-of-function mutations in *RyR2* causing diastolic leakage of Ca^{2+} have been also associated with catecholaminergic polymorphic ventricular tachycardia (CPVT),

characterized by effort-induced polymorphic ventricular arrhythmias and sudden death in the setting of a structurally normal heart at autopsy (Priori *et al*., 2001).

To what extent ARVC2 and CPVT may be related through common mutations in *RyR2* is not yet clear. The interesting finding of the same *RyR2* mutation in both ARVC2 and CPVT patients from the same family suggested that these clinical conditions might correspond to different degrees of phenotypic expression of the same disease (D'Amati *et al.*, 2005)

Transforming growth factor β3 (*TGFβ3*)

Mutations in the 5′ and 3′ regulatory domains of the gene encoding transforming growth factor β3 were detected in a few patients with autosomal dominant ARVC.

Initially, a nucleotide substitution (c.-36G>A) in the 5'-UTR of *TGFβ3* gene was found to cosegregate with the clinical phenotype in a large ARVC1 family. Subsequent mutation screening extended to 30 unrelated ARVC index cases led to identify an additional variant (c.1723C>T) in the 3'-UTR of one proband. *In vitro* functional studies revealed that both mutations significantly increase activity of luciferase reporter gene in C2C12 cells (Beffagna *et al*., 2005).

TGFβ3 is a member of the transforming growth factor superfamily, a large group of regulatory cytokines playing a pivotal role in embryonic development, tissue homeostasis, wound healing, chemotaxis, and cell cycle control.

It is well documented that TGFβs stimulate mesenchymal cells to proliferate and to produce extracellular matrix components. TGFβs induce a fibrotic response in several tissues *in vivo*, by regulating expression of genes involved in extracellular matrix production or degradation (Leask and Abraham 2004). Recent evidences showed that TGFβ-induced endothelial-mesenchymal transition (EMT) contributes to cardiac fibrosis (Zeisberg *et al*., 2007).

Since the reported mutations in *TGFβ3* UTR regions lead to enhanced gene expression *in vitro,* it is likely that they could promote myocardial fibrosis *in vivo.* In agreement with this hypothesis, endomyocardial biopsy in the two probands carrying *TGFβ3* UTR mutations showed extensive replacement-type fibrosis.

Moreover, independent studies revealed that TGFβs can modulate expression of genes encoding desmosomal proteins in different cell types, suggesting a possible role in regulating intercellular junctional complexes (Yoshida *et al.*, 1992; Kapoun *et al*., 2004). It has been hypothesized that over-expression of TGFβ3, caused by mutations in

regulatory gene regions, might affect cell-cell junction stability, leading to a final outcome similar to that observed in ARVC cases due to mutations in desmosomal genes (Rampazzo 2006).

Transmembrane protein 43 (*TMEM43*)

More recently, the gene encoding transmembrane protein 43 was implicated in a distinctive form of autosomal dominant ARVC (ARVC5), characterized by full penetrance and a sex-influenced lethal clinical course. By positional mapping approach, a single missense mutation (S358L) in *TMEM43* gene was identified in ARVC5 patients from a Newfoundland genetically isolated population. This mutation occurs in a highly conserved transmembrane domain of TMEM43 and is predicted to be deleterious (Merner *et al*., 2008). A subsequent study reported the S358L mutation and a novel splice-site sequence variant of unknown significance respectively in two unrelated ARVC patients from a Danish cohort (Christensen *et al*., 2011). TMEM43 protein, also known as LUMA, is localized to the inner nuclear membrane and endoplasmic reticulum. Topological and functional characterization studies showed that TMEM43 contains 4 transmembrane spans, which are necessary for nuclear envelope targeting and homo-oligomerization, and a large hydrophilic domain whose sequence is predicted to be natively unfolded and proposed to provide a binding site for signal proteins. TMEM43 oligomers were proposed to provide a platform for formation and/or organization of protein complexes on nuclear membrane.

TMEM43 interacts with inner nuclear membrane (INM) proteins, as emerin and SUN2, and lamins, intermediate filament proteins forming nuclear lamina and anchoring INM proteins (Bengtsson and Otto 2008; Liang *et al*., 2011). The evolutionary highly conserved amino acid sequence of TMEM43 suggests a pivotal cellular function, however its exact biological role is still largely unknown and no animal model exists. Identification of a peroxisome proliferator response element in *TMEM43* gene provides support for a possible role in an adipogenic pathway regulated by PPARγ (Lemay and Hwang 2006), then a dysregulation of this pathway may explain the fibrofatty replacement of the myocardium in ARVC patients. Observation of reduced immunoreactive signal level for plakoglobin in *TMEM43* mutation carriers suggests that *TMEM43*-associated ARVC may share a final molecular pathway with desmosome-associated ARVC (Christensen *et al*., 2011).

Interestingly, two missense *TMEM43* mutations affecting residues in the hydrophilic

domain were identified in patients affected by Emery-Dreifuss muscular dystrophy-related myopathy, a genetically heterogeneous neuromuscular disorder characterized by muscular dystrophy, joint contractures, and cardiomyopathy with conduction block (Liang *et al*., 2011; Emery 2000). This finding indicates that different protein domains may be involved in different biological functions and *TMEM43* mutations may underlie a wide spectrum of distinct phenotypes.

Desmin (*DES*)

The gene coding for desmin (*DES*) has recently been recognized as a new player in the growing field of ARVC-associated genes (Van Tintelen *et al*., 2009; Otten *et al.*, 2010; Klauke *et al*., 2010). Desmin is the main intermediate filament (IF) protein in mature skeletal and heart muscle cells where it forms a three-dimensional scaffold around myofibrillar Z-discs connecting them to nuclear lamina, mitochondria and desmosomes. This cytoplasmic framework provides structural and functional tissue integrity by coordinating mechanical stress transmission, organelle positioning, organization and assembly of sarcomeres, signal transduction, and apoptosis (Bär *et al*., 2004).

Like all IF proteins, desmin exhibits a tripartite structure which consists of a central rod domain containing four distinct α-helical segments (1A, 1B, 2A, and 2B), flanked by non-α-helical N-terminal “head” and C-terminal “tail” regions (Weber and Geisler, 1985).

In the rod domain, a heptad-repeat arrangement with a typical sequence of hydrophobic and hydrophilic residues guides two desmin polypeptides into formation of a parallel coiled-coil dimer, the elementary unit of each filament (Bär *et al*., 2004). Desmin dimers associate to form tetrameric complexes; lateral association of these tetramers yields so-called unit-length filaments (ULFs) that undergo a longitudinal and radial assembly, generating mature filaments (Herrmann *et al*., 1996; Herrmann and Aebi, 2000).

The head and tail domains are sites of post-translational modifications, by phosphorylation and glycosylation, regulating dynamic aspects of desmin organization and structure during the cell cycle (Heins and Aebi, 1994).

Mutations in *DES* gene are implicated in a subgroup of myofibrillar myopathies, referred to as desmin-related myopathy (DRM). The clinical phenotype of DRM is high variable and includes “isolated” myopathies, dilated, restrictive, and hypertrophic cardiomyopathy, cardiac conduction disease, and combinations of these disorders (Schröder *et al*., 2007).

The first evidence of an association of *DES* mutations with ARVC was published by Van

Tintelen and colleagues which reported identification of a single founder mutation (S13F), affecting the N-terminal head domain of desmin, in 27 individuals from five families with a highly variable cardiac phenotype (Van Tintelen *et al*., 2009). This mutation was previously implicated in a myopathy and in a broad spectrum of cardiomyopathies (Bergman *et al.,* 2007; Pica *et al*., 2008). In the study by Van Tintelen *et al*, most of patients presented dilated or hypertrophic cardiomyopathy with conduction delay phenotypes, whereas only two subjects fulfil ARVC task force criteria. Immunoistochemistry showed an altered distribution pattern of desmosomal proteins and more convoluted and elongated intercalated disks in S13F mutation carriers, suggesting a localized effect of the mutant protein on cellular connections.

In a subsequent report, Otten and colleagues described two different *DES* mutations (N342D and R454W) in two Dutch families showing ARVC-like phenotype, associated with myopathy, or biventricular cardiomyopathy with unknown skeletal muscle involvement (Otten *et al.*, 2010). The N342D mutation involves the segment 2B in the rod domain of desmin and was previously linked to an isolated skeletal muscle phenotype, without evidence of cardiomyopathy (Dalakas *et al.*, 2000). The R454W mutation is located in the C-terminal tail domain of desmin and was previously associated with a hypertrophic obstructive cardiomyopathy (Bär *et al*., 2007). The study of Otten *et al* revealed that the R454W mutation affects the localization of the desmosomal proteins desmoplakin, plakophilin-2, and connexin 43 at the intercalated disk, suggesting that the tail domain of desmin is involved in mechanical coupling.

Finally, a *de novo* desmin mutation (N116S), located in segment 1A of the rod domain, was detected in an ARVC patient with subclinical skeletal muscle alterations and results in a severe impairment of filament formation (Klauke *et al*., 2010).

Overall these data indicates that the clinical phenotype of ARVC-related *DES* mutations differs considerably and the overlap with other cardiomyopathies suggests a possible common pathway for these distinct clinical entities.

Titin *(TTN)*

The gene encoding titin is the last ARVC gene identified so far. A unique report describes detection of a novel *TTN* mutation (T2896I) showing complete segregation with ARVC phenotype in a large family (Taylor *et al*., 2011). Several *TTN* mutations have also been reported in tibialis muscular dystrophy, without any apparent cardiac signs or symptoms (Hackman *et al*., 2002), in dilated cardiomyopathy (Itoh-Satoh *et al.*, 2002;

Gerull *et al*., 2002; 2006), and in hypertrophic cardiomyopathy (Satoh *et al.*, 1999).

Titin is a giant sarcomeric protein, spanning from the Z-disk to the M-band region, with a crucial role in the maintenance of structural and functional sarcomere integrity (Furst *et al*., 1988).

Titin filaments interact with actin and myosin allowing for proper alignment; moreover, they work as “bidirectional springs” regulating the sarcomeric length and contributing to the majority of passive cardiomyocyte tension (Helmes *et al*., 1999).

The extensible portion of titin consists of tandemly linked immunoglobulin (Ig)-like domains, that make up a proximal (near Z-disk) and a distal (near A-I junction) Ig segment, interspersed by the PEVK sequence (rich in the amino acids proline, glutamate, valine, and lysine) and the N2B element constituted by three Ig domains and a unique 572-residue region. Moreover, the protein contains a C-terminal inextensible region including single repeats of Ig and fibronectin type 3 (Fn3) modules, a kinase domain, and several unique-sequence regions. Titin is expressed in both skeletal and cardiac muscle and in myocardium two isoforms (N2B and N2BA) are generated by alternative splicing. The N2BA variant has an additional element in the N2 region (segment N2A), consisting of four Ig domains and a unique 106-residue region, which confers a higher level of elasticity (LeWinter and Granzier 2010).

In addition to the structural role in the sarcomere, titin filaments connect to the so-called “transitional junction” in the final half-sarcomere adjacent to the intercalated disk. In this region a standard I-band ends with a domain that resembles a Z-disc, where N-terminal titin and α-actinin, recognized Z-disc markers, occur (Bennet *et al.*, 2006). This observation suggests a functional link between the desmosome and titin.

The ARVC-related *TTN* mutation identified by Taylor and colleagues is located in the Ig10 domain within the extensible region of titin. The mutant domain results partially folded and more vulnerable to proteolysis; this increased susceptibility to degradation was proposed as a primary step in the disease pathology. However, the exact pathway by which titin proteolysis might lead to ARVC is still unknown.

Pathogenetic mechanisms of ARVC

Despite the important advances in the genetics of ARVC, which have led to identification of several causative mutations in desmosomal and extra-desmosomal genes, much less is known about the early molecular and cellular events underlying the processes of cardiomyocyte injury, fibro-fatty tissue repair, ventricular remodeling and arrhythmias.

Several evidences arising from immunohistochemical observations in affected human myocardium, expression systems *in vitro*, and animal models suggest that the pathogenesis of ARVC probably involves mechanistic links among abnormal biomechanical properties, inflammatory mediators, stem cell biology, and altered signalling pathways.

Desmosomal dysfunction model

The identification of causal mutations in one or more desmosomal genes, in approximately 50% of affected individuals, fostered the view that desmosomal dysfunction might be the final common pathway in the pathogenesis of ARVC.

A desmosomal gene mutation may impair intercellular adhesion and/or intermediate filament function, depending on its location and impact on protein structure and function. The disruption or the absence of desmosomes compromises the ability of cardiomyocytes to handle high mechanical stresses, leading to myocyte disassociation at the intercalated disk. The detached myocytes undergo cell death, either by apoptosis or necrosis, accounting for progressive loss of the ventricular myocardium. In agreement with this hypothesis, evidence of myocyte death has been reported in ARVC patients at the early and symptomatic phases of the disease (Basso *et al*., 2009). Since the regenerative capacity of the myocardium is limited, repair by fibrofatty replacement ensues. The fibrofatty tissue islands within the damaged myocardium are potential sources of arrhythmias.

The right ventricle may be particularly susceptible to mutations compromising intercellular adhesion because of its thinner walls and its normal dilatory response to exercise. Conversely, defects resulting in C-terminal truncation of desmosomal proteins, especially desmoplakin, may disrupt intermediate filament binding leading to dominant and/or severe involvement of the left ventricle, which must withstand high systolic

pressure. However, coexistence of different disease subtypes (classic right-dominant, biventricular, and left-dominant) in ~67% of families suggests a role of modifier genes and/or environmental influences, in addition to the primary mutation, to explain clinical differences (Sen-Chowdhry *et al*., 2007).

Immunoistochemical analysis in myocardial tissue from affected subjects provided initial insights into mechanisms by which mutations in desmosomal genes cause the disease, revealing an altered subcellular distribution of desmosomal proteins at the intercalated disk.

In particular, in subjects with Naxos disease or Carvajal syndrome the mutant proteins, plakoglobin and desmoplakin respectively, are expressed in the cardiac tissue but fail to localize at intercellular junctions. Moreover, in Carvajal patients a marked loss of plakoglobin and desmin signal at the intercalated disk was observed, presumably because the desmoplakin mutation interferes with the normal molecular interactions among junctional proteins (Kaplan *et al*., 2004).

These data suggest a redistribution of mutant proteins from junctions to other cellular locations and provided the first evidence that a mutation in a single desmosomal component may perturb the subcellular distribution of another protein which is not genetically altered. Similarly, the localization of desmosomal proteins was characterized in tissues from ARVC patients carrying dominant mutations in the desmosomal genes *DSP*, *DSG2*, *DSP* and *JUP*, revealing a marked reduction in plakoglobin staining at the intercalated disk in all samples and variable patterns of altered distribution for the other desmosomal proteins (Asimaki *et al*., 2009). The reduced plakoglobin signal appears to be specific for ARVC and does not occur in other forms of heart-muscle disease. Interestingly, it was also observed in ARVC patients with mutations in the extradesmosomal gene *TMEM43* (Christenses *et al*., 2011), suggesting the hypothesis that redistribution of plakoglobin from junctions to cytosol compartments is part of a final common pathway in disease pathogenesis, in which plakoglobin might play a key role in altered signaling pathways.

Several evidences coming from studies in cultured cells and genetically modified animal models provide support for a pivotal signalling function of nuclear PG in repressing the Wnt/β-catenin signalling pathway and inducing adipogenesis in cardiac progenitor cells.

It is known that the canonical Wnt/β-catenin signalling regulates the transcriptional switch between myogenesis versus adipogenesis (Ross *et al*., 2000); moreover, it is primarily involved in differentiation of cardiac progenitor cells and embryonic

development of the right ventricle and its outflow tract (Ai *et al.*, 2007).

Activation of Wnt signalling enhances myogenesis, inhibits adipogenic transcription factors, as C/EBPα and PPARγ, maintains preadipocytes in undifferentiated state and blocks apoptosis in a variety of cells. Conversely, suppression of Wnt signalling, by overexpression of axin or a dominant-negative effect of Tcf-4 mutants, leads to adipogenesis, adipocyte proliferation, fibrogenesis and apoptosis (Ross *et al*., 2000). It has been hypothesized that desmosomal genes mutations impairing desmosome assembly may perturb the normal balance of proteins in junctions, resulting in dislocation of plakoglobin from desmosomes to intracellular pools and subsequent traslocation into the nucleus. Increased levels of nuclear plakoglobin lead to suppression of the canonical Wnt signalling probably through competitive interactions of plakoglobin and β-catenin with Tcf-4 transcription factor. Complexes of plakoglobin and Tcf-4/Lef1 transcription factors bind to DNA more weakly than do complexes containing β-catenin (Zhurinsky *et al*., 2000).

Consistent with this hypothesis, studies in cultured atrial myocyte (HL-1) cell lines and in a mouse model showed that suppression of desmoplakin expression is associated with nuclear localization of plakoglobin, a two-fold reduction in Wnt signalling, enhanced myocyte apoptosis, excess fibrogenesis and adipogenesis, myocardial dysfunction, and ventricular tachycardia (Garcia-Gras *et al*., 2006).

Moreover, nuclear localization of plakoglobin was associated with decreased expression of connective tissue factor (CTGF), which is a negative regulator of adipogenesis, and enhanced expression of adipogenic markers, as bone morphogenic protein (BMP7), kruppel-like factor 15 (KLF15), and noncanonical Wnt5b molecule, as well as insulin growth factor binding protein 5 (IGFBP5) which is implicated in several biological functions, including muscle atrophy, cell senescence, survival, differentiation, fibrosis, and inflammatory response.

Genetic fate-mapping experiments in mice suggested that adipocytes in ARVC originate from a subset of second heart field progenitor cells regulated by Mef2C transcription factor. Cardiac progenitor cells have not yet fully committed to a myocyte lineage and preferentially differentiate into adipocytes in response to suppression of canonical Wnt signalling due to increased levels of nuclear plakoglobin. These findings were corroborated by observations in autoptic heart specimens from ARVC patients showing coexpression of second heart field markers and adipogenic transcription factors in rare cells within fibroadipocytic areas (Lombardi *et al.*, 2009; Lombardi *et al*., 2011). The

predominant involvement of the right ventricular free wall in classical ARVC may be related to the fact that the second heart field progenitor cells give rise to the right ventricle and its outflow tract (Cai *et al*., 2003). Moreover, since the phenotypic spectrum of ARVC includes also non classic left-dominant and biventricular subtypes, it was proposed that subepicardial progenitor cells might play a role in disease pathogenesis, because they spread into right and left ventricles and give origin to the myocardium and interstitial cells (Pilichou *et al*., 2011).

Overall, these evidences support the view of dysregulated Wnt signaling as a fundamental pathogenetic mechanism in ARVC.

The desmosomal dysfunction model for ARVC pathogenesis may also explain the genesis of arrhythmias in an early disease stage, preceding fibrofatty substitution, by gap junctions remodelling and alterations in sodium current kinetics in response to impairment or deficiency of desmosomal components. Although fibro-fatty tissue islands are well-recognized arrhythmogenic substrates, ARVC patients may present with severe arrhythmias also in the absence of significant structural changes.

Several evidences support the general concept that the extent to which cardiac cells are electrically coupled by gap junctions depends on the presence of sufficient mechanical stabilization of the intercalated disk by adhesion junctions.

In vitro observation demonstrated that the establishment of adhesion junctions consisting of N-cadherin, desmoplakin, α-catenin, and plakoglobin precedes the formation of gap junctional plaques between cultured adult rat ventricular cardiomyocytes (Kostin *et al.,* 1999). Moreover, induced deletion of N-cadherin gene in adult mice results in disassembly of the intercalated disk structure and a prominent decrease Cx43 levels (Kostetskii *et al*., 2005).

Ultrastructural studies in myocardial tissues from gene-positive ARVC patients showed intercalated disk remodelling associated with mislocalization and decreased number of desmosomes (Basso *et al*., 2006). Immunohistochemical and electron microscopy investigation on myocardium from subjects affected with Naxos disease or Carvajal syndrome revealed a clear reduction in Cx43 signal at the intercalated disk, along with a decreased number and size of gap junctions (Kaplan *et al*., 2004). Diminished Cx43 immunoreactivity at intercalated disks was also observed in dominant forms of ARVC associated with mutations in desmosomal genes (Tandri et al., 2008; Asimaki *et al.*, 2009) or in desmin gene (Van Tintelen *et al*., 2009; Otten *et al*., 2010).

Moreover, Oxford and colleagues demonstrated that inhibition of PKP2 expression, by

small interfering (si)RNA, in primary cultures of ventricular cardiomyocytes leads to a decrease in total Cx43 content, a redistribution of Cx43 from the intercalated disk to intracellular pools, and a significant reduction in dye transfer between cells which indicates compromised intercellular communication. In addition, pulldown experiments indicated that Cx43 and PKP2 can coexist in the same macromolecular complex (Oxford *et al*., 2007). A further study showed that siRNA-mediated PKP2 knockdown in cardiomyocytes results in disintegration of *area composita* junction structures (Pieperhoff *et al*., 2008).

More recently, a novel direct interaction between DSC2a isoform and Cx43 was described.

Immunoistochemical analysis on myocardial tissue from an ARVC patient carrying a truncation DSC2a mutation revealed reduced total Cx43 levels and changes in Cx43 phosphorylation. Subsequent functional studies demonstrated that the DSC2a mutant is deficient in binding Cx43, as well as JUP and DSP (Gehmlich *et al.*, 2011).

These findings raise the possibility that desmosomal proteins are directly involved in connexin stabilization and indicate that the integrity of adhesion junctions at the intercalated disk is a prerequisite for normal targeting and function of gap junctions. Accordingly, impaired mechanical coupling, due to defects in cell–cell adhesion or discontinuities between adhesion junctions and cytoskeleton, destabilizes gap junctions and may contribute to arrhythmogenesis by inducing slow and discontinuous conduction (Saffitz 2005).

Gap junctions remodelling occurs early in ARVC, in cardiac regions showing no significant structural or functional alterations, unlike other cardiomyopathies in which it becomes most apparent during advanced disease stage associated with considerable structural changes (Nattel *et al*., 2007; Asimaki *et al*., 2009). This evidence suggests a disease-specific mechanism and provides further support for a role of gap junction remodelling in promoting arrhythmia in ARVC.

Moreover, other ion channels could be involved as well. A recent study demonstrated that PKP2 associates with the major α subunit of the cardiac sodium channel Nav1.5 and that knockdown of PKP2 expression leads to a decrease in amplitude and a shift in sodium current kinetics in adult ventricular myocytes (Sato *et al*., 2009). Optical mapping expreriments revealed that loss of PKP2 expression results in slow conduction and increases propensity to re-entrant arrhythmias in cardiac cell monolayers (Deo *et al.*, 2011). Overall these results suggest the hypothesis that changes in desmosome

integrity may disrupt molecular complexes relevant to electrical function sufficiently to initiate and maintain arrhythmic events, emphasizing the view of the cardiac intercalated disk as a functional unit where cross-talk between different molecular complexes maintains synchrony within cell populations.

Role of inflammation

Myocyte loss in either ventricle may be associated with inflammatory infiltrates, composed mainly of T lymphocytes and observed in up to 75% of hearts at autopsy (Thiene *et al*., 2007). Inflammation is a potential source of ventricular arrhythmia and may contribute to disease progression underlying the clinical phenomenon of “hot phases”, characterized by periodic exacerbations of an otherwise stable or quiescent disease (Basso *et al*., 2009).

Nevertheless, etiology and role of myocardial inflammation in ARVC remains unresolved. The inflammatory response might be a reaction to cell death or the consequence of infective or immune mechanisms. Virus have been detected in the myocardium of some ARVC patients suggesting a possible connection between viral myocarditis and disease pathogenesis. Alternatively, viral infection could be an epiphenomenon unrelated to ARVC or cell degeneration may favour viral settlement in the myocardium (Calabrese *et al*., 2006).

Another possibility is that inflammatory cytokines play a direct role in ARVC pathogenesis. This “cytokine hypothesis” proposes that a precipitating event, such as myocardial tissue injury, triggers innate stress response leading to production of pro-inflammatory cytokines by nucleated cells in the heart and subsequent release into the bloodstream. These inflammatory mediators, as interleukin-1β (IL-1β), interleukin-6 (IL-6) and tumour necrosis factor-α (TNF-α), exert direct toxic effects on the heart contributing to the deterioration of cardiovascular function, by various mechanisms including myocyte hypertrophy, ventricular dysfunction and remodelling, and increased cardiac myocyte apoptosis (Anker and von Haehling 2004). It is known that TNF-α and IL-1β can stimulate the expression of inducible nitric oxide synthase (iNOS) leading to strand breaks, p53 accumulation and apoptosis, which in turn evokes an inflammatory response (Geng *et al*., 1994; Messmer *et al.*, 1995).

This evidence suggests that the inflammatory response in ARVC may not only be an initial response to a triggering event, such as a viral infection, but it may also be

enhanced because of apoptosis induced by pro-inflammatory cytokines.

However, the cytokine hypothesis has not been formally investigated and no data on a possible association between activation of pro-inflammatory cytokines and disease are available.

In a recent study, cardiac inflammation was non-invasively assessed by analysis of plasma inflammatory cytokine levels and cardiac ^{67}Ga scintigraphy, demonstrating that in ARVC patients plasma levels of pro-inflammatory cytokines interleukin (IL)-1β, IL-6 and tumor necrosis factor (TNF)-α, as well as the ^{67}Ga uptake in the right ventricular wall, are significantly higher that in controls. These findings, however, did not allow to distinguish whether inflammation is an initial response to an infection or is secondly induced by apoptosis and the clinical implications remain to be clarified (Campian *et al.*, 2010).

Finally, data coming from studies on animal models of ARVC suggested that inflammation may promote cardiac hypertrophy through β-catenin signalling.

Several studies indicate that β-catenin/Tcf/Lef targets are dominant regulators of cardiomyocyte growth and overexpression of a stabilized mutant form of β-catenin can drive hypertrophic growth in cardiomyocytes by a Wnt-independent mechanism (Chen *et al*., 2006; Haq *et al.*, 2003). Conversely, cardiac-restricted β-catenin haploinsufficiency inhibits cardiac hypertrophy in response to pressure overload (Qu *et al.*, 2007).

It was proposed that increased levels of IL-6 and IL-1β, following myocardial damage in ARVC, may induce activation of the PI3K/AKT pathway and inhibition of GSK-3β, promoting β-catenin-mediated hypertrophy (Li *et al.*, 2011).

Role of apoptosis

Apoptosis in ARVC was proposed as an important process that could account, at least in part, for the progressive loss of myocardial cells in the disease.

Apoptotic myocardial cell death is a consistent *post mortem* finding in both right and left ventricles (Mallat *et al.*, 1996). Moreover, *in vivo* evidences of apoptosis in endomyocardial biopsies from ARVC patients were obtained by transmission electron microscope (TEM), TUNEL assay, and ^{99m}Tc-annexin V scintigraphy (Valente *et al*., 1996; Campian *et al*., 2011). Interestingly, apoptotic myocytes were observed in areas of the myocardium which are not subjected to invasion by adipocytes and fibrous tissue, suggesting that the loss of myocardial cells through apoptosis is a primary process

preceding the fibro-fatty replacement. Further studies revealed increased expression of the apoptotic genes, as *CPP32,* encoding caspase 3, and *BAX,* encoding BCL2-associated X protein, in ARVC samples but not in age-matched normal controls (Yamaji *et al*., 2005). In addition, cell-line studies showed that plakoglobin regulates expression of the *BCL2* antiapoptotic gene*,* encoding B-cell CLL/lymphoma 2 (Hakimelahi *et al.*, 2000). Finally, it is well documented that the Wnt/β-catenin signalling pathway modulates the apoptotic response in preadipocytes (Longo *et al*., 2000).
Despite these evidences, the contribution of programmed cell death in pathogenesis and progression of ARVC remains unclear.

Animal models of ARVC

In recent years, animal models recapitulating important aspects of the human ARVC phenotype have contributed to a better understanding and in-depth characterization of molecular mechanisms underlying the disease, because of the unique ability to control both environmental influences and genetic background. Transgenic, knockin, knockout and overexpression models mimicking the human ARVC phenotype have been reported. Moreover, naturally occurring animal models for ARVC have been described.

Desmoplakin

To date, three murine lines have been developed for *DSP* gene. The first described is a germline knockout mouse model showing high embryonic lethality of homozygous mutants, due to desmosome instability and loss of tissue integrity. Analysis of embryos revealed a critical role for desmoplakin in desmosome assembly and stabilization, as well as in establishing intermediate filament cytoskeletal architecture (Gallicano *et al*., 1998). Partial rescue of desmoplakin expression in extraembryonic tissues promoted survival of embryos not beyond gastrulation, with major defects in heart muscle, neuroepithelium and skin epithelium (Gallicano *et al*., 2001). More recently, Garcia-Gras and colleagues showed that cardiac-restricted *DSP* deletion impairs heart morphogenesis leading to embryonic lethality in homozygous mice. A higher survival rate was found in the heterozygous animals exhibiting age-dependent penetrance of heart involvement with a 20% incidence of sudden cardiac death by 6 month of life. The

cardiac phenotype included fibroadipocytic replacement of myocytes, enhanced myocyte apoptosis, ventricular dysfunction, and ventricular arrhythmias, recapitulating the human ARVC disease. The authors demonstrated that cardiac-restricted *DSP* deletion in hemizygous mice led to accumulation of plakoglobin within nonjunctional compartments, including the nucleus. Moreover, expression levels of adipogenic genes, as PPARγ, C/EBP-α and adiponectin, were increased, whereas expression of genes targeted by the Wnt/β-catenin signalling pathway, as c-myc and cyclin D1, was reduced. These observations suggested the hypothesis that *DSP* knockdown results in nuclear translocation of JUP and suppression of the canonical Wnt/β-catenin signalling through Tcf/Lef1 transcription factors, leading to adipogenesis, fibrogenesis and myocyte apoptosis, as observed in human ARVC (Garcia-Gras *et al.*, 2006). Subsequently, in order to identify the cellular origin of adipocytes in ARVC, the same group generated three lines of *DSP*-deficient lineage tracer mice regulated by different cardiac lineage promoters (αMyHC, Nkx2.5, or Mef2C), in which *DSP* expression was conditionally suppressed while simultaneously labeling cells with a reporter protein. Absence of liveborn homozygous *DSP*-deficient mice indicated high embryonic lethality, as previously reported. Conversely, heterozygous mice survived and exhibited excess fibroadiposis, along with increased numbers of adipocytes in the hearts. Detection of reporter protein expression in adipocytes from the Mef2C-regulated lineage tracer mice revealed an origin from the second heart field progenitors.

Moreover, rare cells coexpressed adipogenic transcription factors and the second heart field markers Isl1 and Mef2C in the lineage tracer mouse hearts and in myocardial tissue from ARVC patients.

The authors concluded that adipocytes in ARVC originate from the second heart field progenitor cells that switch to adipogenesis as a result of suppressed canonical Wnt signaling by nuclear plakoglobin (Lombardi *et al*., 2009).

An alternative approach was used to characterize specific effects of ARVC-related *DSP* mutations. Transgenic mice overexpressing a cardiac-restricted C-terminal *DSP* mutation (R2834H) were generated using the heart-specific α-myosin heavy chain promoter. The mutant mice displayed increased cardiomyocyte apoptosis, cardiac fibrosis and lipid accumulation, as well as ventricular enlargement and dysfunction of both ventricles by 6 month of age. Interestingly, marked ultrastructural abnormalities of the intercalated disks were observed, along with loss of desmin-desmoplakin interaction and redistribution of several junctional components including JUP, PKP2, β-catenin, and

Cx43. Moreover, large amounts of JUP and β-catenin were present in the Triton-X soluble fraction, mostly cytoplasmic, suggesting potential transcriptional changes contributing to cardiac phenotype.

Overall, the authors concluded that DSP is essential for maintaining cardiac tissue integrity. Accordingly, DSP abnormalities can cause ARVC as a result of desmosome instability, cardiomyocyte death, intercalated disk remodelling and alteration of lipid metabolism. Of note, no effects on cardiac rhythm and no increased prevalence of sudden cardiac death were described in these animal models. Conversely, cardiac-specific overexpression of N-terminal DSP mutant (V30M and Q90R) in transgenic mice resulted in embryonic lethality due to profound ventricular dilation (Yang *et al.*, 2006).

Plakophilin-2

Although *PKP2* is the gene most commonly associated with ARVC, animal models of *PKP2* mutations are not yet available.

Only a *PKP2* knockout murine model was described by Grossmann and colleagues and showed a lethal phenotype in homozygous mutants, due to abnormal heart morphogenesis at mid-gestation. Homozygous *PKP2*-deficient embryos exhibited reduced trabeculation, disarrayed cytoskeleton, ruptures of cardiac walls, and blood accumulation in the pericardic cavity. Moreover, desmoplakin did not colocalize with junctional proteins at the intercalated disk but was dispersed over the cytoplasm, forming granular aggregates. Surprisingly, desmoglein-2 was largely absent from desmosomal junctions in the mutant hearts suggesting that PKP2 is a stabilizing binding partner of desmosomal cadherins.

In contrast to the myocardium, the ultrastructure of junctions in epithelial tissues was not altered. These findings indicated that PKP2 is essential for assembly of junctional proteins and for maintaining architectural stability of the cardiac intercalated disk (Grossmann *et al.*, 2004).

Plakoglobin

Similar to germ-line *DSP* and *PKP2* knockout, introduction of a null *JUP* mutation in mice is embryonic lethal. Two *JUP* knockout mouse models were independently generated by distinct groups, showing some contradictory findings. Homozygous mutants described by Ruiz and co-workers died at mid-gestation due to severe cardiac defects. Analysis of embryos revealed absence of desmosomes and consequent

redistribution of DSP and DSG2 in heart, but not in epithelial tissues. The remaining junctional structures at the intercalated disks were drastically altered and exhibited impaired architectural stability and function (Ruiz *et al*., 1996). Similarly, in the *JUP* null murine model developed by Bierkamp and colleagues homozygous mutants were embryonic lethal, although some embryos developed further and died around birth. However, subsequent evaluation of embryos showed skin blistering and subcorneal acantholysis, along with cardiac dysfunction. Ultrastructural analysis revealed that desmosomes were greatly reduced in number and structurally altered both in the skin and in the heart (Bierkamp *et al*., 1996).

Overall, both knockout mouse models indicate that the absence of plakoglobin significantly affects desmosome formation and architecture of the intercalated disks in the heart, resulting in tissue instability, but disagree about the role of JUP in epithelial desmosomes.

In the same year, a further study showed that haploinsufficient $JUP^{+/-}$ mice exhibited right ventricular dilation and dysfunction, as well as spontaneous ventricular arrhythmias, by 6 months of age. This phenotype was exacerbated by daily swimming, supporting the view that endurance training could accelerate disease progression in ARVC patients. However, based on histology and electron microscopy, there was no evidence of cardiomyocyte abnormalities, fibrofatty replacement, and alterations of myocardial structure or desmosome integrity. The absence of histological and structural changes in heterozygous *JUP*-deficient mice is concordant with occasional reports that the clinical cardiac manifestations of Naxos disease or ARVC may occur in younger patients without significant histological abnormalities which develop later, as a result of disease progression (Kirchhof *et al*., 2006). In a subsequent study, the same group demonstrated that a therapy aimed at reducing ventricular pressure and volume load in heterozygous *JUP*-deficient mice prevented training-induced development of ventricular enlargement and conduction slowing and normalized inducibility of ventricular tachycardia (Fabritz *et al*., 2011).

Very recently, inducible cardiac-restricted $JUP^{-/-}$ mice exhibited many histopathologic features of human ARVC, as altered desmosome ultrastructure, decreased signal of desmosomal proteins at the intercalated disks, apoptosis, progressive cardiomyocyte loss, inflammation, fibrous tissue replacement, and cardiac dysfunction. However, despite gap junction remodelling, this murine model did not recapitulate the arrhythmic phenotype. Interestingly, the authors showed increased levels of unphosphorylated β-

catenin, transcriptionally active, localized at the intercalated disk, as well as in the cytoplasm.

The activated β-catenin was also found complexed with Tcf-4 and β-catenin/Tcf/Lef target genes, as *c-Myc* and *c-Fos*, involved in regulation of hypertrophy, were up-regulated. Moreover, a significant increase in inactive GSK-3β phosphorylated forms and active PKB/AKT was observed.

Overall, these observations suggested the idea that ablation of plakoglobin in cardiac-restricted *JUP* knockout mice led to redistribution of desmosomal proteins and myocyte loss associated with an inflammatory response. Sustained stimulation of IL-6 and IL-1β following myocardial damage induce activation of AKT and inhibition of GSK-3β, resulting in stabilization of β-catenin and upregulation of target genes implicated in cardiac hypertrophy (Li *et al.*, 2011).

In the same year, an other cardiac-restricted *JUP* knockout mouse was generated by a different group and exhibited several interesting differences compared to that described above. This murine model largely recapitulated the human ARVC phenotype, showing ventricular dilation and aneurysm, cardiac dysfunction, fibrosis, and absence of desmosome structure at the intercalated disks. The mutant mice also developed spontaneous ventricular arrhythmias and slow conductivity with disease progression. Connexin 43 signal at the intercalated disk was absent in regions of myocyte loss and fibrotic replacement. Moreover, β-catenin was up-regulated and immunostaining revealed that it was present at the intercalated disk, but not in the cytosol or nucleus. Analysis of β-catenin transcriptional activity and expression levels of target genes, as *Cyclin D1* and *c-Myc*, revealed that β-catenin signaling was not altered.

These evidences indicated that the enhanced β-catenin expression primarily compensated for the loss of JUP in the constitution of adherens junctions but not in desmosomes at the intercalated disk, without altering overall β-catenin transcriptional activities. Conversely, the TGFβ signaling was up-regulated and the authors speculated that the enhanced TGFβ activities in *JUP* mutant hearts was triggered by the intensified myocardial wall stress due to the compromised cell–cell mechanical coupling following desmosome disruption.

This finding raises the possibility that TGFβ signaling might be involved in the pathogenesis of ARVC, consistent with implication of TGFβ signaling in myocyte cell death regulation, including both apoptosis and necrosis, cardiac fibrosis and hypertrophy (Li *et al*., 2011).

In addition to the evidences coming from mouse models, morpholino-induced knockdown of *JUP* expression in zebrafish revealed significant effects on cardiogenesis. Morphant embryos exhibited decreased heart size, reduced heartbeat, cardiac edema, and valvular dysfunction leading to intrachamber reflux. Desmosomes and adherens junctions at the intercalcated disks were lower in number and showed a more diffuse ultrastucture in the morphant hearts. Moreover, Wnt target gene expression was enhanced in the heart and throughout the embryo, indicating that plakoglobin competes with β-catenin in Wnt/β-catenin signalling. The authors also demonstrated that inhibition of this increase in Wnt signalling, by co-injecting an optimal dose of the Wnt inhibitor Dkk1, rescued the cardiac phenotype in morphant embryos.

The loss of JUP resulted in increased β-catenin protein expression, due to protein stabilization or increased translation, since β-catenin mRNA levels were similar in morphant and control embryos. β-catenin compensated for the loss of plakoglobin in adherens junctions but not in desmosomes, as indicated by colocalization of β-catenin with E-cadherin. These observations were consistent with findings in inducible cardiac-restricted $JUP^{-/-}$ mice (Martin *et al*., 2008).

Desmocollin-2

A zebrafish model system was used to investigate the physiological effects of an ARVC-related *DSC2* mutation (c.631-2A>G) which creates a premature stop codon and leads to marked reduction in the mutant transcript level in patient specimens. Morpholino-induced knockdown of *DSC2* gene resulted in a cardiac phenotype with dose-dependent bradycardia, chamber dilatation, abnormal cardiac contractility, and progressive pericardial edema. Morphant embryos also exhibited reduced desmosomal areas and loss of desmosomal extracellular electron-dense midline in the myocardial tissue. Rescue of the morphant phenotype was obtained by coinjection of wild-type human *DSC2* mRNA but not with mutant mRNA, suggesting that physiologic levels of DSC2 are critical for early cardiac morphogenesis, normal desmosome formation and cardiac function. In addition, these results confirmed the *in vivo* loss of function of the truncated mutant protein (Heuser *et al*., 2006).

Desmoglein-2

A knockout mouse model for *DSG2* gene was developed by Eshkind and coworkers in 2002 and showed high embryonic lethality. Homozygous mutants and a considerable

number of heterozygous mice died at or shortly after implantation, indicating that DSG2 is essential for embryonic stem cell viability and proliferation. Moreover, immunofluorescence analysis of *DSG2*$^{-/-}$ blastocysts revealed altered distribution of PKP2 and DSP, whereas β-catenin and E-cadherin appeared to be unaffected (Eshkind *et al*., 2002).

A more recent study characterized the effect of an ARVC-related *DSG2* mutation (N266S) by generating transgenic mice with cardiac-restricted overexpression of the mouse homologue variant *(dsg2*-N271S). This mouse model recapitulated pathognomonic features of human ARVC, as sudden death at young age, spontaneous ventricular arrhythmias, cardiac dysfunction, biventricular dilation and aneurysms, myocardial atrophy, and fibrosis. The phenotype was dependent on the transgenic expression level.

The authors demonstrated that myocardial injury was initiated by necrotic myocyte death triggering an inflammatory response and massive calcification within the myocardium, followed by fibrous tissue replacement as repair process. Moreover, observation of structurally normal desmosomes in the hearts of both transgenic mice and ARVC patients suggested a dominant-negative effect of mutant protein on desmosome function rather than structure (Pilichou *et al*., 2009).

Finally, a homozygous *DSG2* mutant mouse model (DSG2$^{mt/mt}$), lacking major parts of the adhesive extracellular domains EC1 and EC2, allowed to study the consequences of a mutated endogenous desmosomal protein. These mutant mice exhibited features of dilative cardiomyopathy and ARVC, with dilation of heart chambers leading to cardiac insufficiency and eventually premature death. Cardiomyocyte death by calcifying necrosis and replacement by fibrous tissue also occurred. Highly proliferative fibrotic foci were observed in 2-week-old mutants, associated with increased apoptosis and abundant cardiomyocyte necrosis; whereas the fibrotic lesions of older mutants showed little proliferation. These findings suggested that active replacement processes, induced by local injuries of the heart muscle, were terminated by formation of inactive scar tissue. Disease progression and cardiac response correlated with an initial increase in mRNA levels of several cardiac stress markers playing antihypertrophic and cardioprotective effects (c-myc, CTGF, GDF15) in mice with apparently normal heart muscle, followed by higher synthesis of antifibrotic natriuretic peptides (ANF and BNF) in older animals with fibrosis and cardiomyocyte death.

Overall, these data highlighted the acquired nature of the disease (Krusche *et al.*, 2011).

AIM OF THE STUDY

The PhD project described in the present thesis concerns the molecular genetics of Arrhythmogenic Right Ventricular Cardiomyopathy (ARVC).

ARVC is a potentially lethal genetic disorder characterized by fibrofatty replacement of ventricular myocardium and ventricular arrhythmias; it significantly increases the risk of sudden cardiac death, which may be prevented by timely detection and intervention.

Hight phenotypic heterogeneity, age-related penetrance and lack of conspicuous abnormalities in the early “concealed” phase of the disease greatly complicate the diagnosis. Genetic testing is of most value in enabling early identification of asymptomatic mutation carriers.

However, causative mutations in known ARVC genes have been detected in about 50% of index cases; therefore, additional and still unknown disease-genes must be involved.

This study aimed to estimate the relative prevalence of mutations among ARVC genes encoding desmosomal proteins (*PKP2*, *DSP*, *DSG2*, *DSC2,* and *JUP*) in a cohort of 80 Italian unrelated index cases. Moreover, identification of novel disease-loci and genes was attempted by genome wide scan in three ARVC family showing no mutations in any of the known genes. For each family, different approaches were adopted, including linkage study, Copy Number Variations analysis, and exome sequencing.

Identification of novel ARVC genes is of great importance for understanding the molecular pathogenesis of this disease, as well as for increasing the power of genetic screening and developing successful targeted therapies.

2. MATERIALS and METHODS

2.1 Mutation screening

Study population

The study population consisted of eighty unrelated index cases of Italian descent with a diagnosis of ARVC. All participating patients and their relatives gave informed consent to clinical and genetic studies.

Probands and family members were clinically evaluated according to the major and minor diagnostic criteria established by the International Task Force of the European Society of Cardiology/International Society and Federation of Cardiology (Marcus *et al.*, 2010).

Clinical evaluation was made in the University of Padua Medical School – Azienda Ospedaliera and the study protocol included a detailed personal/family history, physical examination, 12-lead ECG, 2-dimensional echocardiogram, signal-averaged ECG (SAECG), Holter monitoring, stress test ECG, and cardiac magnetic resonance imaging (MRI) in some cases. Additional invasive procedures, including angiography and endomyocardial biopsy, were performed only when deemed necessary.

Genetic analysis

For each patient, genomic DNA was extracted from peripheral blood leukocytes using a modified salting-out procedure.

The coding exons and also 50 to 150 bp lanking intronic regions of PKP2, DSP, DSG2, DSC2 and JUP genes were screened for mutations in all eighty index cases. Each sequence was amplified from genomic DNA by polymerase-chain reaction (PCR) assay. The analysis was performed by denaturing high-performance liquid chromatography (DHPLC, Transgenomic, NE, USA) and direct sequencing. The allele frequencies of all novel detected variants were estimated by screening of a control group of 250 healthy and ethnically-matched subjects (500 chromosomes). The available family members of the probands were analyzed for the presence of the mutations identified in the index cases.

Salting-out DNA extraction

The following protocol is a modification of the salting-out procedure (Miller et al., 1988), evaluated at the Human Genetic Laboratory, University of Padua, Italy.

Genomic DNA was isolated from peripheral blood leukocytes using 10 mL of whole blood.

MATERIALS:

- N-N solution (NaCl 0.9%; Nonidet 0.1%)
- TEN buffer (Tris-HCL 10mM; EDTA 2mM, pH 8.0; NaCl 400mM)
- 20% SDS solution
- Saturated NaCl solution
- Chloroform
- Isopropanol
- 70% ethanol
- TE buffer (10mM Tris-HCl; 1mM EDTA; pH 8.0)
- Vacuette EDTA K3 tube (evacuated blood collection system, Greiner bio-one)
- 15mL tubes
- 50mL tubes
- Sterile Pasteur pipettes
- Centrifuge
- Vortex mixer
- Oven

PROCEDURE:

Whole blood is collected in disodium-EDTA containers and stored at -20ºC. To facilitate haemolysis of Red Blood Cells it is recommended to store a fresh sample for a few hours in a freezer, as freezing destroys the red cells.

After thawing, 10 ml of whole blood are transferred to a sterile conical centrifuge tube (50 ml volume) to which 40 ml of N-N solution must be added.

The solution is left for 10 min at room temperature with occasional mixing by inversion followed by centrifugation for 30 min at 3000 x g (4°C).

After centrifugation, the supernatant is discarded and a white pellet is observed at the

bottom of the tube. N-N solution wash and centrifugation steps are repeated twice.
It is important to breakdown the pellet and rinse it well in N-N solution in order to clean the white blood cells.
The red supernatant is removed by aspiration and 4 ml of TEN buffer are added to the pellet which must be broken up by vigorous vortexing.
After adding 300 µl of 20 % SDS, the tubes are incubated at 80°C for 3 hours under mixing.
After the incubation, 1 ml of saturated NaCl solution is added to the samples.
Then, the tubes are mixed vigorously (by vortex) and the emulsion is centrifuged for 10 min at 3000 x g at room temperature.
The supernatant is transferred into a clean and sterile conical centrifuge tube (15 ml), using a sterile Pasteur pipette, and an equal volume of chloroform is added to the sample.
The mix is swirled and centrifuged for 10 min at 3000 x g at room temperature.
After centrifugation, the upper aqueous phase (containing DNA) is transferred into a clean and sterile conical centrifuge tube (15 ml), followed by the addition of an equal volume of isopropanol.
DNA is precipitated by gentle swirling of the tube and is observed visually as a white thread like strand.
The sample is centrifuged for 15 min at 3000 x g at room temperature.
After centrifugation, the supernatant is discarded and 1-2 ml of 70% ethanol is added to the pellet. The solution is centrifuged for 10 min at 3000 x g at room temperature.
After centrifugation, the supernatant is discarded and the previous step is repeated.
After discarding the supernatant, the pellet is dried from excess ethanol by leaving the tubes open and inverted at room temperature for an hour.
The dried pellet is resuspended in 300-500 µl TE buffer and left overnight on a rotator.

DNA quantification

DNA concentration was determined using NanoDrop ND-1000 UV-Vis spectrophotometer (CELBIO).
Absorbance readings of 1 µl of each sample at 260 nm and 280 nm provided the DNA and protein concentration, respectively. The ratio of sample absorbance at 260 and 280 nm was used to assess the purity of DNA, checking the presence of protein, phenol or other contaminants that absorb strongly at or near 280 nm. In addition, the

spectrophotometric analysis provided the absorbance ratio at 260 and 230 nm, as secondary measure of DNA purity. Samples with ratio values (A_{260}/A_{280} and A_{260}/A_{230}) between 1.8 and 2.0 were accepted as “pure” DNA solutions.

The quantified DNA samples were diluted in sterile nuclease-free water to a final concentration of 50 ng/µl and used for subsequent polymerase chain reactions.

DNA amplification by Polymerase Chain Reaction (PCR)

All exons and intron-exons junctions of PKP2, DSP, DSG2, DSC2 ,and JUP genes were amplified by Polymerase Chain Reaction (PCR) assay. The primers were designed by PRIMER 3 software (http://frodo.wi.mit.edu/primer3/), based on the sequence data in GenBank (Table 2.1). Multiple primer pairs were used for large exons.

PCR reactions were carried out in a 25 µl volume containing 50 ng of DNA, 10 pmoles of each primer (10 pmol/µl, MWG), 100 µM deoxinucleotide triphosphate (dNTPs 1mM, Invitrogen), 1X PCR Buffer (Applied Biosystems or Promega), 1.5mM $MgCl_2$ (25 mM, Applied Biosystems or Promega), and 0.8 U of Taq Gold DNA Polymerase (5U/µl, Applied Biosystems) or 0.625 U of GoTaq DNA polymerase (5U/µl, Promega), depending on the amplicon.

DNA amplification was performed in a Peltier PTC-200 thermal cycler (MJ Research) using standard or touch-down protocols. Amplicon sizes, primer sequences, amplification and analysis conditions are reported in Appendix A.

Due to the high GC content in the nucleotide sequence, exon 1 of PKP2 gene was amplified with the GC-RICH PCR System (Roche diagnostic GmbH), according to the manufacturer's protocol.

The presence of amplified DNA fragments was checked by electrophoresis, loading an aliquot of PCR product onto a 2% w/v agarose gel stained by Gel Red (Biotinum).

Each amplicon was visualized under ultraviolet trans-illumination and identified by comparing with a known molecular-weight marker.

Human gene	*cDNA accession number*	*Translation sequence*
PKP2	NM_004572	NP_004563
DSP	NM_004415	NP_004406
DSG2	NM_001943	NP_001934
DSC2	NM_024422	NP_077740
JUP	NM_002230	NP_002221

Table 2.1. Genbank Accession numbers of cDNA and translation sequences for human ARVC genes.

Mutation screening by DHPLC

Background

Denaturing high-performance liquid chromatography (DHPLC) is a high-capacity low-cost mutation scanning technique, based on a ion-pair reversed-phase chromatography. The stationary phase is a hydrophobic matrix containing nonporous alkylated polystyrene-divinylbenzene particles. Double-stranded DNA molecules are retained on the chromatography column mainly via electrostatic interactions mediated by the triethylammonium acetate (TEAA) adsorbed at the interface between the stationary phase and the hydroorganic mobile phase. DNA elution is obtained by a linear increasing gradient of organic solvent (acetonitrile) in the mobile phase; the eluting fragments are detected by UV absorbance at 260 nm.

DHPLC reveals the presence of single nucleotide substitutions, as well as small insertions and deletions, exploiting the differential melting properties of homoduplex and heteroduplex DNA fragments; these species are formed upon mixing, denaturing and re-annealing of PCR amplicons containing a heterozygous mutation. Under partial denaturing thermal conditions, the heteroduplex, characterized by a mismatch in their sequence, undergo more extended denaturation and are eluted earlier than their corresponding homoduplex molecules. As result of this differential retention, elution of a sample containing a sequence variation appears as multiple peaks in the chromatogram (Figure 2.1). Some mutations, however, yield only a single broadened peak, for this reason it is recommended to compare the chromatographic profile of each sample against a wild-type reference.

To identify homozygous mutations, heteroduplex must be generated by mixing mutant and wild type samples in a ratio of 1:1.

Temperature determines the sensitivity and its optimum is predicted, by computation, in the range from 48°C to 68°C, depending on the amplicon sequence and GC-content

For a given fragment, the algorithm provides the melting profile and the optimal analysis temperature, corresponding to 70–80% of helical fraction, for each domain.

Several studies have documented the high sensitivity (>96%) and specificity (>99%) of DHPLC in detecting mutations (Xiao and Oefner, 2001).

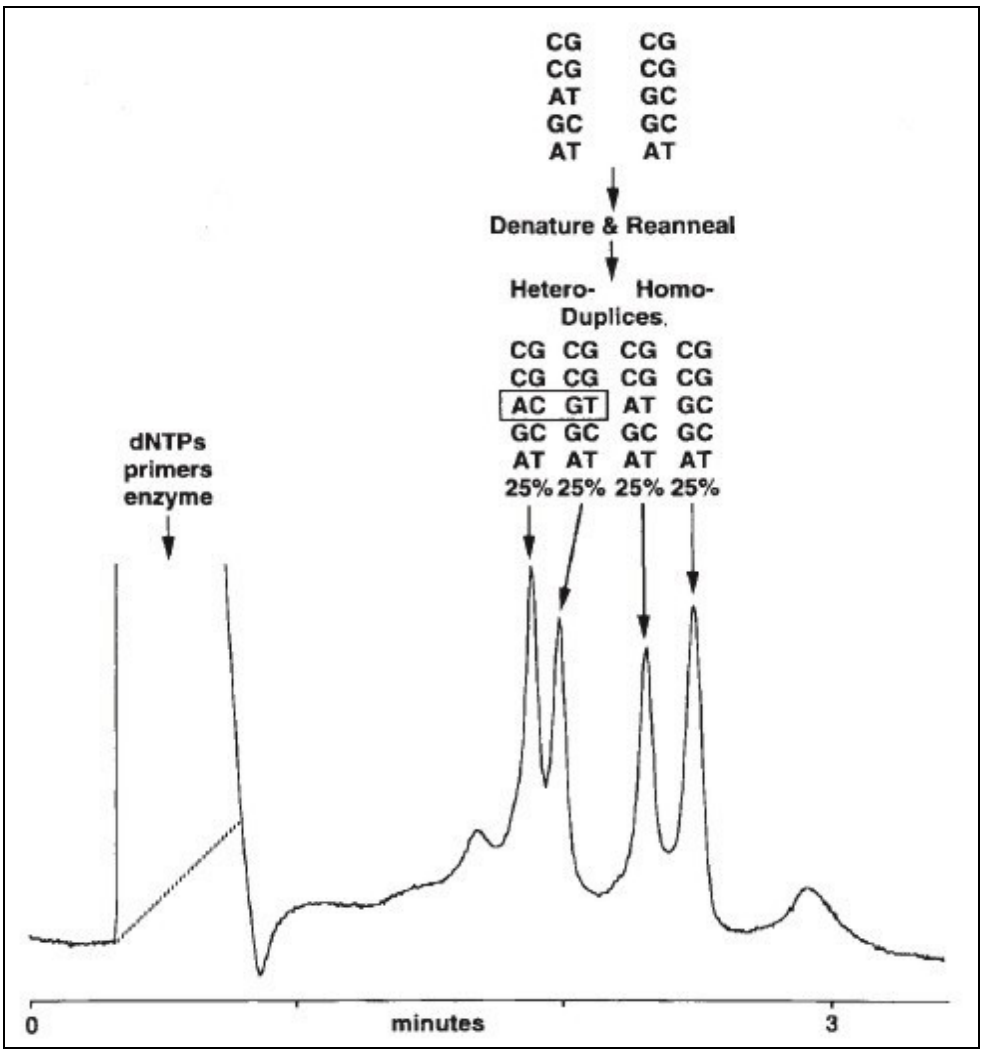

Figure 2.1. Principle of mutation detection by DHPLC. DHPLC compares two or more chromosomal fragments as a mixture of denatured and re-annealed PCR products. In the presence of a sequence variation, a mixed population of homoduplex and heteroduplex DNA molecules is generated. At partially denaturing temperatures, the less stable heteroduplex are retained shorter than the two perfectly matched homoduplex. The degree of destabilization of the four DNA species is mainly the result of differences in neighboring stacking interactions and determines their order of elution (from Xiao and Oefner, 2001, with permission).

DHPLC analysis

DHPLC analysis was performed using a WAVE DNA Fragment Analysis System 35000 HT with a DNASep HT cartridge (Transgenomic).

PCR fragments were denaturated for 5 minutes at 95°C and then gradually re-annealed by decreasing the sample temperature to 25°C over 40 minutes, to promote possible formation of heteroduplex. Approximately 50-200 ng of sample (3-10 µl of PCR product)

were injected into the chromatographic column and eluted by a linear acetonitrile gradient, at a flow rate of 0.9 mL/min in the standard analysis mode or 1.5 mL/min in the rapid analysis mode. The gradient was obtained by mixing buffer A (0.1M TEAA; pH 7.0) and buffer B (0.1M TEAA; pH 7.0; 25% acetonitrile) in the mobile phase and increasing buffer B of 2%/min. Temperatures for successful resolution of heteroduplex molecules were predicted by Wave Navigator software (Transgenomic), which uses a implementation of Fixman-Freire's algorithm (Fixman and Freire; 1977) to calculate the probability that each base is in the helical duplex form or in the single-stranded form. Most of the exons required two to three temperatures for mutation analysis due to the different melting domains in the corresponding DNA fragment. Amplicons size and analysis conditions are listed in Appendix B.

Heteroduplexes and homoduplexes were detected by monitoring the absorbance at 260 nm.

Samples showing an aberrant elution profile, compared with a wild-type control, were re-amplified and analysed by sequencing, to establish location and nature of the variant base(s).

DNA sequencing

PCR amplicons were purified with the PCR Product Pre-sequencing Kit (USB, Amersham Pharmacia Biotech), containing two Hydrolytic enzymes, Shrimp Alkaline Phosphatase (SAP) and Exonuclease I (EXO) to remove unincorporated dNTPs and excess primers.

A 5 µl volume of PCR reaction mixture was mixed with 0.5 µl of SAP enzyme (2 U/µl) and 0.5 µl of EXO I enzyme (10 U/µl) under the following conditions: incubation at 37°C for 15 minutes and inactivation of enzymes at 80°C for 15 minutes.

The purified PCR products were sequenced at the BMR-Genomics (Padua, Italy), by ABI Prism 3730XL DNA sequencer (Applied Biosystems), with the BIG DYE dideoxy-terminator chemistry (Applied Biosystems).

Sequencing reaction was performed using 3 ng of DNA every 100 bp of fragment lenght and 10 pmol of primer.

Electropherograms were analysed with Chromas v1.5 (Technelsium) and Lasergene (SeqMan II, DNASTAR) softwares to edit, assemble, and translate sequences.

The sequencing results were compared with the reference sequence in GenBank for

each gene. When a putative mutation was identified, amplicons from an independent PCR reaction were resequenced to confirm the base variation. The presence of the new variants, not included in the database dbSNPs, was examined in 250 unrelated healthy subjects, to exclude DNA polymorphisms.

Genome-wide scan

Clinical ascertainment and collection of families

A genome wide scan by linkage study and Copy Number Variations (CNVs) analysis was performed on three independent families with recurrence of ARVC, showing no causative mutations in any of the desmosomal disease genes.

The index case of each family and all available relatives were investigated at the Department of Cardiology - University of Padua.

The affection status was established according to the recently modified diagnostic Task Force criteria (Marcus *et al*., 2010).

Written informed consent was obtained from all individuals.

A total of 79 subjects were available for the study across the three families. Blood samples were collected from all participants and genomic DNA was extracted using a modification of the salting-out procedure, previously described.

The pedigree of each family is shown in Appendix B.

Linkage analysis

Background

Linkage analysis is commonly used in gene mapping studies to determine if there is significant evidence for co-segregation (linkage) of alleles at a marker locus and alleles at a hypothetical disease locus. The rate at which two alleles are transmitted together to the next generation is related to the probability of a crossing-over event (or recombination) between the loci and hence to their distance along the chromosome (Ott, 1994).

A genome-wide set of a few hundred or a few thousand genetic markers is typed in families with multiple affected members and, in the multipoint analysis, several marker loci are simultaneously tested for linkage with the disease. The pivotal idea in this strategy is to limit the location of the disease gene to a small chromosomal region, exploiting the known position of the linked markers. In the parametric analysis, the parameters of the disease model need to be specified, i.e. the mode of inheritance, the penetrance, and the population frequency of the disease allele.

The LOD (logarithm of odds) score method is the most widely used approach to

parametric linkage analysis (Morton, 1955); it provides a statistical evaluation of the co-segregation of markers and disease allele. The LOD score calculation compares the likelihood of the data if the markers are linked to the disease locus, at a particular recombination rate θ (<0.5), to the likelihood of the data if the loci are unlinked (θ=0.5). The $\log_{10}$ of this likelihood ratio is the LOD score (Z). A LOD score of 3.0 is the threshold of statistical significance for accepting linkage, corresponding to an odds ratio of 1000:1; conversely, linkage hypothesis can be rejected if Z < –2.0. Values of Z between –2 and +3 are inconclusive. When the linkage for different families is investigated, using the same markers and the same genetic model, the overall probability of linkage is the product of the probabilities in each individual family, therefore LOD scores can be added together.

Genotyping

Individual genotyping was carried out using the High−density SNP marker set Infinium HumanCNV370-Duo BeadChip (Illumina, San Diego, CA, USA), which includes 370,404 SNP markers with average spacing of 7.9 Kb.

Selection of exon-centric SNPs and putative functional markers (non-synonymous, splice sites, synonymous, etc.), with high heterozygosity and uniform genome-wide distribution, maximizes the information content, improving the likelihood of detecting a recombination event. The BeadChip content and features are listed in Table 2.2.

The Illumina technology uses single tube whole-genome amplification followed by hybridization capture to 50-mer probe arrays and SNP genotyping by single-base extension reaction (SBE) (Figure 2.2). Genotypes were automatically called using Illumina BeadStudio software.

For each family member, 200 ng of genomic DNA (gDNA) was analysed with the SNP arrays from the Burlo-CBM SNP Genotyping Service of Trieste (http://www.cbm.fvg.it/) on Illumina Iscan System (Illumina, San Diego, CA, USA), according to the manufacturer's protocol.

Number of Markers	370,404	
Genomic coverage (Mean/Median/r^2>0.8)	**Caucasian (CEU)**	0.87/1.0/0.81
	Han Chinese/Japanese (CHB+JBT)	0.82/0.95/0.68
	Youruba (YRI)	0.59/0.58/0.34
Minor Allele Frequency (*) (Mean/Median)	**CEU**	0.25/0.25
	CHB+JBT	0.23/0.23
	YRI	0.22/0.22
Spacing (Kb) (Mean/Median)	7.9/5.0	
Marker categories	**Markers within 10kb of a known RefSeq Gene**	164,485
	Non-Synonymous SNPs (**)	7,181
	MHC(†)/ADME(∓)/Indel SNPs	5058/2022/0
	Sex Chromosome Content (X/Y/PAR loci)	12,556/ 1,412/361
CNV coverage	**Number of DGV(§) Regions Represented**	3.034
	Number of Markers in DGV Regions	79,631
	Average Markers per Region	26.2
	Targets Novel CNV Regions (~9K)	Yes

Table 2.2: HumanCNV370-Duo BeadChip features (www.illumina.com).

(*) Based on HapMap release 22 data
(**) Based on Ref Seq and Ensemble databases
(†) MHC region as defined by de Bakker and colleagues
(∓) Markers within 10kb of a known ADME related gene
(§) Toronto Database of Genomic Variants (http://projects.tcag.ca/variation) containing 3,644 CNV regions as of March 2007

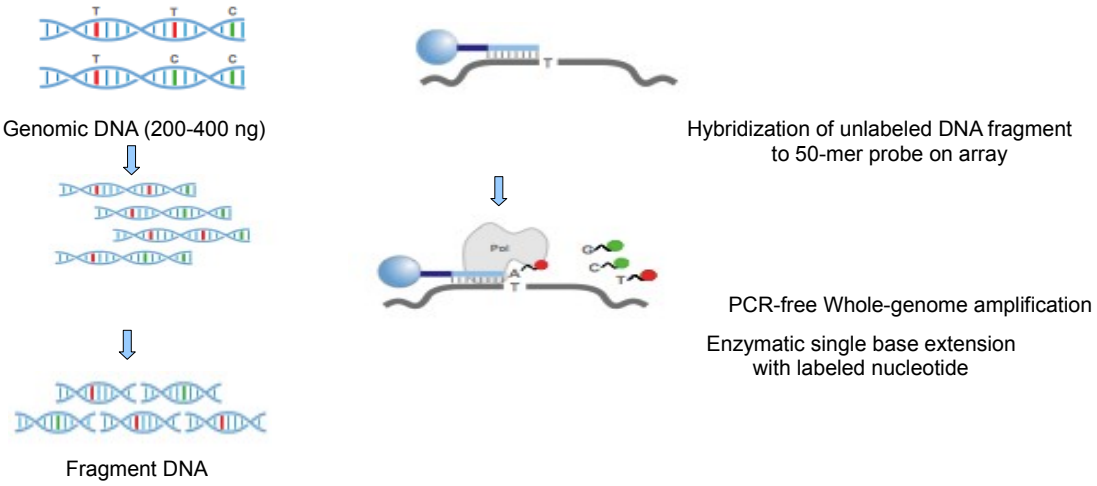

Figure 2.2. Illumina whole-genome genotyping on DNA arrays (www.illumina.com). **Step 1.** The Illumina protocol begins with a whole-genome amplification reaction to amplify the input gDNA by over 1000-2000X. This genome representation is fragmented to approximately 300 to 600 bp, precipitated, resuspended, and hybridized onto a BeadChip. **Step 2.** After capture of the target loci, the SNPs are scored using a single-base extension (SBE) reaction. SBE employs a single probe sequence 50 bp long (attached to the bead) designed to hybridize immediately adjacent to the SNP query site. The arrayed SNP locus-specific primers are extended with a single hapten-labeled dideoxynucleotide. Allelic discrimination is achieved using two color differentially labeled terminators. Finally, the haptens are detected in a multilayer immunohistochemical sandwich assay and genotype calls are generated by Illumina's software (Gunderson et al; 2006).

Data manipulation and quality checking

The genotyping results were provided as a text file (*.txt) for each subject, containing the analysed SNPs, sorted by name, the called genotype for each marker, and the signal intensity values (Figure 2.3). The raw data were processed by Plink software v1.07 (Purcell *et al*., 2007) to obtain a single file (*.snp) including all genotyping data of each family, with markers sorted according to their physical map position (Figure 2.4). Genetic distances between markers were determined using the deCODE genetic map (Kong *et al.*, 2002) and base pair positions, as well as the marker's order, were obtained from the human reference sequence assembly (february 2009, hg19 release) (http://genome.ucsc.edu).

The SNP dataset was selected, by Plink, using several quality criteria.

All allele calls were checked for Mendelian inconsistencies and markers with genotype errors were removed. The reliability of the called genotypes was evaluated based on the call rate (defined as the percentage of successful genotype calls among subjects), removing SNPs with call rates <95%.

To avoid potential bias caused by rare alleles, only SNPs with Minimum Allele Frequency >1% were considered for the analysis. Tests for Hardy-Weinberg equilibrium (HWE) deviations were performed by Plink using an exact test (Wigginton *et al*., 2005) and markers showing an average P value <0.001 were excluded.

Finally, SNPs in the same physical position or mapped on multiple loci were not included in the analysis.

SNP Name	Sample ID	Allele 1	Allele 2	Log R Ratio	B Allele Freq
rs10203812	5401	A	G	-0.2491	0.5225
rs1020382	5401	A	A	0.0696	0.0028
rs10203851	5401	A	C	-0.1465	0.5123
rs1020388	5401	A	C	-0.2342	0.5611
rs10203916	5401	A	A	0.197	0.0005
rs10203925	5401	A	A	-0.235	0
rs10203992	5401	A	A	-0.1774	0
rs10204012	5401	C	C	0.1091	1
rs1020407	5401	C	C	0.1443	1
rs10204079	5401	G	G	-0.1489	1
rs10204095	5401	A	A	-0.1398	0
rs10204096	5401	A	G	0.0066	0.4495
rs1020410	5401	A	G	0.0322	0.4988
rs10204137	5401	A	A	-0.0567	0.0038

Figure 2.3. Example of *.txt file reporting raw genotyping results of a single sample. From the left column: marker name; sample ID; allele calls; total fluorescent intensity signals from both alleles (Log R Ratio); relative ratio of the fluorescent signals between two alleles at each SNP (B Allele Frequency).

SNP_ID	5422	5401	5421	5412	7209	5418	7208	7955	5406	5404
rs35672141	AA	AA	BB	AA	AB	AA	BB	AA	AA	AA
rs7531583	AA	AB	BB	AB	AB	AB	BB	AB	AB	AA
rs742359	BB	AB	BB	AB	BB	AB	BB	AB	AB	BB
rs3737626	BB	BB	BB	BB	BB	BB	BB	BB	BB	BB
rs6681938	BB	BB	BB	BB	AB	BB	BB	BB	BB	BB
rs4648592	BB	AB	BB	AB	BB	AB	BB	AB	AB	BB
rs7525092	BB	AB	BB	AB	BB	AB	BB	AB	AB	BB
rs2474460	AA	AA	BB	AA	AB	AA	BB	AA	AA	AA
rs3820011	BB	AB	AB	AB	BB	AB	BB	AB	AB	BB

Figure 2.4. Example of *.snp file obtained from raw data, using Plink software. The first column lists all analysed SNPs, sorted according to their physical map position specified in the map file *.map. Genotyping data, recoded into binary form (as A/B), are arranged in the columns, one for each family members, according to the pedigree information specified in the file *.pro.

Linkage analysis statistical methods

The genome-wide linkage study was performed using a multipoint approach that extracts inheritance information at every point of the genome, based on genotypes at any number of markers simultaneously considered. Through the graphical user interface EasyLinkage Plus (Lindner and Hoffmann, 2005), a parametric analysis was conducted by GeneHunter software version 2.1 (Kruglyak *et al*., 1996) which implements the Lander-Green algorithm (Lander *et al*., 1987) to infer information about the inheritance pattern in a pedigree. An autosomal dominant model with 0.0001 disease allele frequency and 0.02 phenocopy rate was specified. Equal allele frequencies for the markers tested were assumed.

Taking into account the incomplete penetrance of the disease, a conservative "affected-only" approach was assumed coding as "unknown" the phenotype of all unaffected family members, in order to avoid decrease of LOD score values due to low penetrance. To get a good resolution of the whole genome and to reduce the number of false positive linkage peaks, the analysis was performed varying marker density across four levels: 1 marker every 1, 0.7, 0.5, or 0.3 cM. For all regions showing positive LOD score values, the haplotypes of markers were reconstructed using Viterbi algorithm implemented in GeneHunter software and displayed by HaploPainter program (Thiele *et al*., 2005). After haplotype analysis, upper and lower borders of each critical interval were refined by GeneHunter, based on recombination events observed in affected individuals.

Homozygosity Haplotype analysis

The Homozygosity Haplotype analysis was performed in Family #2 to confirm the linkage results.

Homozygosity Haplotype (HH) is a non-parametric approach allowing a genome-wide search for shared autosomal segments derived from a common ancestor, using high density SNP genotype data (Miyazawa *et al.*, 2007).

The HH method uses a haplotype described by only homozygous SNPs and obtained removing all heterozygous markers from the sample dataset.

Within families or genetically isolated populations, patients who inherited the same mutation from a common ancestor share a chromosomal segment around the disease gene. This shared genomic region is identical by descent (IBD) and can be identified, by

the HH analysis, as a Region with a Conserved Homozygosity Haplotype (RCHH), the genetic length of which is longer than a cutoff value.
An RCHH is defined by a set of concordant homozygous SNP in two or more subjects, that are identified through comparison of homozygosity haplotypes among multiple patients (Figure 2.5).

The HH program was run with the genotypes of all affected family members, setting a cutoff value of 3.0 cM to search RCHHs, as recommended by the authors to minimize the rates of false positives and false negatives.

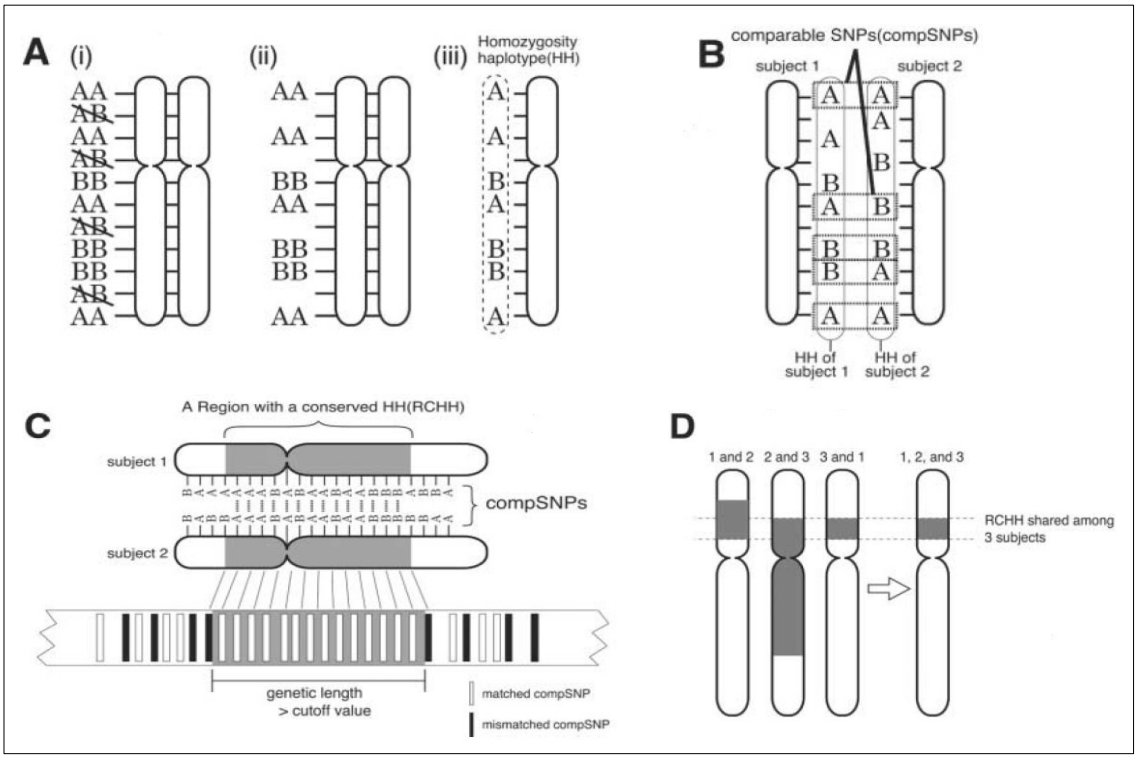

Figure 2.5. Principle of HH analysis. **A.** An Homozygosity Haplotype (HH) is a uniquely phased haplotype described by only homozygous SNPs. “A” and “B” indicate the major and the minor allele for each marker, respectively. **B.** SNPs that are homozygous in two or more subjects are defined “comparable SNPs”, with concordant (matched comparable SNPs) or discordant (mismatched comparable SNPs) genotypes. **C.** A Region with a Conserved Homozygosity Haplotype (RCHH) is a run of type-matched comparable SNPs with genetic length longer than a cutoff value. D. The overlapped RCHH shared among multiple patients predicts the presence of a Region from a Common Ancestor (RCA). (From Miyazawa *et al*., 2007, with permission).

Copy Number Variations (CNVs) Analysis

The occurrence of structural variations in each family was evaluated using PennCNV software (Wang *et al.,* 2007). Through a Hidden Markov Model, this algorithm infers the most likely copy number state from the signal intensity data at each SNP, represented as normalized total fluorescent intensity values from both alleles (Log R Ratio) and normalized relative ratio of fluorescent signals between two allels (B Allele Frequency).

The gcmodel file was included in the analysis to correct for “genomic waves”, which consist of variations in signal intensities due to highly GC-rich regions and affecting the accuracy of CNVs calling (Diskin *et al.*, 2008).

Quality control analysis was performed by PennCNV software, considering the following criteria: standard deviation for autosomal Log R Ratio >0.28, median B Allele Frequency >0.55 or <0.45, B Allele frequency drift >0.002, and waviness factor >0.05. Moreover, to reduce the number of false positives, CNV calls were required to include at least 5 probes and to span genomic regions >10 Kb in size.

Quantitative real-time PCR (qPCR)

In order to confirm the presence of the PKP2 gene deletion in 8 members of Family #1, as predicted by PennCNV software, quantitative real-time PCR was performed using primers specific for exon 2, exon 7 and exon 13 of PKP2 gene.

To normalize the target gene copy number, Beta-actin (ACTB) and TATA-binding protein (TBP) genes were used as internal references.

All primers were designed through Primer3 software (http://frodo.wi.mit.edu/primer3/) (Table 6; Appendix A).

Genomic DNA from eight subjects carrying the PKP2 gene deletion, three family members with a normal gene copy number (based on PennCNV calls), and a matched control sample was amplified by real-time PCR on an ABI PRISM 7900HT Fast Sequence Detection System (Applied Biosystems).

qPCR reactions were carried out in triplicate for each sample, in a final volume of 10 µl, containing 10 ng of genomic DNA, 2X SYBR Green PCR Master Mix (DyNAmo™ HS SYBR® Green qPCR Kit, Finnzymes), and the appropriate concentrations of each primer. Amplification conditions consisted of initial denaturation step at 95°C for 10 minutes, followed by 40 cycles at 95°C for 15 seconds and at 62°C for 1 minute. The ΔΔCt quantification method was used to determine the relative gene copy number in each sample. Validation experiments were performed using the standard curve method

with five serial dilutions of genomic DNA from control subjects. PCR efficiencies (E) for all exons were calculated according to: $E = [10^{(-1/slope)} - 1] \times 100$, where E = 100 corresponds to 100% efficiency. Efficiencies were identical and the relative gene copy number was calculated by $2^{-\Delta\Delta Ct}$, as previously described (Livak and Schmittgen, 2001).

Selection of candidate genes on chromosome 19p13.3

The UCSC Human Genome Browser database (hg19, february 2009 release) (http://genome.ucsc.edu) was used to determine annotated known genes, ORFs, and predicted/hypothetical genes located in the 19p13.3 critical region, identified by linkage analysis in Family #2.

Evaluation of positional candidate genes was performed according to their expression in myocardium and function, taking into account the current knowledge about the disease. Information was collected using several human genome resources including the following online databases:

- UCSC Human Genome Browser
- NCBI (http://www.ncbi.nlm.gov)
- Ensembl (http://www.ensembl.org)
- GeneCards (http://www.genecards.org)
- OMIM (http://www.ncbi.nlm.nih.gov/OMIM)
- PubMed (http://www.ncbi.nlm.nih.gov/pubmed).

Reverse Transcription Polymerase Chain Reaction (RT-PCR)

The cardiac expression of Protein Tyrosine Phosphatase Receptor-type Sigma (PTPRS) gene, identified as good candidate for mutation screening in Family #2, was verified by Reverse Transcription Polymerase Chain Reaction (RT-PCR) using RNA from human heart (Stratagene).

As an initial step, 1 µg of mRNA was activated adding 1 µg of random hexamer primers (500 µg/µl, Promega) and RNase-free water to a final volume of 5µl and incubating the mix 5 minutes at 70°C and 5 minutes at 4°C.

The activated RNA was reverse-transcribed using 10 nmoles of dNTPs (10 mM, Invitrogen), 1X ImProm-II Reaction Buffer (Promega), 60 mmoles of $MgCl_2$ (25 mM, Promega), 40 U of rRNAsin RNase Inhibitor (40 U/µl, Promega), 1 µl of ImProm-II Reverse Transcriptase (Promega), and nuclease-free water to a final volume of 25 µl.

The RT reaction was performed under the following conditions: annealing at 25°C for 5 minutes, extension at 42°C for one hour, enzyme inactivation at 70°C for 15 minutes, and reaction stop at 4°C for 10 minutes.

The resulting cDNA was used as template for PCR to amplify the fragment corresponding to exons 20-21 with specific primers (Table 2.3).

The primers were designed by PRIMER 3 software (http://frodo.wi.mit.edu/primer3/), based on the sequence data of the longest isoform of PTPRS gene (NM_002850).

PCR reaction was carried out in a reaction volume of 25 µl containing 1 µl of cDNA, 10 pmoles of each primer (10 pmol/µl, MWG), 100 µM of deoxinucleotide triphosphate (dNTPs 1mM, Invitrogen), 1X PCR Buffer II (Applied Biosystems), 1.5 mM $MgCl_2$ (25 mM, Applied Biosystems), and 0.8 U of DNA Taq Gold polymerase (5 U/µl, Applied Biosystems).

The following standard amplification protocol was used: enzyme activation at 95°C for 12 minutes, 37 cycles of denaturation at 95°C for 30 seconds, annealing at 62°C for 30 seconds and extension at 72°C for 45 seconds, followed by final extension step at 72°C for 10 minutes and reaction stop at 4°C for 5 minutes.

PCR reactions were performed in a Peltier PTC-200 thermocycler (MJ Research).

The presence of amplified product was checked by electrophoresis on 2% w/v agarose gel stained by Gel Red (Biotinum) and exposed to ultraviolet light.

Primer Forward 5'-3'	Primer Reverse 5'-3'	Amplicon size (bp)
AAGAAGCTCATCACGCACCT	AGTGGCACCATCACAATGAA	236

Table 2.3: Sequence of primers used to amplify exons 20-21 of PTPRS gene from cDNA and amplicon size.

Mutation screening of Protein Tyrosine Phosphatase Receptor-type Sigma (PTPRS) gene

A search for pathogenic sequence changes in all coding exons, intron-exon boundaries, and untranslated regions of PTPRS gene was undertaken by PCR amplification from genomic DNA of the proband of Family #2 and subsequent direct sequencing.

PRIMER 3 software (http://frodo.wi.mit.edu/primer3/) was used to design all primers pairs, based on the sequence data of the longest isoform of PTPRS gene

(NM_002850).

PCR reactions were performed in a final volume of 25 µl containing 50 ng of genomic DNA, 10 pmoles of each primer (10 pmol/µl, Invitrogen), 100 µM deoxinucleotide triphosphate (dNTPs 1mM, Invitrogen), 1X PCR Buffer (Applied Biosystems or Promega), 1.5mM $MgCl_2$ (25 mM, Applied Biosystems or Promega), and 0.8 U of Taq Gold DNA Polymerase (5U/µl, Applied Biosystems) or 0.625 U of GoTaq DNA polymerase (Promega), depending on the amplicon.

DNA amplification was carried out in a Peltier PTC-200 thermal cycler (MJ Research) using standard or touch-down protocols. All primer sequences and cycling conditions are reported in Table 7; Appendix A.

An aliquot of each PCR product was subjected to electrophoresis on 2% w/v agarose gel, stained by Gel Red (Biotinum). Amplicons were identified by comparing with a known molecular-weight marker, under UV light.

After amplification, DNA fragments were purified and sequenced as described above.

Sequencing results were analyzed by Chromas v1.5 (Technelsium) and Lasergene (SeqMan II, DNASTAR) softwares. Whenever a sequence variant was detected, a search on dbSNP database (www.ncbi.nlm.nih.gov/projects/SNP/*)* was performed to exclude DNA polymorphisms.

Exome sequencing

The whole-exome sequencing was performed in two affected subjects of Family #2 (IV-9 and IV-12) and Family #3 (II-4 and II-7), at the Beijing Genomics Institute (BGI) (http://en.genomics.cn/).

Exome capture

Enrichment of coding exons and flanking intronic regions was carried out using SureSelect Human All Exon 50 Mb Kit (Agilent).

The array content covers 98.9% of 21,326 protein-coding genes from the Consensus Coding Sequence Region (CCDS, March 2009 release) (http://www.ncbi.nlm.nih.gov/projects/CCDS/), Refgen (April 2009 release) (http://genome.ucsc.edu/) and Ensembl Gene databases (release 54) (www.ensembl.org/), and 94.2% of 719 microRNA genes from the human microRNA database (v13.0) (http://www.mirbase.org/), providing a total capture size of approximately 50 Mb (Xu *et al*., 2011).

For each sample, individual library preparations, hybridizations, and captures were performed, following the manufacturer's protocols.

To construct the sequencing library, genomic DNA (3 µg) was randomly sheared by Covaris instrument and paired-end sequencing adapters were ligated to both ends of 150-200 bp DNA fragments. The adapter-flanked templates were purified by the Agencourt AMPure SPRI beads (Beckman Coulter Genomics) and fragments with insert size about 250 bp were amplified by ligation-mediated PCR (LM-PCR) (Mueller and Wold, 1989). To enrich the exonic DNA in each prepped library, purified LM-PCR products were hybridized to the capture array consisting of single-stranded biolinylated RNA oligonucleotides. Hybridized fragments were bound to streptavidin coated magnetic beads and, after washing and RNA digestion, captured products were amplified by PCR.

The basic experimental process of exome capture is illustrated in Figure 2.6.

The final sequencing libraries were validated by Bioanalyzer analysis (Agilent) and quantitative PCR to assess magnitude of enrichment and quantity of each library.

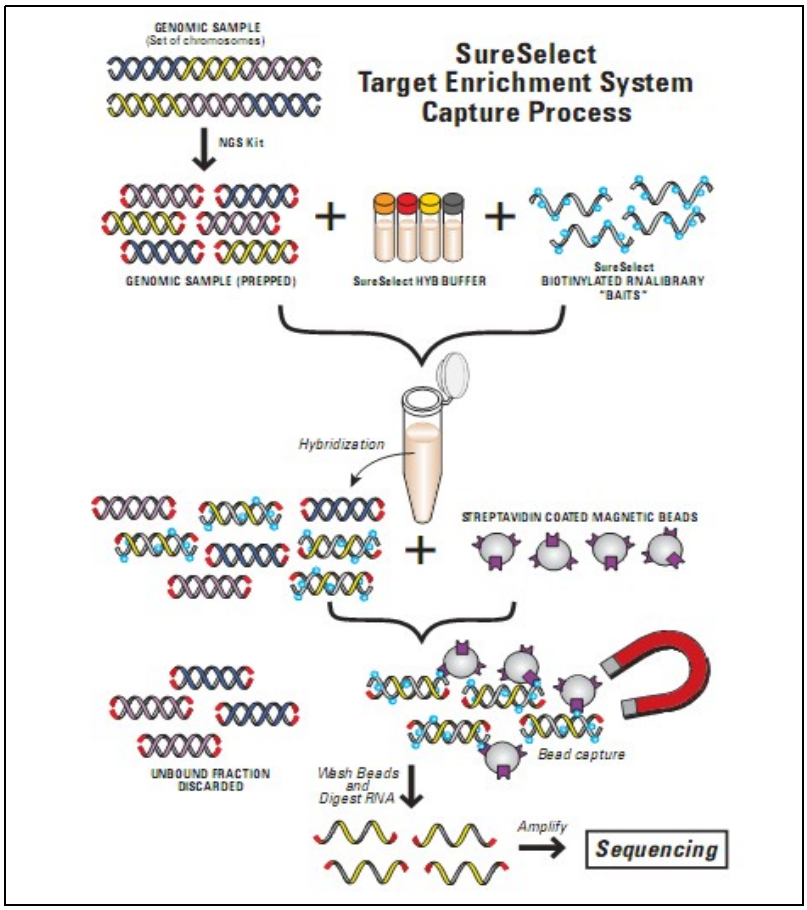

Figure 2.6: Agilent Sure Select system exome capture (www.agilent.com).

Sequencing

Sequencing of enriched libraries was done on HiSeq2000 platform (Illumina) to a depth providing a mean coverage of 50X on targeted regions. Sequences were generated as 90 bp reads from each end of DNA templates (paired-end), following the manufacturer's instructions.

The Illumina technology relies on solid-phase bridge PCR (Adessi *et al*., 2000; Fedurco et al., 2006) to amplify each DNA template from the captured sequencing library (Figure 2.7) The resulting DNA fragments are sequenced using the reversible terminator chemistry (Bentley *et al*., 2008; Turcatti *et al*., 2008) (Figure 2.8).

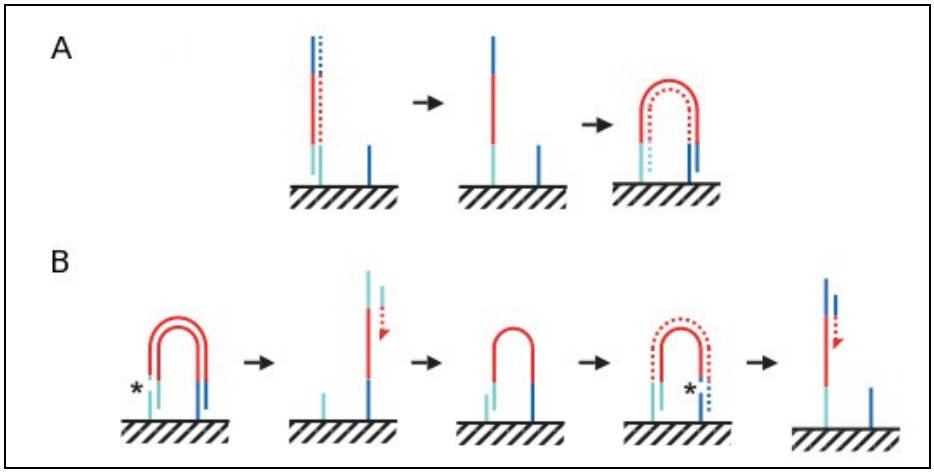

Figure 2.7: Bridge PCR. **A.** The flow cell surface (hatched) is coated with two different populations of oligonucleotides 5'-attached by a flexible linker and complementary to the adapters (in light and dark blue) of the library DNA fragments (in red). Single-stranded library molecules are annealed to the immobilized oligonucleotides and a new strand (dotted) is synthesized from the original template which is then removed by denaturation. The copied strand bends over and the adapter sequence at the 3' end hybridizes to another complementary oligonucleotide, forming a bridge and allowing the synthesis of a second covalently bound strand (dotted). The bridge PCR generates clusters of about 1000 clonal amplicons tethered to a single physical location on a flow cell.

B. After cluster generation, one strand is selectively cleaved within the adaptor sequence (gap marked by an asterisk) and the complementary strand is sequenced by annealing the first sequencing primer. To perform paired-end sequencing, the synthesized reads are removed by denaturation and a few bridge amplification cycle is repeated to generate the reverse strand (dotted). The amplicons are linearized by cleavage of the original strand (gap marked by an asterisk) to provide the template for the second sequencing read. (Adapted from Bentley *et al.*, 2008).

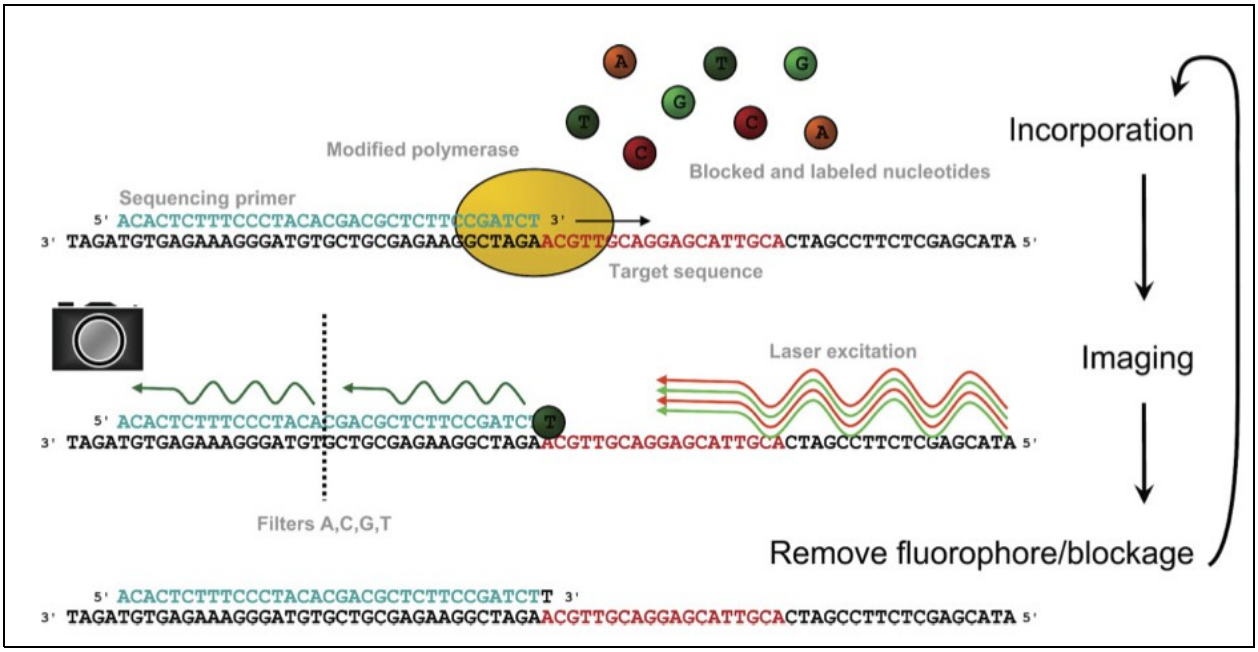

Figure 2.8. DNA sequencing by reversible terminator chemistry. DNA templates are sequenced by repeated cycles of single base extension using a modified DNA polymerase and a mixture of four modified deoxynucleotides, each labelled with a different removable fluorophore and bearing a reversible blocker at the 3' hydroxyl position. The incorporation of the first nucleotide is followed by imaging in four channels through different filters. The subsequent cleavage of both the fluorescent label and the blocker allows the addition of the next base. (From Kircher and Kelso, 2010).

Bioinformatic analysis

Raw image files were processed for base-calling by Illumina Sequencing Analysis Pipeline (version 1.7) with default parameters. Sequence reads were mapped to the UCSC reference human genome (hg 19, NCBI build 37.1) (http://genome.ucsc.edu) by SOAPaligner/SOAP2 software (v2.21) (Li *et al*., 2009) with maximum 3 mismatches and setting the following parameters: -a -b -D -o -u -p -2 -m -x -s 40 -l 35 -v 3 (http://soap.genomics.org.cn/). Depth and coverage for each exon were then calculated using the CCDS database (April 2011 release).

SOAPsnp software (Ruiqiang *et al.*, 2009) was used to call consensus genotypes, defined as diploid genotypes for genomic positions subjected to SNP calling and including capture target regions as well as 200 bp flanking regions.

The parameters were set as follows: -i -d -o -r 0.0005 -e 0.001 -u -L 150 -T -s -2 (http://soap.genomics.org.cn/).

Genotypes that differ from reference were extracted as candidate SNPs.

For insertion and deletion (indel) detection, reads were aligned to the reference genome by BWA software (Li and Durbin, 2009) and the Genome Analysis ToolKit (GATK) (DePristo *et al*., 2011) was used to identify the breakpoints.

The low quality variations were filtered out using the following criteria: Phred-like quality score ≥20 (Li *et al*., 2008), sequencing depth between 4 and 10000000, estimated copy number of a nearby region ≤2, and distance between two SNPs ≥5 bp.

The remaining high-confidence variants were annotated for novelty, based on non-overlap with data from dbSNP131 (www.ncbi.nlm.nih.gov/projects/SNP/), 1000 genomes project (pilot 1, 2, 3) (www.1000genomes.org), eight HapMap exomes (Ng *et al*., 2009), YanHuang project (yh.genomics.org.cn/download.jsp) and two databases belonging to BGI, and for potential functional effect predicted by SIFT (sift.jcvi.org/*).* The aminoacid substitution was predicted damaging if the score is ≤0.05 and tolerated if the score is >0.05.

Mutation validation

Sanger sequencing of PCR amplicons from genomic DNA was performed to confirm the variants in genes mapped on the critical regions identified by linkage analysis and to verify co-segregation with the ARVC phenotype within each family.

All PCR primers were designed by PRIMER 3 software (http://frodo.wi.mit.edu/primer3/), based on the sequence data in GenBank.

PCR reactions were carried out in a 25 µl volume containing 50 ng of DNA, 10 pmoles of each primer (10 pmol/µl, Invitrogen), 100 µM deoxinucleotide triphosphate (dNTPs 1mM, Invitrogen), 1X PCR Buffer (Applied Biosystems), 1.5mM $MgCl_2$ (25 mM, Applied Biosystems), and 0.8 U of Taq Gold DNA Polymerase (5U/µl, Applied Biosystems).

DNA amplification was performed in a Peltier PTC-200 thermal cycler (MJ Research) using a standard or touch-down protocol.

An aliquot of PCR product was subjected to electrophoresis on 2% w/v agarose gel stained by Gel Red (Biotinum). Each amplicon was visualized under UV light and identified by comparing with a known molecular-weight marker.

After amplification, DNA fragments were purified and sequenced as described and sequencing results were analysed by Chromas v1.5 (Technelsium) and Lasergene (SeqMan II, DNASTAR) softwares. All variants were confirmed by at least two independent sequences using different primers.

3. RESULTS

3.1. Mutation screening in desmosomal ARVC genes

All coding exons and 50 to 150 bp flanking intronic sequences of *PKP2*, *DSP*, *DSG2*, *DSC2* and *JUP* genes were screened for mutations by Denaturing Hight Pressure Liquid Chromatography (DHPLC) and direct sequencing, in 80 unrelated Italian index cases fulfilling the diagnostic Task Force criteria (Marcus *et al.*, 2010). For about 50% of them, family history reported the occurence of additional cases of ARVC.

A control group of 250 unrelated, ethnically-matched, healthy subjects (500 alleles) was used to estimate the allele frequency of detected variants. DNA variations found in more than 1% of control chromosomes were considered as polymorphisms.

Single point mutations were identified in 26 index cases (32.5%). Moreover, 10 index cases (12.5%) resulted to carry two mutations in the same gene or in different genes. No mutation were detected in the remaining 44 probands (55%), suggesting involvement of additional and still unknown disease-genes.

A total of 46 variants were identified in this study and the same variation occurred in different patients in six cases. The genes most frequently involved were *PKP2*, *DSP* and *DSG2,* accounting respectively for 34.8%, 30.4%, and 26.1% of the total mutations, whereas *DSC2* and *JUP* variants account for 4.3%.

Among the 40 different mutations, 25 (62.5%) altered single amino acids (missense mutations), 10 (25%) were small insertions or deletions causing frame-shift, and 5 (12.5%) coded for a premature stop codon (nonsense mutations) (Table 3).

Whenever possible, genetic analysis was extended to available family members in order to evaluate the segregation of each mutation identified in the index case.

Type of mutation	***PKP2* mutations**	***DSP* mutations**	***DSP* mutations**	***DSC2* mutation**	***JUP* mutations**	**Total**
Missense	6	9	7	1	2	**25**
Frameshift	5	2	2	1	0	**10**
Nonsense	2	2	1	0	0	**5**
Total	**13**	**13**	**10**	**2**	**2**	**40**

Table 3: Type and number of different mutations detected in desmosomal genes in 80 Italian ARVC index cases.

Single mutation in *PKP2* gene

Eight different heterozygous point mutations (4 frame-shift, 2 missense and 2 nonsense) were identified in 12 out of 80 investigated index cases (15%). In three cases, the same variant occurred in more than one subject (Table 3.1). In addition, several polymorphisms described in dbSNP database were found (not showed).

Exon	Nucleotide substitution	Amino acid change	Type of variation	Protein domain	Index case code	Reference
1	c.145_148delCAGA	p.T50SfsX61	Deletion, frame-shift	N-terminal	2, 14, 54	Gerull *et al.*, 2004; Syrris *et al*., 2006; Dalal *et al.*, 2006; Wu *et al*., 2009; den Haan *et al*., 2009; Tan *et al*., 2010; Quarta *et al*., 2011
3	**c.964_965delGGInsC**	**p.G322PfsX30**	**Del/Ins, frame-shift**	**N-terminal**	**19**	**novel**
3	c.397C>T	p.Q133X	Nonsense	N-terminal	34	Van Tintelen *et al*., 2006; Bhuyan *et a*l., 2009; Cox *et al.*, 2011
3	c.631C>T	p.Q211X	Nonsense	N-terminal	51, 13	Qiu *et al*., 2009; Xu *et al*., 2010
5	c.1211_1212InsT	p.V406SfsX4	Insertion, frame-shift	Arm-2	44	Van Tintelen *et al*., 2006; Bhuyan *et a*l., 2009; Xu *et a*l., 2010; De Bortoli *et al*., 2010; Cox *et al.*, 2011
9	**c.1841T>C**	**p.L614P**	**Missense**	**Arm-5**	**58**	**novel**
10	c.2013delC	p.K672RfsX12	Deletion, frame-shift	Arm-5	76, 43	Dalal *et al.*, 2006
12	c.2333T>C	p.I778T	Missense	Arm-7	5	Xu *et al*., 2010; Bauce *et al.*, 2011

Table 3.1: *PKP2* mutations identified in a cohort of 80 ARVC probands. Mutation screening was performed in the longest isoform of PKP2 (PKP2b). Numbering of the *PKP2* nucleotides starts at ATG and refers to Genbank Accession number NM_001005242; translation sequence was compared to reference NP_004563.

Three patients resulted to carry a four base-pair deletion in *PKP2* exon 1 (c.145_148delCAGA), which causes a frame-shift leading to addition of a premature termination codon within the N-terminal head domain (p.T50SfsX61). This mutation was

previously described by several independent groups. Genetic analysis extended to available family members of proband #2 identified this variant in five individuals, of which only one was affected, three resulted asymptomatic, and one showed minor signs not fulfilling the diagnostic criteria. Moreover, two affected subjects did not carry p.T50SfsX61 variation, suggesting the presence of al least another causative mutation within this family (Figure 3.1).

A novel mutation resulting in a predicted truncated protein at the N-terminal domain was detected in one index case and was absent from the control population; a deletion of two nucleotides along with a single base pair insertion (c.964_965delGGInsC) in *PKP2* exon 3 causes a frame-shift and addition of 30 amino acid residues before a premature stop codon (p.G322PfsX31). The other two frame-shift mutations (p.V406SfsX4 and p.K672RfsX12), due to a single base pair insertion and deletion, respectively (c.1211_1212InsT and c.2013delC), were previously reported in the literature and affect conserved *Arm* repeat domains of PKP2.

The missense variations p.I778T and p.L614P are located in distinct *Arm* domains of PKP2 and only the p.I778T is reported in literature.

p.L614P is a novel variant, not found in the control group, causing a non conservative amino acidic substitution and involving a highly conserved residue among different species, belonging to the LxNLS motif, which is characteristic of *Arm* repeats and could represent a binding site for yet unidentified PKP2 ligands, as observed in the case of β-catenin (Choi and Weis 2005).

Finally, two known nonsense mutations (Q133X and Q211X), both affecting the N-terminal head, cause insertion of a premature termination codon with consequent loss of all *Arm* domains.

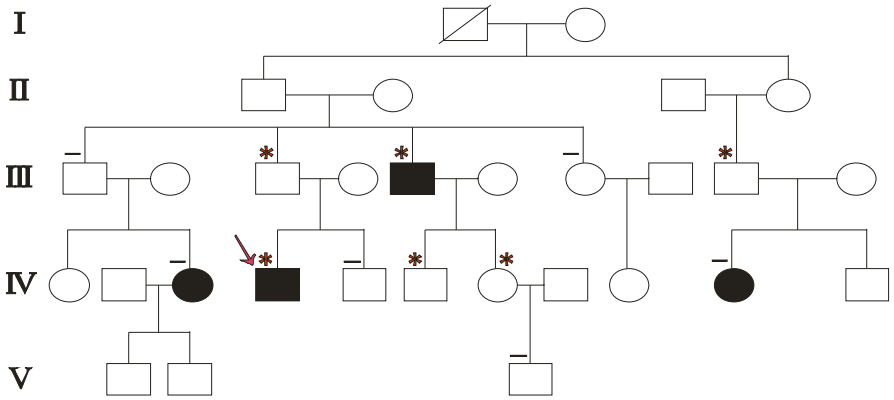

Figure 3.1: Pedigree of the family of patient #2. Proband is indicated by an arrow. Black, white and grey symbols represent clinically affected and unaffected individuals, and subjects of unknown disease status, respectively. The asterisk denotes the presence of mutation; the trait denotes the absence of mutation.

Single point mutations in *DSP* gene

Six out of 80 investigated probands (7,5%) resulted to carry a single heterozygous mutation in *DSP* gene. Variations identified in this cohort of index cases include one frameshift, two nonsense, and four missense variants, previously described in the literature (Table 3.2).

Several polymorphisms reported in dbSNP database were also detected (not showed).

Exon	Nucleotide substitution	Amino acid change	Type of variation	Protein domain	Index case code	Reference
1	c.88G>A	p.V30M	Missense	SR3	57	Yang *et al.*, 2006; Xu *et al*., 2010; Bauce *et al*., 2010; Bauce *et al.*, 2011; Kapplinger *et al.*, 2011
11	c.1408A>G	p.K470E	Missense	SH3	40	Basso *et al*., 2006; Bauce *et al*., 2011; Al-jasser *et al*., 2011
13	c.1696G>A	p.A566T	Missense	SR6	12	Basso *et al.*, 2006; Cox *et al.,* 2011
20	c.2821C>T	p.R941X	Nonsense	CT linker domain	4	Quarta *et al*., 2011
23	c.3203_3204delAG	p.E1068VfsX19	Deletion, frame-shift	Rod	79	Bauce *et al.*, 2011
23	c.3337C>T	p.R1113X	Nonsense	Rod	51	Sen-Chowdhry *et al*., 2008; Asimaki *et al*., 2009; Quarta *et al.*, 2011; Cox *et al.,* 2011; Bauce *et al.,* 2011

Table 3.2: *DSP* mutations identified in a cohort of 80 ARVC probands. Mutation screening was performed in DSP-I, which is the isoform expressed in cardiac muscle. Numbering of the *DSP-I* nucleotides starts at ATG and refers to Genbank Accession number NM_004415; translation sequence was compared to reference NP_004406.

The missense variant p.V30M is located within the spectrin repeat SR3 in the N-terminal head of desmoplakin, involved in interaction with armadillo proteins within the desmosomal plaque. Methionine in position 30 of DSP does not show phylogenetic conservation in vertebrates; however, *in vitro* studies demonstrated that this missense substitution impairs normal localization of DSP, probably causing loss of binding to JUP, as indicated by protein-protein interaction analysis (Yang *et al*., 2006).

The missense variant p.K470E involves a residue within the Src homology 3 (SH3) domain; a recent study demonstrated that this substitution compromises the structural integrity of the N-terminal plakin domain causing local conformational alterations, although the global fold was maintained (Al-Jasser *et al*., 2011). The missense mutation p.A566T alters a highly conserved residue among different species, located in the spectrin repeat SR5 of DSP, and results in a non-conservative amino acidic substitution.

A novel nonsense mutation (c.2821C>T, p.R941X), causing the introduction of a stop codon within the CT linker domain, was detected in one proband and resulted absent from the control population. The predicted truncated protein completely lacks the Rod domain, which forms homodimeric coiled-coil structures, and the C-terminal region

interacting with desmin intermediate filaments. The same mutation was recently described also by Quarta and colleagues (Quarta *et al*., 2011).

Genetic analysis of available family members identified the variant p.R941X in three subjects, two of them were clinically affected, while one did not show evidence of disease.

Finally, two mutations (p.E1068VfsX19 and p.R1113X) affect the central Rod domain and both result in a predicted truncated protein lacking most Rod domain and the whole C-terminal region.

Single point mutations in *DSG2* gene

Six heterozygous *DSG2* mutations were identified in 6 (7.5%) out of 80 investigated index cases, including two frame-shift and four missense variants (Table 3.3). Several polymorphisms present in dbSNP database were also found (not showed).

Exon	Nucleotide substitution	Amino acid change	Type of variation	Protein domain	Index case code	Reference
4	c.298G>C	p.G100R	Missense	EC1	8	Pilichou *et al*., 2006; Basso *et al*., 2006; Bauce *et al*., 2011
7	**c.727G>T**	**p.D243Y**	**Missense**	**EC2**	**10**	**novel**
8	c.1003A>G	p.T335A	Missense	EC3	77	den Haan *et al*., 2009; Xu *et al*., 2010; Tan *et al*., 2010; Bauce *et al*., 2010; Christensen *et al*., 2010; Quarta *et al*., 2011; Cox *et al*., 2011
13	c.1912G>A	p.G638R	Missense	IA	39	De Bortoli *et al*., 2010; Bauce *et al*., 2011
14	c.2036delG	p.G678AfsX4	Deletion; frame-shift	IA	40	Pilichou *et al*., 2006
15	c.2983delG	p.G997VfsX20	Deletion; frame-shift	RUD	48	Bauce *et al*., 2011

Table 3.3: *DSG2* mutations identified in a cohort of 80 ARVC probands. Numbering of the *DSG2* nucleotides starts at ATG and refers to Genbank Accession number BC099657; translation sequence was compared to reference NP_001943.

Among the missense mutations, three (p.G100R, p.D243Y, and p.T335A) affect evolutionary conserved residues located in distinct extracellular domains (EC1, EC2, and EC3, respectively), involved in Ca^{2+}-dependent homophilic interactions with other

desmosomal cadherins. Each of these variations causes a non-conservative amino acidic substitution which could potentially destabilize the rod-like structure of cadherin domains impairing the homophilic binding.

Both p.G100R and p.T335A mutations were previously described in literature, while p.D243Y is a novel variant, not found in the control population. Of note, p.T335A mutation predisposes also to idhiopatic dilated cardiomyopathy, as other mutations in desmosomal genes (Garcia-Pavia *et al*., 2011; Elliott *et al*., 2010).

Another novel missense variation (p.G638R), not found in the control population, alters an evolutionary highly conserved residue and causes a non-conservative amino acidic substitution in the intracellular anchor of DSG2.

Finally, two single base pair deletions cause frame-shift and premature termination of translation (p.G678AfsX2 and p.G997VfsX20), resulting in predicted truncated proteins which would lack the whole intracellular regions and the terminal domain (TD), respectively.

Single point mutations in *DSC2* gene

Only one (1,25%) index case out of 80 resulted to carry a known mutation in *DSC2* gene (Table 3.4).

Several polymorphisms described in dbSNP database were also identified (not reported).

Exon	Nucleotide substitution	Amino acid change	Type of variation	Protein domain	Index case code	Reference
3	c.304G>A	p.E102K	Missense	Propeptide	36	Beffagna *et al*., 2007; De Bortoli *et al*., 2011; Quarta *et al*., 2011

Table 3.4: *DSC2* mutation identified in a cohort of 80 ARVC probands. Mutation screening was performed in the longest isoform of DSC2 (DSC2a). Numbering of the *DSC2* nucleotides starts at ATG and refers to Genbank Accession number NM_024422; translation sequence was compared to reference NP_077740.

The missense mutation p.E102K affects a conserved residue located in the propeptide domain of DSC2. Although in mouse and rat dsc2 protein, E102 is replaced by aspartic acid, these two amino acids exhibit very similar physico-chemical properties. *In vitro* functional studies demonstrated that this variation impairs the

normal localisation of DSC2, as the mutant protein was almost exclusively distributed throughout the cytoplasm (Beffagna *et al.*, 2007).

Single point mutations in *JUP* gene

Only one *JUP* mutation was identified in 1 proband out of 80 investigated (1,25%) (Table 3.5). Several polymorphisms present in dbSNP database were detected (not reported).

Exon	Nucleotide substitution	Amino acid change	Type of variation	Protein domain	Index case code	Reference
8	c.1172G>A	p.S391N	Missense	Arm-5	15	**novel**

Table 3.5: *JUP* mutation identified in a cohort of 80 ARVC probands. Mutation screening was performed in the longest isoform. Numbering of the JUP nucleotides starts at ATG and refers to Genbank Accession number NM_002230; translation sequence was compared to reference NP_002221.

The missense variation p.S391N was not previously described in literature and resulted absent from the control population. This mutation occurs in the Arm-5 domain, involved in interaction of JUP with other desmosomal components, and causes a conservative amino acidic change, as both Serine and Asparagine are hydrophilic residues. However, Asparagine shows a different sterical crowding and a greater structural rigidity, due to presence of the aminic group and the double bond of the carbonilic group in its lateral chain, both absent in Serine. Moreover, the involved amino acid is evolutionary highly conserved among different species.

Multiple mutations in desmosomal genes

Ten probands (12,5%) out of 80 carried more than one mutation in the same gene (compound heterozygotes) or different genes (double and triple heterozygotes) (Table 3.6).

COMPOUND HETEROZYGOTES						
Index case code	**Gene**	**Exon**	**Nucleotide substitution**	**Amino acid change**	**Protein domain**	**Reference**
18	*PKP2*	6	c.1468C>T	p.R490W	Portion between Arm-2 and Arm-3	Fressart *et al*., 2010; Gandjbakhch *et al*., 2011
		7	c.1577C>T	p.T526M	Arm-4	den Haan *et al*., 2009; Quarta *et al*., 2011
11	***DSP***	**23**	**c.4973C>T**	**p.S1658F**	**Rod**	**novel**
		24	**c.7039A>G**	**p.I2347V**	**C-terminal**	**novel**
51	*DSG2*	9	c.1254_1257insATGA	p. E419X	EC4	Pilichou *et al.*, 2006, Basso *et al*., 2006; Bauce *et al*., 2011
		15	c.2983delG	p.G997VfsX19	RUD	Bauce *et al*., 2011
DOUBLE AND TRIPLE HETEROZYGOTES						
Index case code	**Gene**	**Exon**	**Nucleotide substitution**	**Amino acid change**	**Protein domain**	**Reference**
21	*PKP2*	1	c.145_148delCAGA	p.T50SfsX61	N-terminal	Gerull *et al*., 2004; Syrris *et al*., 2006; Dalal *et al.*, 2006; Wu *et al*., 2009; den Haan *et al*., 2009; Tan *et al*., 2010; Quarta *et al*., 2011
	DSG2	13	c.1912G>A	p.G638R	IA	De Bortoli *et al*., 2010; Bauce *et al*., 2011
30	*DSG2*	6	c.689A>G	p.E230G	EC2	Bauce *et al*., 2011
	DSP	23	c.5324G>T	p.R1775I	Rod	Bauce *et al*., 2005; Bauce *et al*., 2011
44	***DSP***	**23**	**c.3894_3895insGGTC**	**p. M1299GfsX6**	**Rod**	**novel**
	JUP	**11**	**c.1787C>T**	**p. S596L**	**Arm-11**	**novel**
3	*PKP2*	7	c.1655T>G	p.F552C	Arm-4	De Bortoli *et al.*, 2010
	DSC2	16	c.2687_2688insGA	p.A897KfsX4	ICS	Syrris *et al*., 2006; den Haan *et al*., 2009; De Bortoli *et al.*, 2010; Klauke *et al*., 2010; Gehmlich *et al.*, 2010; Fressart *et al.*, 2010; Elliott *et al.*, 2010; Christensen et al.,

						2010; Quarta *et al.*, 2011; Cox *et al.*, 2011
	DSP	9	c.1124A>T	p. N375I	N-terminal	De Bortoli *et al.*, 2010; Bauce *et al*., 2011
32	DSP	23	c.3203_3204delAG	p. E1068VfsX19	Rod	Bauce *et al.*, 2011
			c.5218G>A	p.E1740K	Rod	Cox *et al.*, 2011
	DSG2	15	c.2773C>T	p. P925S	RUD	Bauce *et al*., 2011
39	DSP	23	c.3764G>A	p.R1255K	Rod	Bauce *et al*., 2005; Xu *et al*., 2010
	PKP2	3	c.631C>T	p.Q211X	Head	Qiu *et al*., 2009; Xu *et al*., 2010
		12	c.2333T>C	p. I778T	Arm-7	Xu *et al*., 2010, Bauce *et al.*, 2011
56	*PKP2*	3	c.627C>G	p. S209R	N-terminal	Xu *et al.*, 2010
		12	c.2447_2448delCC	p.T816RfsX10	Arm-8	Xu *et al*., 2010
	DSG2	5	c.437G>A	p. R146H	EC1	Xu *et al.*, 2010

Table 3.6: Multiple mutations identified in desmosomal ARVC genes in a cohort of 80 probands.

Three cases of compound heterozygosity were observed. The index case #18 resulted to carry two different missense mutations in *PKP2* gene (p.R490W and p.T526M). Both these variations were novel and absent from the Italian control group. Very recently, p.R490W was reported in ARVC patients from French population (Fressart *et al*., 2010) and p.T526M was found in probands from North America (den Haan *et al*., 2009).

The p.R490W mutation alters a residue belonging to a 44-amino acid sequence, between the second and the third Arm domain of plakophilin-2, determining a non-conservative amino acidic substitution, as serine and tryptophan residues show different physico-chemical properties. However, the transition c.1468C>T, causing p.R490W, affects the alternatively spliced exon 6 of *PKP2* gene, included only in the longest isoform PKP2b.

The pathogenic potential of p.R490W, as other variants located in *PKP2* exon 6, is still not well defined.

A recent study demonstrated that PKP2a is the dominant isoform in human heart tissue, while *PKP2* exon 6 is an Alu-derived sequence with very low expression level. Moreover, the authors showed that p.R490W was not associated with aberrant exon 6 splicing or mutant mRNA downregulation in the mutation carrier sample (Gandjbakhch *et al*., 2011).

The p.T526M variation also causes a non-conservative amino acidic substitution in the Arm-4 domain, however the involved residue is not evolutionary highly conserved. Moreover, this variant was reported as a rare polymorphism by den Haan and colleagues due to presence in healthy control subjects (den Haan *et al*., 2009).

The index case #11 was heterozygous for two different *DSP* mutations (p.S1658F and p.I2347V), both not previously described in literature and absent in the control group. The p.S1658F variant causes a non-conservative amino acidic substitution in the central rod domain of DSP, since a hydrophilic serine is replaced by a hydrophobic phenylalanine residue, carrying a bigger sterical crowding due to the aromatic group in the lateral chain. However, the involved amino acid is not highly conserved among different species. Conversely, the p.I2347V is a conservative variation altering an evolutionary highly conserved amino acid in the C-terminal domain of the protein. Genetic analysis extended to available family members identified both mutations in the proband's sister which is clinically affected. These variations were inherited in *trans* and none of single mutation carriers showed evidence of disease.

Finally, the index case #51 resulted to carry two known mutations in *DSG2* gene: a four base-pair insertion in exon 9 (c.1254_1257insATGA) causing addition of a single amino acid before a premature stop codon (p.E419X) and a single base-pair deletion in exon 15 (c.2983delG) leading to frame-shift and premature termination of translation several aminoacids downstream (p.G997VfsX19). Both mutations result in predicted truncated proteins, lacking the whole cytoplasmic region and the terminal domain (TD) of DSP, respectively.

Genetic analysis of proband's parents revealed that p.E419X mutation was inherited from the paternal side, while p.G997VfsX19 was present in the proband's mother.

In addition to compound heterozygotes, several cases of double or triple heterozygotes occurred.

The index case #21 showed di-genic heterozygosity for the known *PKP2* deletion causing p.T50SfsX60 and for a novel missense variant in *DSG2* gene (p.G638R). Both these variations were also observed as single mutations in other patients investigated in the present study.

The proband #30 was double heterozygous for a known *DSP* mutation (p.R1775I) and a novel *DSG2* variant (p.E230G), not found in the control population. Both these missense variations occur in evolutionary highly conserved residues and result in non-conservative amino acidic substitutions.

Two novel variants, absent from the control population, were identified in proband #44 showing a severe form of ARVC: a *DSP* frame-shift mutation (p.M1299GfsX6) due to a four base pairs insertion in exon 23 (c.3894_3895insGGTC), and a non conservative missense *JUP* mutation (p.S596L) affecting Arm-11 domain.

Genetic analysis extended to available family members showed that *DSP* mutation was inherited from the paternal line, while JUP mutation was present in the proband's mother (Figure 3.2). The patient's son carrying only the *DSP* mutation, as well as the twins carrying both variants did not show evidence of disease, although it may be due to their young age.

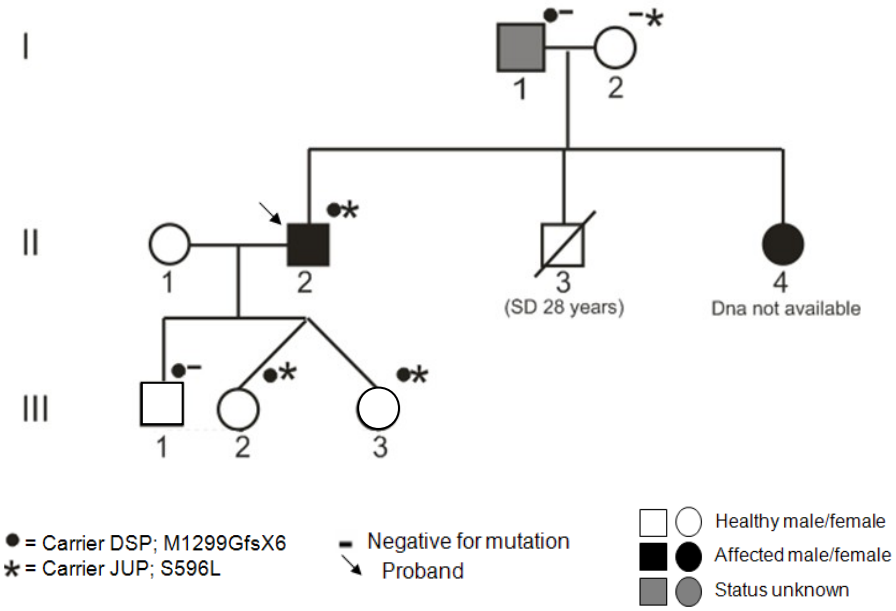

Figure 3.2: Pedigree of family of patient #44.

Four cases of triple heterozygotes were observed in this study.

The proband #3, with a severe form of ARVC, carried a *DSP* missense mutation (p.N375I), a *PKP2* missense mutation (p.F552C) and a *DSC2* frame-shift variant (p.A897KfsX4). Both *PKP2* p.F552C and *DSP* p.N375I were novel mutations, not found in the control population, causing non-conservative amino acidic substitutions and occurring in evolutionary conserved residues, although PKP2 F552 is not conserved in some species.

The *DSC2* variant p.A897KfsX4 is due to a two base-pair insertion in exon 17, resulting in frame-shift and premature termination of translation. It was previously reported by

Syrris and colleagues as pathogenic mutation (Syrris *et* al., 2006). However, this variation was also found in our Italian control group with minor allele frequency of 1.5% (De Bortoli *et al*., 2010) and, then, in several healthy subjects from other populations, with minor allele frequency ranging from 0.8% to 1.69% (Klauke *et al*., 2010; Fressart *et al*., 2010; Elliott *et al*., 2010; Christensen *et al*., 2010), confirming our classification as polymorphism. The last five amino acids of DSC2a, involved in the p.A897KfsX3 variation, show relative variance among different species. Moreover, the alternatively spliced exon 17, encoding for the intracellular cadherin-like sequence (ICS) of DSC2a, is untraslated in DSC2b, which is the major isoform in the human heart. Accordingly, p.A897KfsX3 variation affects only the isoform a of DSC2. *In vitro* functional studies showed that p.A897KfsX4 variation impaired the proper desmosomal localization of DSC2a, as the mutant protein was detected in the cytoplasm (De Bortoli *et al*., 2010). Moreover, an independent study demonstrated weaker binding of the DSC2a A897fsX3 mutant to JUP and DSP, while interaction with PKP2 was virtually unaffected (Gemlike *et al.,* 2010). Nevertheless, the pathogenic role of this *DSC2* variant in determining the disease remains controversial.

The genetic study extended to available family members revealed that only the index case carried all the three variants. Interestingly, the proband's niece (III,1, Figure 3.3), which is clinically affected, did not carry any of these variations, suggesting the presence of additional mutation/s underlying the pathogenic phenotype in this subject in known or not yet identified genes.

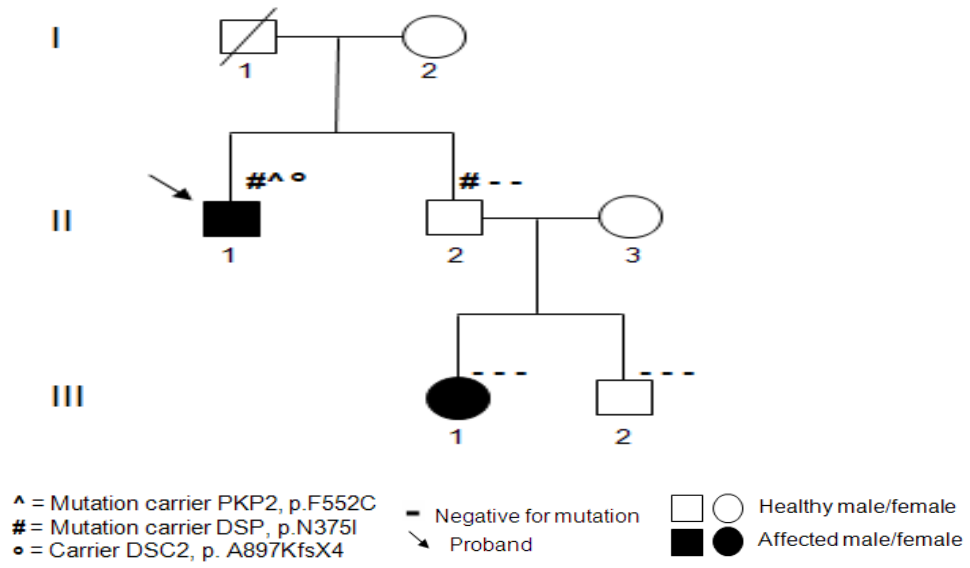

Figure 3.3: Pedigree of family of patient #3.

The proband #32 was heterozygous for three mutations, not previously reported in literature and absent from the control population: a *DSG2* missense variation affecting the RUD domain (p.P925S) and two different *DSP* mutations in the central Rod region (p.E1068VfsX19 and p.E1740K). The p.E1068VfsX19 was also detected as single mutation in another patient. Both novel missense variants alter evolutionary highly conserved residues and cause non-conservative amino acidic substitutions in respective proteins. Very recently, the p.E1740K mutation was also described in two ARVC patients from Netherlands (Cox *et al*., 2011).

Genetic screening of available family members revealed that *DSG2* mutation and *DSP* frameshift mutation were present in the proband's father, while the *DSP* missense mutation was inherited from the maternal side. Among mutation carriers in this family, only the proband's sister which is coumpund heterozygous for *DSP* mutations, showed a severe phenotype.

The index case #39 resulted to carry two *PKP2* mutations (p.Q211X and p.I778T) and a *DSP* missense substitution (p.R1255K). Both *PKP2* variants were also identified as single mutations in two different patients. The p.R1255K *DSP* variation, previously described in literature, causes a conservative amino acidic change, as both arginine and lysine are positively charged residues with similar physico-chemical properties, although arginine could establish higher number of hydrogen bonds than lysine.

Finally, three novel variants, absent from the control population, were identified in the proband #56, showing a severe form of ARVC: two *PKP2* mutations (p.T816RfsX10 and p.S209R) and a *DSG2* variant (p.R146H). The p.T816RfsX10 variation is due to a two-nucleotide deletion (c.2447_2448delCC) in *PKP2* exon 12, leading to frame-shift and addition of a premature stop codon; the predicted truncated protein lacks a portion of Arm-8 domain. The p.S209R mutation causes a non-conservative amino acidic change in the N-terminal domain of PKP2, as a polar serine is replaced by a positively charged arginine, although the involved residue is not highly conserved among different species.

Conversely, the p.R146H *DSG2* variation affects an evolutionary highly conserved amino acid in the extracellular cadherin domain EC1 and could potentially destabilize the rod-like structure of EC domain, impairing the homophilic intercellular binding between desmosomal cadherins. Although p.R146H is a conservative change, as both arginine and histidine are basic residues, histidine brings a wider sterical crowding due to presence of the imidazole ring in its side-chain.

3.2 Genome-wide scan

Genetic screening of all desmosomal ARVC genes in 80 Italian index cases excluded point mutations in 44 probands (55%), three of them belonging to independent families with recurrence of ARVC.

In these families a genome-wide scan was performed in order to map novel loci and, possibly, to identify the involved genes. A total of 79 subjects were genotyped using High−density SNP marker set Infinium HumanCNV370-Duo BeadChip, including 370,404 SNP markers. In each family, a linkage study was performed to identify critical genomic regions segregating with the disease phenotype and then to select candidate genes for mutation screening. Moreover, the presence of large genomic deletions or duplications (>1 Kb), shared by all affected individuals within each family, was evaluated by Copy Number Variations (CNVs) analysis.

In addition, in Family #2 and in Family #3 a combined strategy of linkage analysis and exome sequencing was adopted to identify novel ARVC genes.

Family #1

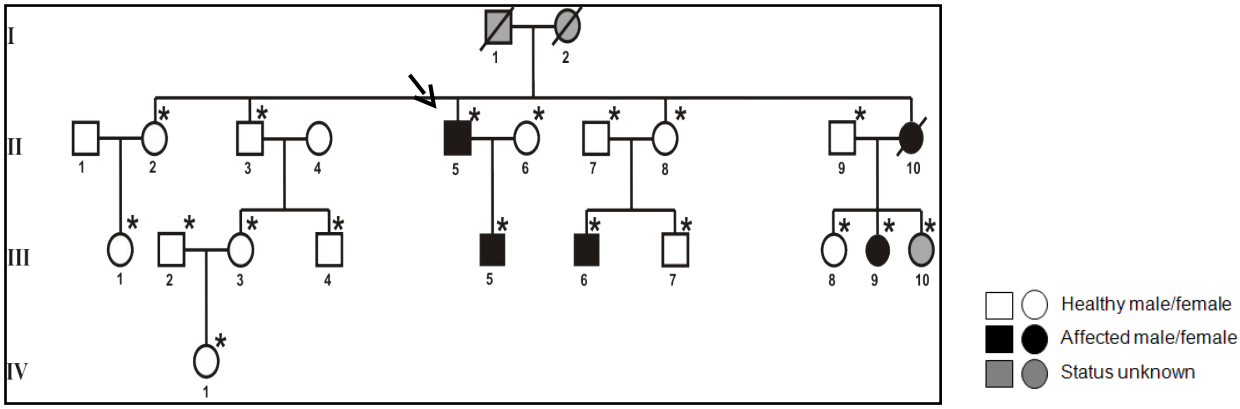

Figure 3.4: Pedigree of Family #1. Asterisks denote genotyped subjects. The proband is indicated by the arrow.

Linkage analysis

In Family #1 (Figure 3.4), multipoint linkage analysis, using an affected-only approach, gave positive parametric (p)LOD scores for 16 chromosomal regions. None of these linkage signals reached the threshold of statistical significance for accepting linkage

(pLOD >+3.0), as the maximum pLOD value was 1.17, observed in 11 genomic regions (Figure 3.5).

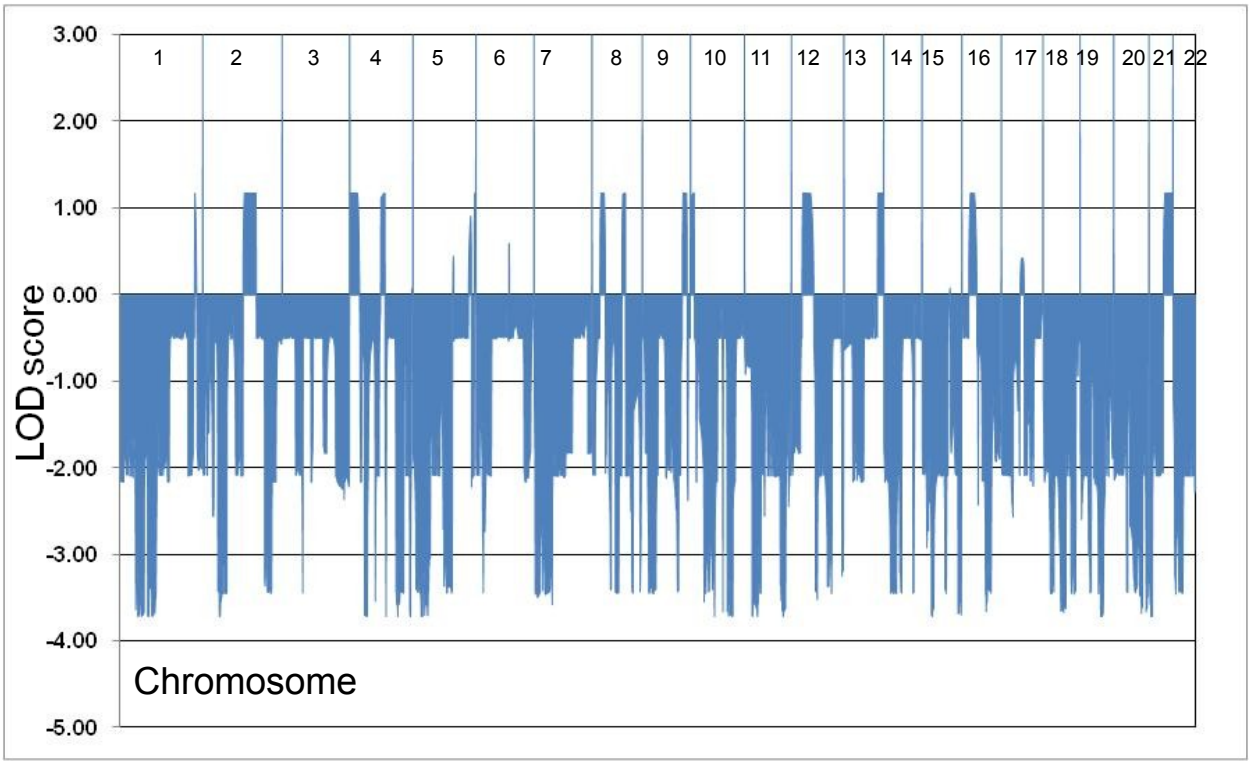

Figure 3.5: Graphical representation of genome-wide multipoint linkage results obtained for Family #1.

Analysis of marker segregation showed a common haplotype, shared by all affected family members, on each of 11 suggestive linkage regions. Taking into account the incomplete penetrance of the disease, only recombination events occurring in affected subjects were considered to define a critical interval on each region. (Table 3.8).
Interestingly, the genomic region on 12p12.3-q13.3 included the *PKP2* ARVC locus (12p11.21) (Figure 3.6).
Since no point mutations in *PKP2* gene were identified in the index case, a genome-wide CNVs analysis was performed to evaluate the presence of large genomic rearrangements (deletions or duplications >1kb in size), shared by all affected family members.

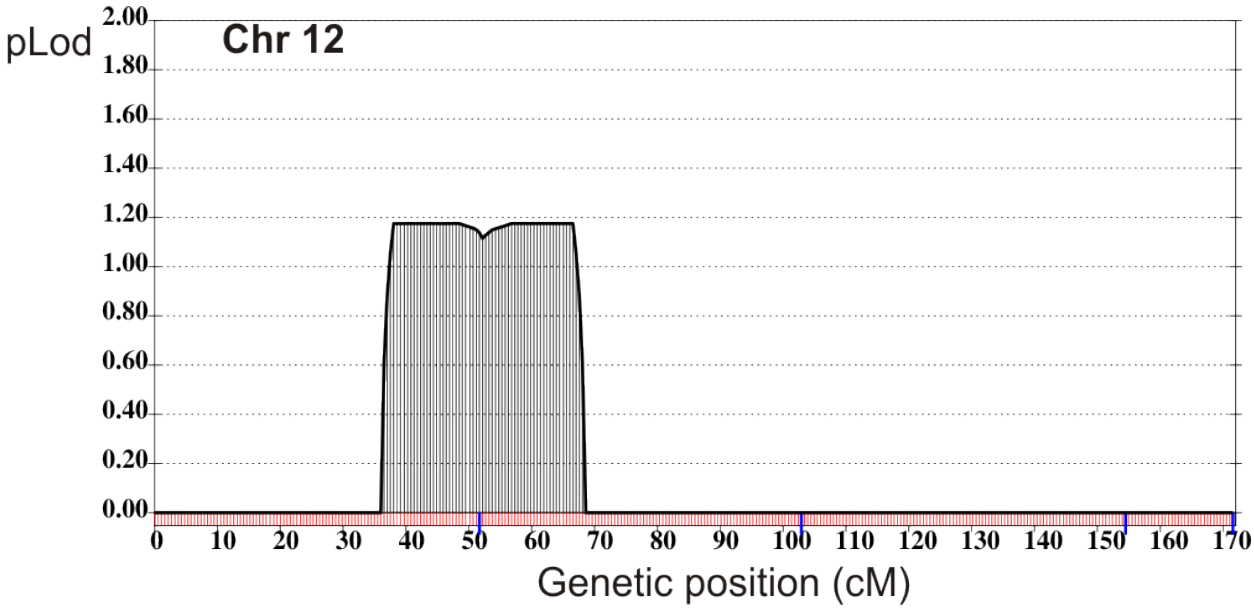

Figure 3.6: Plot of pLOD scores obtained for markers on chromosome 12, in Family #1.

Chromosome	Size	Markers defining critical interval
2q14.3-q31.1	49 Mb	rs2034138; rs7586400
4p16.3-p15.32	16.6 Mb	rs4690284;rs1395291
4q22.2-q25	16.7 Mb	rs6856229; rs243985
8p22-p21.2	9.6 Mb	rs2170116; rs901170
8q22.1-q22.3	8.6 Mb	rs12542917; rs2511724
9q33.3-q34.2	7.6 Mb	rs2417024; rs457420
10p15.3-p15.1	3.9 Mb	rs9419461; rs2765650
12p12.3-q13.3	40.5 Mb	rs1541588; rs3214051
13q33.3-q34	7 Mb	rs1408569; rs4883652
16p13.2-p12.1	16.5 Mb	rs1273394; rs12933889
21q22.13-q22.3	8.6 Mb	rs2836096; rs2839309

Table 3.8: Critical intervals for several genomic regions showing a maximum pLOD scores of 1.17 for associated markers, in Family #1. A common marker haplotype, shared by all affected subjects, was observed for each chromosomal region.

Copy Number Variation (CNVs) analysis

The whole SNP genotype dataset of Family #1 was analyzed by PennCNV software and a total of 511 CNVs were identified.

Among all the detected CNVs, a heterozygous deletion of 122.5 Kb on chromosome 12p11.21 (Table 3.9), was identified in all affected family members, three healthy subjects and one individual with minor signs of disease, not fulfilling the diagnostic Task Force criteria (Figure 3.7). Figure 3.8 shows the results of CNVs analysis on chromosome 12 for a subject carrying the deletion.

This deletion encompassed the entire *PKP2* gene (Figure 3.9) and was not present in any of the available databases: 1000 Genomes Project (http://www.1000genomes.org), Database of Genome Variants (http://projects.tcag.ca/variation), and Decipher (http://decipher.sanger.ac.uk).

No other CNVs common to all affected family members were observed.

This is the first case of copy number variation identified in an ARVC Italian family by using high-density SNPs arrays. Very recently, the same deletion was detected in an ARVC Dutch patient, by Multiplex Ligation-dependent Probe Amplification (Cox *et al*., 2011).

Chromosome	Telomeric position (bp)	Centromeric Position (bp)	Size (Kb)	Number of SNPs included	Boundary SNPs
12p11.21	32942278	33064825	122.548	26	rs6488089; rs7295486

Table 3.9: Hemizygous deletion identified on chromosome 12p11.21 in all affected subjects of Family #1.

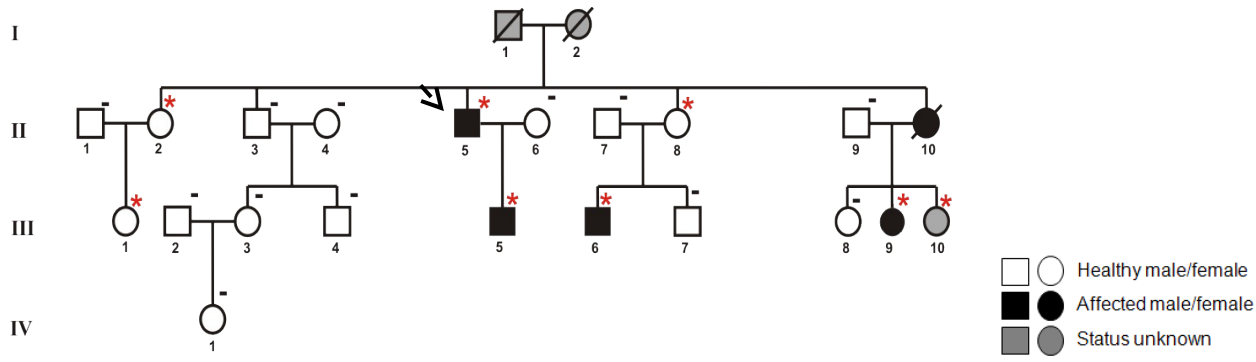

Figure 3.7: Pedigree of Family #1. Asterisks denote subjects carrying the heterozygous *PKP2* deletion. Traits denote a normal gene copy number.

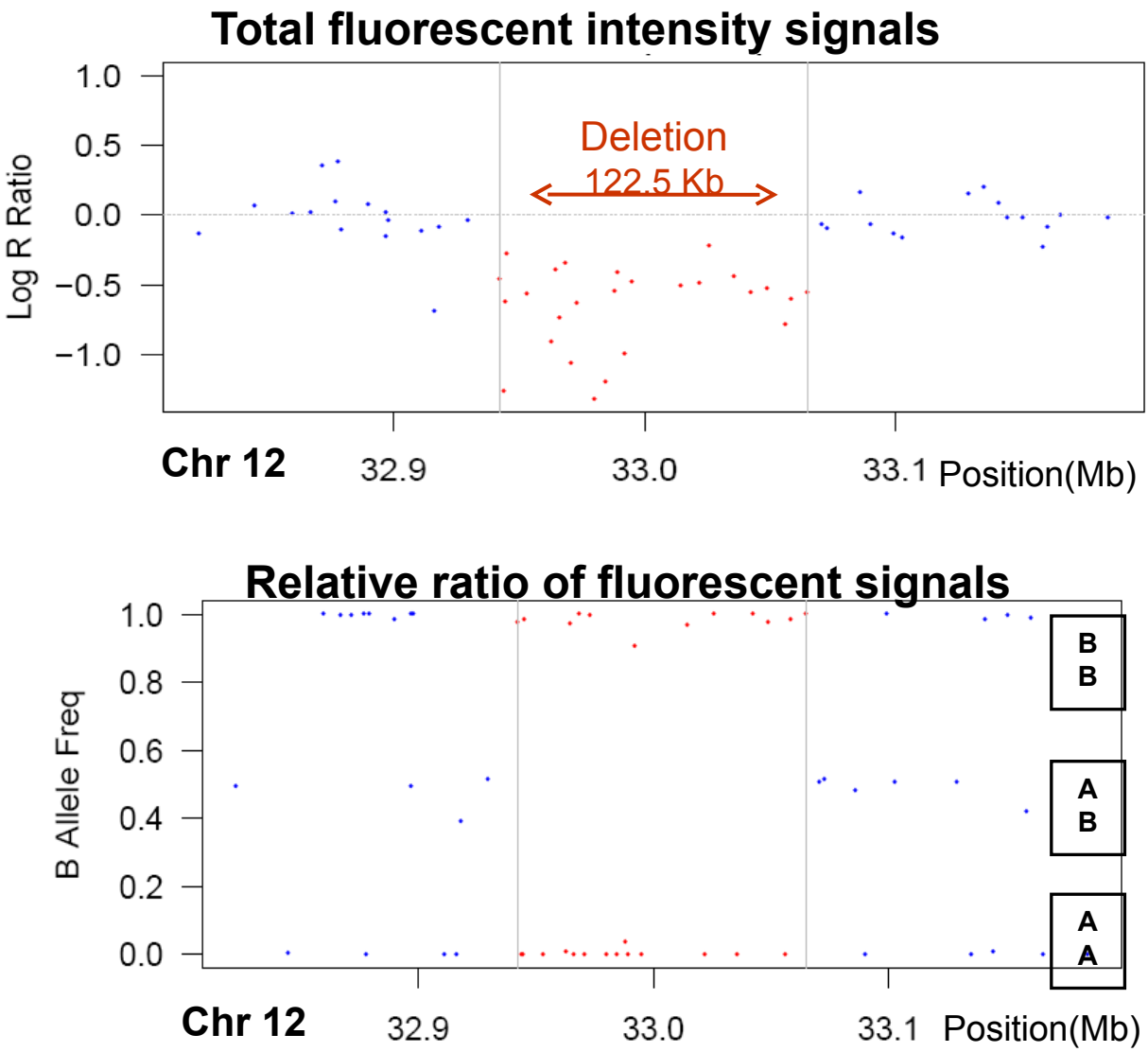

Figure 3.8: Results of CNVs analysis on chromosome 12 for a subject carrying the deletion. Log R ratios (a) and B allele frequencies (b) are plotted against chromosome 12 position. Red dots denote SNPs included in the deleted region, blu dots indicate markers outside the deletion. **a)** Log R ratio (LRR) represents the total fluorescent intensity signals from both alleles at each SNP. A normal chromosome region shows LRR values centered around zero. Hemizygosity appears as a drop in log R ratio (red dots below 0.0). The deletion length is displayed as distance between the two grey vertical lines and included 26 SNPs.

b) B allele frequency (BAF) represents the relative ratio of fluorescent signals between two alleles at each SNP. A normal chromosome region shows three BAF genotype clusters, represented as AA, AB, and BB genotypes in boxes. Within the deleted region, heterozygote SNP calls are missed (lack of dots at 0.5).

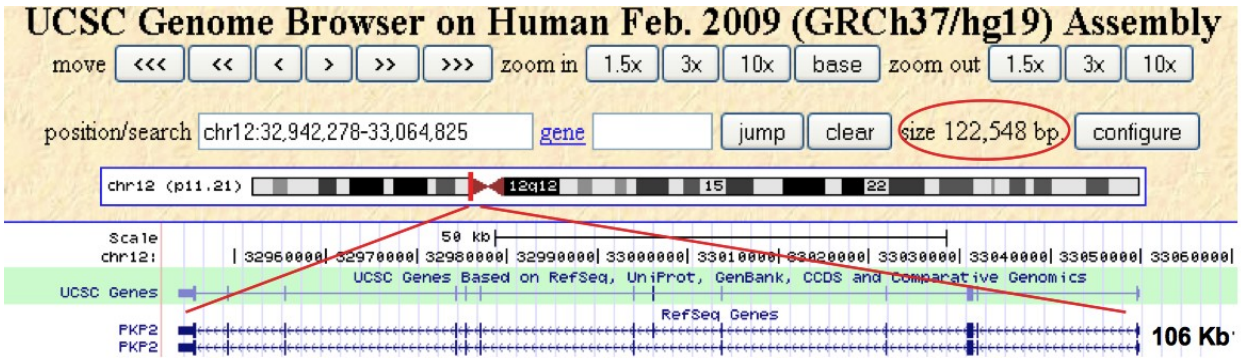

Figure 3.9: Illustration of the deleted region on chromosome 12p11.21. The deletion (red rectangle) encompasses the entire *PKP2* gene. The zoomed region displays the exon-intron organization of *PKP2* gene.

PKP2 gene dosage by quantitative real-time PCR

Gene dosage performed by quantitative real-time PCR with primers specific for *PKP2* exon 2, exon 7, and exon 13 confirmed the deletion in the genomic DNA from all eight subjects, as predicted by PennCNV software.

Real-time PCR results indicated a relative copy number of about 0.5 for each *PKP2* exon in the heterozygous deletion carriers, compared to three family members with a normal copy number (based on PennCNV calls) and 1 external control sample (Figure 3.10).

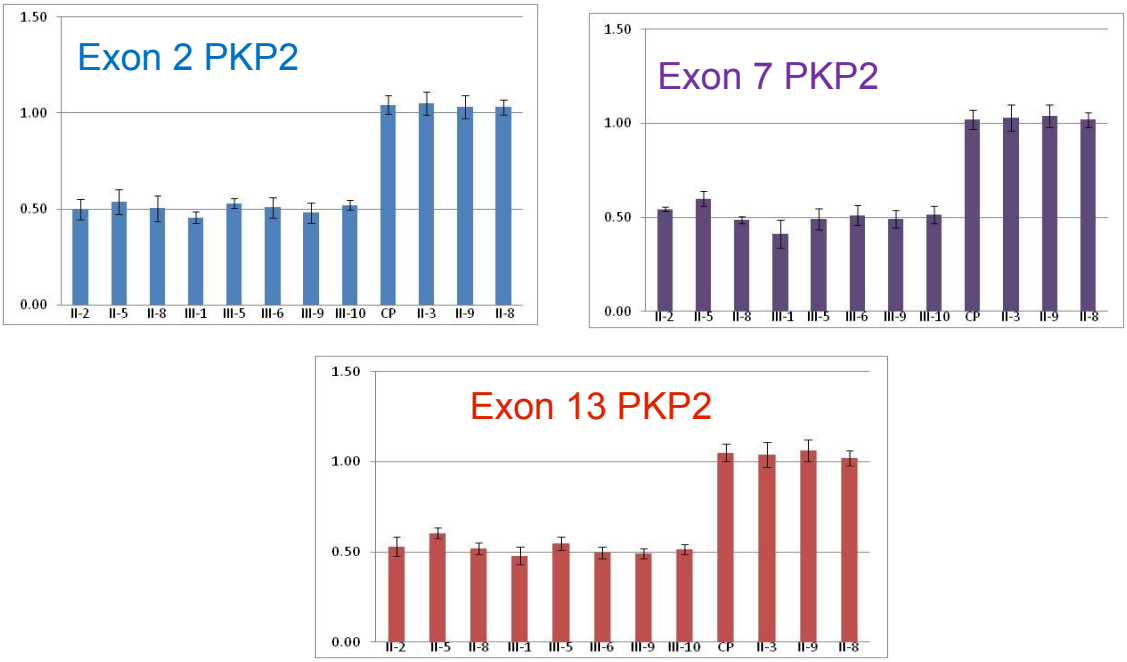

Figure 3.10: *PKP2* gene dosage by quantitative real-time PCR in control individual (CP) and family members. The target gene copy number was normalized to the reference gene TATA-binding protein (TBP). Each experiment was done in triplicate. Error bars represent standard deviation of replicates. Similar results (not showed) were obtained using Beta-actin as internal reference gene.

Family #2

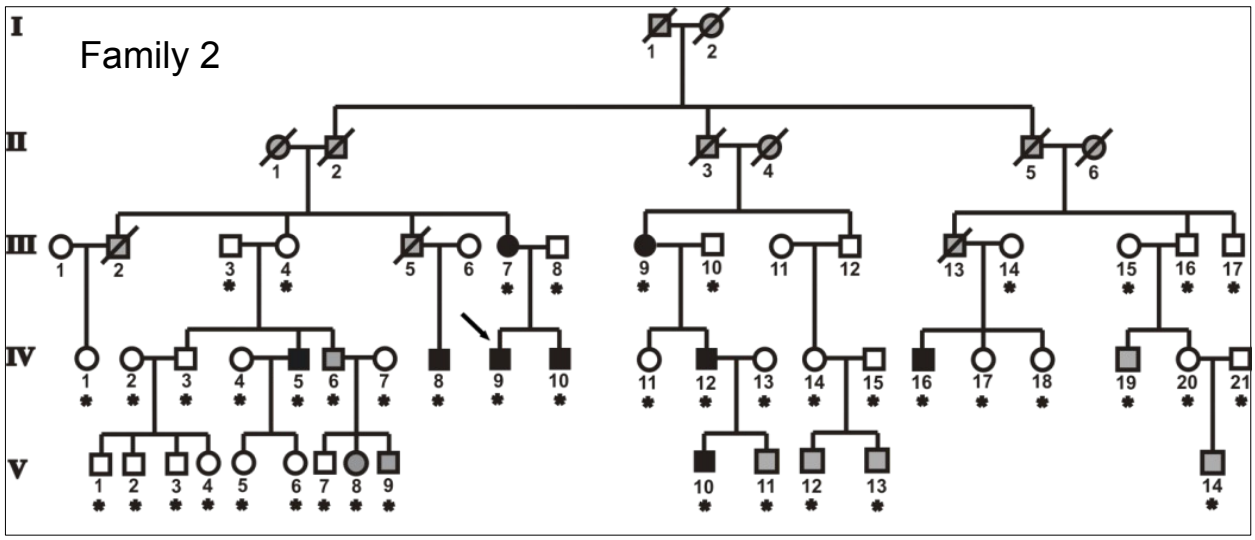

Figure 3.11: Pedigree of Family #2. Asterisks denote genotyped subjects. The proband is indicated by the arrow.

Linkage analysis

In Family #2 (Figure 3.11) multipoint linkage analysis, using an affected-only approach, allowed to exclude linkage of ARVC to markers in 86% of the genome (pLOD <-2) and yielded a single, significant linkage peak on chromosome 19p13.3, with a maximum parametric (p)LOD score of 3.85 at rs171094 (21.78 cM) (Figure 3.12). Figure 3.13 shows graphical plot of pLOD values obtained for markers mapped on chromosome 19p13.3.

This linkage signal was detected in all four analysis with different marker spacing (1cM, 0.7cM, 0.5cM, 0.3cM), indicating that it was not affected by number and set of SNPs selected.

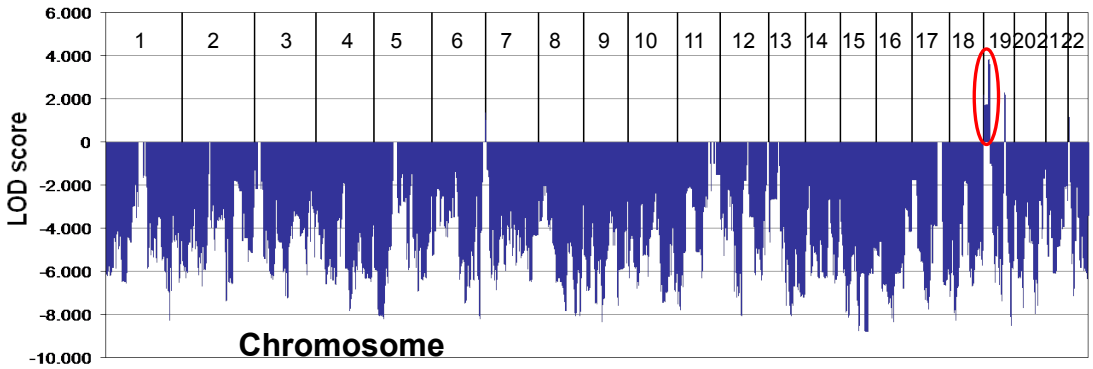

Figure 3.12: Graphical representation of genome-wide multipoint linkage results obtained for Family #2.

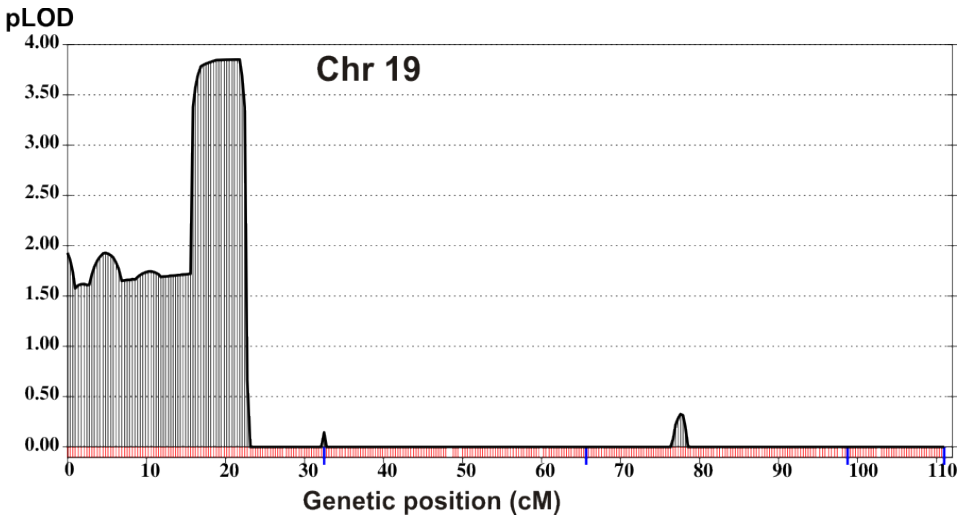

Figure 3.13: Graphical plot of pLOD values obtained for markers mapped on chromosome 19p13.3, in Family #2.

Analysis of haplotype segregation on chromosome 19p13.3 showed a common region shared among all affected subjects (Figure 3.14). Patients IV-16 and IV-12, both affected, presented telomeric (at 16.46 cM) and centromeric (at 22.22 cM) recombination events, respectively, refining the critical interval to a ~2 Mb (6 cM) region, between rs7246083 and rs308195 markers (Table 3.10).

Chromosome	Telomeric position (bp)	Centromeric position (bp)	Size (bp)	Marker defining critical interval
19p13.3	4866451	6836760	1970310	rs7246083; rs308195

Table 3.10: Critical region on chromosome 19p13.3, shared by all affected subjects in Family #2.

This at risk haplotype also occurred in nine additional family members, five of them were asymptomatic, one showed minor signs not fulfilling the diagnostic Task Force criteria, and three were not clinically investigated since deceased. Interestingly, subject III-2 suddenly died at 35 years; unfortunately, the autopsy report was not available to ascertain the cause of death (Figure 3.15).

Since this novel ARVC locus (19p13.3) is the fifteenth reported so far, it should be named ARVC15.

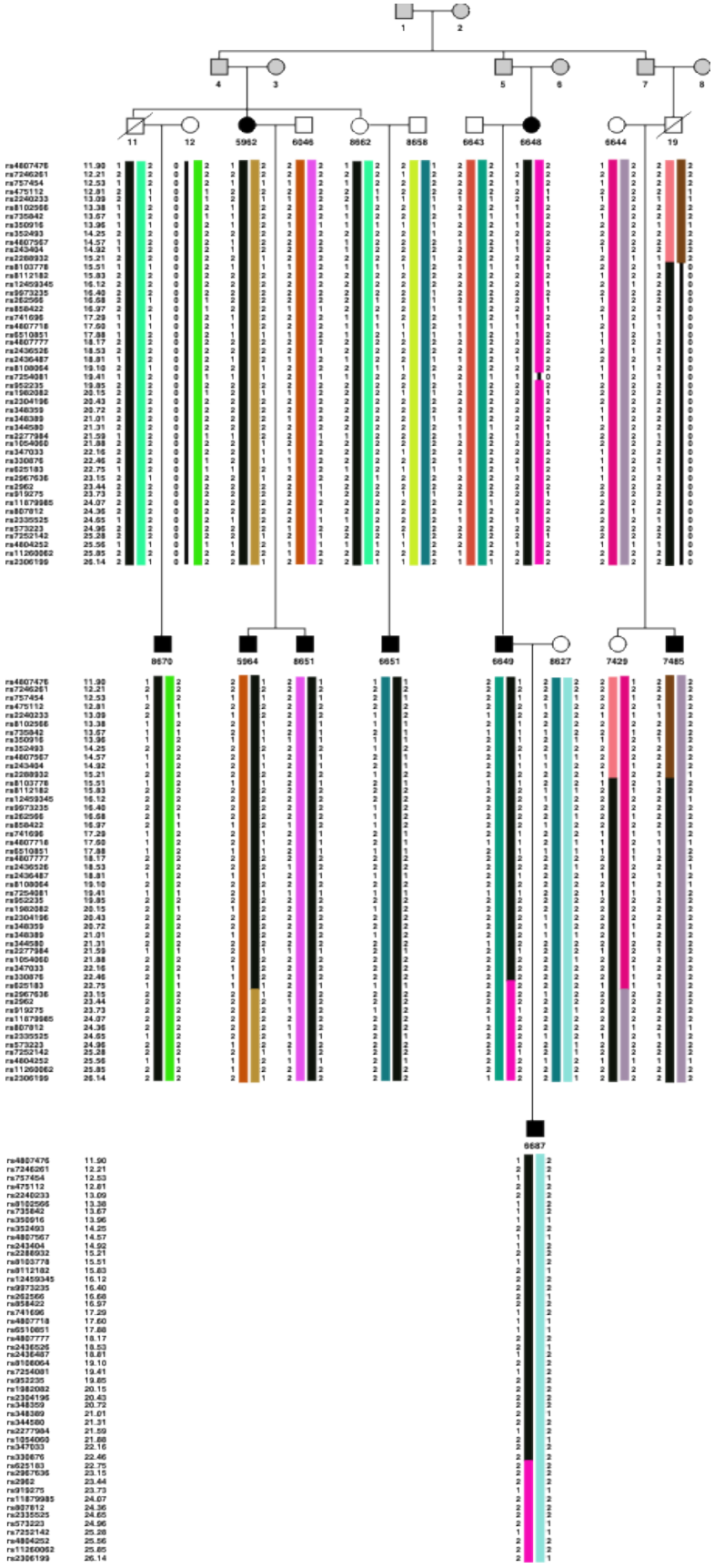

Figure 3.14: Haplotype of markers on chromosome 19p13.3, for Family #2. The at-risk haplotype is shown in black.

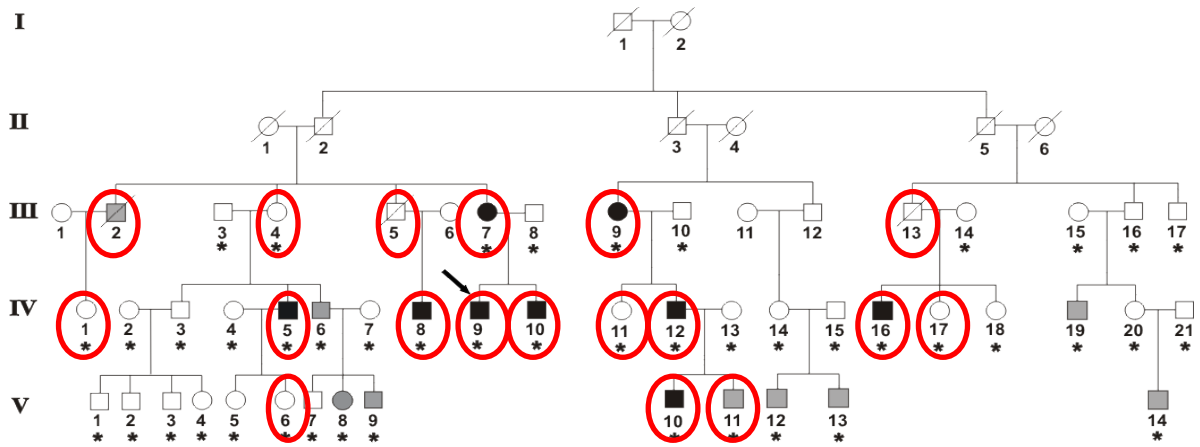

Figure 3.15: Pedigree of Family #2. Asterisks denote genotyped subjects. Red circles denote the presence of at risk haplotype.

Homozygosity Haplotype (HH) analysis

Non parametric Homozygosity Haplotype (HH) analysis, using High-Density SNP genotype data from affected family members only, confirmed the ARVC15 locus, identifying a single shared Region with a Conserved Homozygosity Haplotype (RCHH) on chromosome 19p13.3, matching the critical interval defined by linkage analysis. The RCHH resulted smaller (about 3 Kb at the centromeric limit) compared to the linkage region (Table 3.11).

Chromosome	Telomeric position (bp)	Centromeric position (bp)	Size (bp)	Marker defining RCHH
19p13.3	4866451	6833777	1967327	rs7246083; rs186295

Table 3.11: Output of Homozygosity Haplotype analysis in Family #2.

Copy Number Variation (CNVs) analysis

The whole SNP genotype dataset of Family #2 was analyzed by PennCNV software and a total of 1281 CNVs.

No CNVs shared by all nine affected subjects were observed.

Candidate gene selection within ARVC15 locus

A total of 44 genes and 2 ORFs mapped to the 1.97 Mb ARVC15 critical region.

Among genes expressed in myocardium, *Protein Tyrosine Phosphatase Receptor-type Sigma (PTPRS)* appeared a good candidate gene for mutation screening because of its possible role in intercellular adhesion.

The protein encoded by this gene, known as RPTPσ, PTP-P1 or LAR-2, belongs to the subfamily LAR-PTP of receptor-type protein tyrosine phosphatase and binds to components of desmosomes and adherens junctions, as plakoblobin and β-catenin. It directly regulates phosphorylation level of these proteins, thereby affecting their interactions with cadherins and stability of cell-cell junctions (Kypta *et al*., 1996; Muller *et al*., 1999). It is well documented that tyrosine phosphorylation of plakoblobin and β-catenin regulates the stability of junctional complexes. Enhanced phosphorylation of tyrosine residues on β-catenin is associated with loss of cadherin-actin connection, disassembly of adherens junctions and decreased cell-cell adhesion (Lilien and Balsamo 2005; Sallee *et al*., 2006). Similarly, tyrosine phosphorylation of plakoglobin affects its interaction with components of desmosomes and adherens junctions (Miravet *et al*., 2003).

The cardiac expression of *PTPRS* gene was confirmed by RT-PCR using RNA from human heart.

Mutation screening of *PTPRS* gene

Mutation screening of 38 exons, intronic flanking regions and untranslated regions (UTRs) was performed by direct sequencing in the proband's DNA. DNA sequencing of *PTPRS* coding and untranslated regions (UTRs) in the proband identified several common polymorphisms described in dbSNPs database (not showed), but no potentially pathogenic mutations.

Exome-sequencing

Considering the large number of genes mapped on the ARVC15 locus, the identification of the disease-gene in this family was attempted by exome-sequencing.

All coding exons (as defined in the Consensus Coding Sequence Database CCDS, March 2009 release) and 200 bp flanking intronic regions were captured and sequenced in two affected family members (IV-9 and IV-12).

Overall, 102 and 82.8 million paired-end sequencing reads, comprising 9.2 and 7.5 billion bases, were generated for patients IV-9 and IV-12, respectively.

Among the total reads, 87.7% (for patient IV-9) and 88.8% (for patient IV-12) were aligned to the UCSC human reference genome (hg19 release).

64.2% (for patient IV-9) and 65.8% (for patient IV-12) of the total bases mapped to the targeted and enriched exons. Capture specificity (defined as percentage of uniquely mapped reads aligning to target region) was 72.4% and 74.2% for patients IV-9 and IV-12, respectively.

The detected variants were filtered for the alignment quality, sequence quality score, and sequencing depth of the site, to get high-confidence variants.

After filtering, more than 50.000 SNPs and 5000 Insertion/Deletion (InDels) were identified in the whole exome of each patient (Tables 3.12, 3.13).

These high-confidence SNPs and InDels were compared against those present in several databases (dbSNPs131, HapMap eight exomes, 1000 Genomes Project, YanHuang project, and two databases belonging to BGI) and the shared variants were removed, in order to reduce the candidate pool.

Within this set of variants, a total of 43 SNPs and 104 InDels common to both family members were found.

Categories	Patient IV-9	Patient IV-12
Total number of SNPs	59269	58611
Missense	8276	8667
Readthrough	59	55
Nonsense	97	102
Spice site (1)	1978	2060
Synonymous-coding	6900	7378
5'-UTR	6486	6456
3'-UTR	1925	1816
Intron	32310	30823
Intergenic	1265	1254
Homozygous	27062	25209
Heterozygous	32234	33402

Table 3.12: Summary of SNPs identified in two affected subjects (IV-9 and IV-12) of Family #2.

(1) Intronic SNPs within10 bp of exon/intron boundary.

Categories	Patient IV-9	Patient IV-12
Total number of InDels	5589	5312
Frameshift	307	307
Cds-Indel	220	241
Spice site (1)	387	375
Promoter	27	26
5'-UTR	595	549
3'-UTR	213	196
Intron	3775	3551
Intergenic	65	67
Homozygous	2376	2188
Heterozygous	3213	3124
Total insertions	2585	2374
Total deletions	3004	2938
Ins-coding (2)	267	255
Del-coding (3)	260	293

Table 3.13: Summary of InDels identified in two affected subjects (IV-9 and IV-12) of Family #2.

(1) Intronic SNPs within10 bp of exon/intron boundary.

(2) Insertion in coding sequence

(3) Deletion in coding sequence

Unfortunately, among 147 variants shared by the two subjects none involved genes mapped to the critical region on chromosome 19p13.3.

One novel variant (c.955A>G) was detected only in patient IV-9 in *Ubiquitin-like with PHD and Ring Finger domains 1* (*UHRF1)* gene, located in the critical interval and encoding a protein belonging to a subfamily of RING-finger type E3 ubiquitin ligases.

However, Sanger sequencing did not confirm the presence of this variations in patient IV-9.

To evaluate the sequence coverage depth of the 19p13.3 region, sequencing reads were aligned to the UCSC human reference sequence (February 2009 assembly of the human genome; hg19 GRCh37) (http://genome.ucsc.edu/). The alignment revealed a mean coverage <15X for 67 exons of several genes mapped on the 19p13.3 region, indicating that these regions were insufficiently covered and need to be re-sequenced.

The Figure 3.16 shows a portion of alignment.

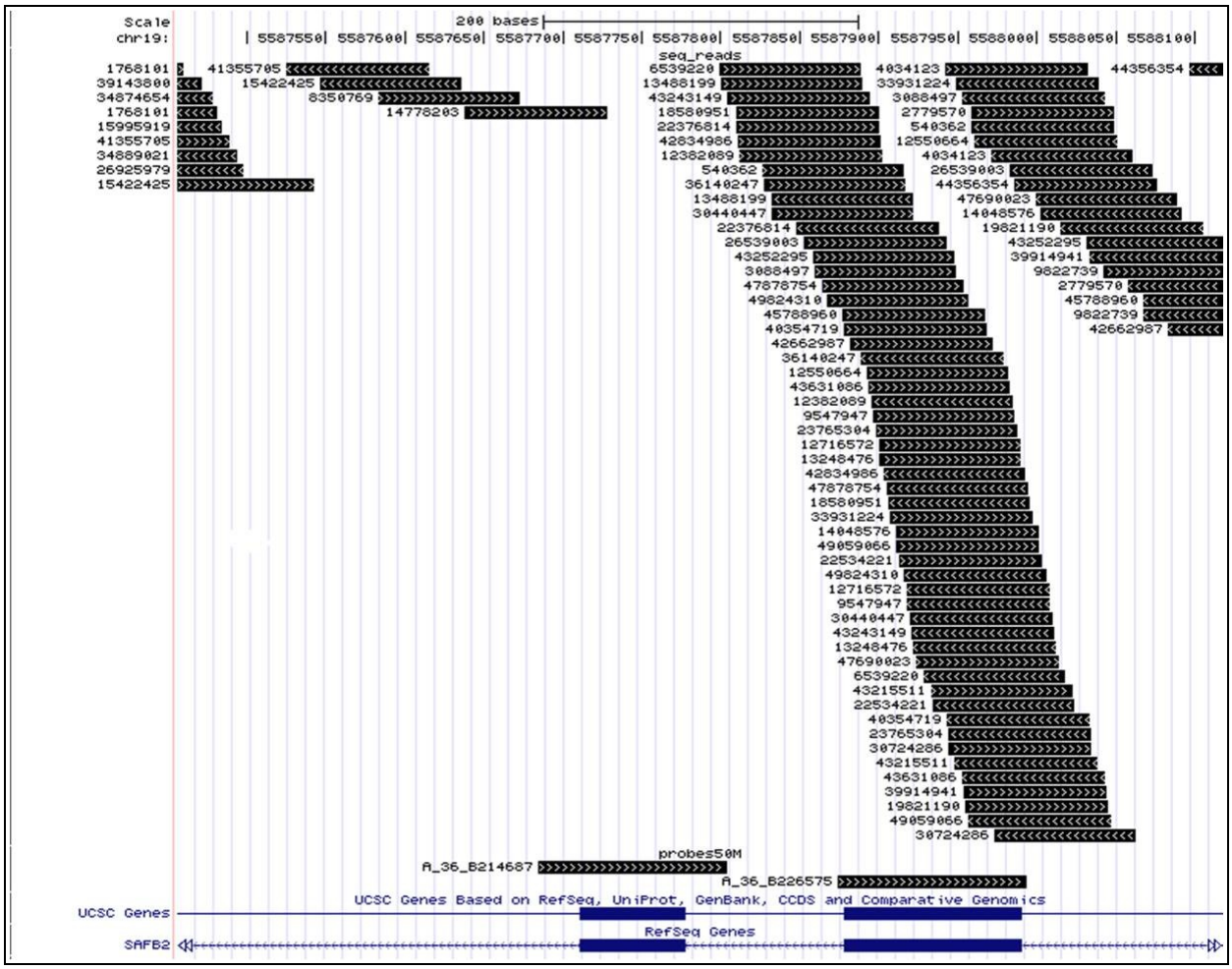

Figure 3.16: Sequencing reads of patient IV-9 aligned to the human reference sequence of *SAFB2* exon 19 and exon 20. *SAFB2* is one of 44 genes mapped on 19p13.3 critical region. Black bars indicate sequencing reads (on the top) and probes (on the bottom), blu bars represent *SAFB2* exons. Only one sequencing read (14778203) covered a portion of *SAFB2* exon 20. Conversely, exon 19 was covered by a large number of reads.

Family #3

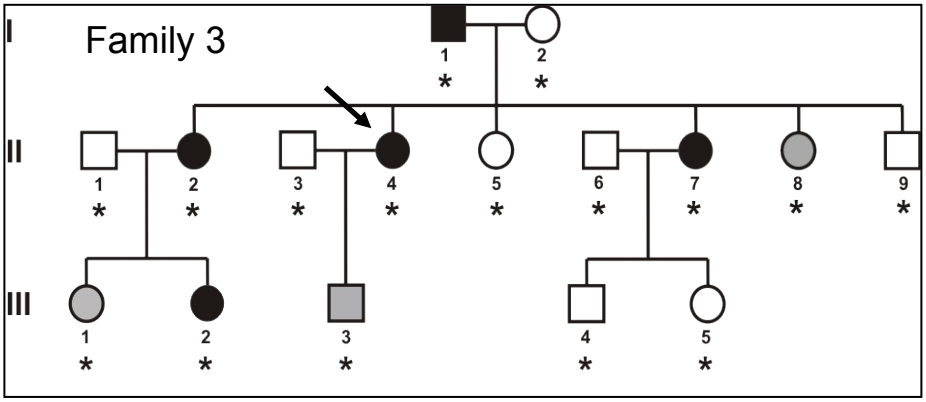

Figure 3.17: Pedigree of Family #3. Asterisks denote genotyped subjects. The proband is indicated by the arrow.

Linkage analysis

In Family #3 (Figure 3.17), multipoint linkage analysis, using an affected-only approach, gave a maximum parametric (p)LOD score of 0.90 for 17 chromosomal regions, inconsistent with linkage (Figure 3.18)

Analysis of marker segregation showed a common haplotype, shared by all affected family members, on each of 16 suggestive linkage regions. Taking into account the incomplete penetrance of the disease, only recombination events occurring in affected subjects were considered to define a critical interval on each region (Table 3.14).

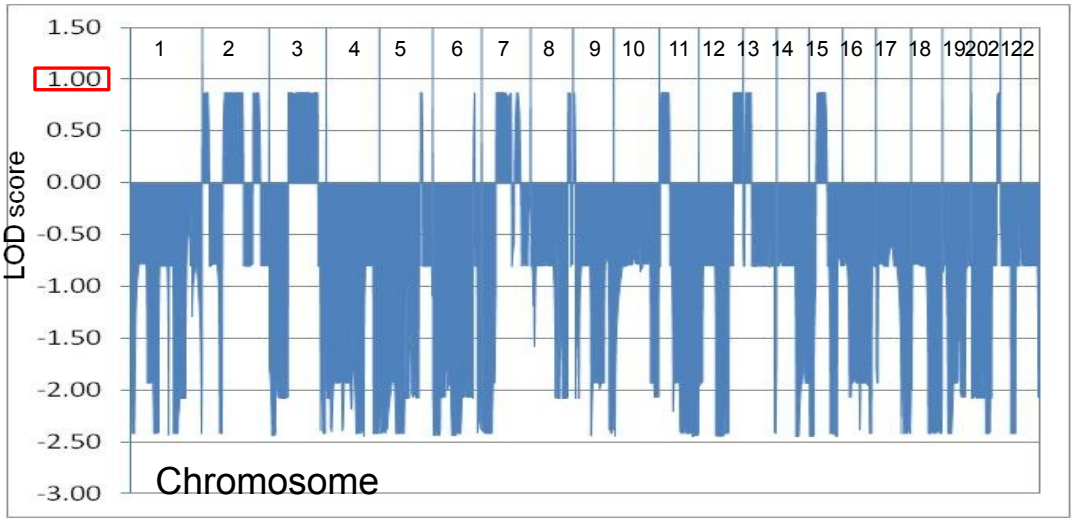

Figure 3.18: Graphical representation of genome-wide multipoint linkage results obtained for Family #3.

Chromosome	Start position (bp)	End position (bp)	Size	Markers defining critical interval
2p25.3-p25.1	18856	10672033	10.65 Mb	rs11901199;rs1641147
2p16.1-q23.3	55053174	153100680	98 Mb	rs993362;rs7355335
2q33.1-q36.1	202532447	224941842	22.4 Mb	rs1208083;rs2123714
3p21.1-q27.1	54330010	183818416	129.5 Mb	rs6445639;rs7627615
5q33.2-q34	152972201	160276677	7.3 Mb	rs778821;rs4559036
6q25.2	152926517	155375989	2.45 Mb	rs2695253;rs7774757
7p14.2-q22.3	36492045	106591791	70 Mb	rs3801302;rs1636804
7q32.3-q34	130640611	142115211	11.5 Mb	rs969827;rs4726529
8q24.22-q24.3	134541542	140969818	6.4 Mb	rs2945779;rs732803
9p24.3-p24.2	191843	2218129	2 Mb	rs3008128;rs17455320
9q33.3-q34.11	128792958	132336394	3.5 Mb	rs4838313;rs1220680
11p15.4-p14.3	3847261	23106436	19.25 Mb	rs1055639;rs2433454
12q24.22-q24.33	117234524	133312853	16 Mb	rs7314211;rs7313293
13q12.22-q13.1	22794240	33587652	10.8 Mb	rs4770248;rs398655
15q14-q23	34026710	69949516	36 Mb	rs8030095;rs4777170
20p13	63799	698987	635 Kb	rs1418258;rs6117279
20q13.32-q13.33	58088597	62877004	4.8 Mb	rs6128602;rs1535211

Table 3.8: Critical intervals for several genomic regions showing a maximum pLOD value of 0.90 for associated markers, in Family #3. A common marker haplotype, shared by all affected subjects, was observed for each chromosomal region.

Copy Number Variation (CNVs) analysis

The whole SNP genotype dataset of Family #2 was analyzed by PennCNV software and a total of 438 CNVs.

No CNVs shared by all affected subjects were observed.

Exome-sequencing

Considering the results obtained from CNVs analysis and the large number of genomic regions showing positive linkage peaks, none of which reached the threshold of statistical significance, the identification of the causative mutation was attempted by exome-sequencing.

All coding exons (as defined in the Consensus Coding Sequence Database CCDS, March 2009 release) and 200 bp flanking intronic regions were captured and sequenced

in two affected family members (II-4 and II-7).

Overall, 89.5 and 91.3 million paired-end sequencing reads, comprising 8.0 and 8.2 billion bases, were generated for patients II-4 and II-7, respectively.

Among the total reads, 89% (for patient II-4) and 86% (for patient II-7) were aligned to the UCSC human reference genome (hg19 release) and 64.5% of the total bases mapped to the targeted and enriched exons.

Capture specificity (defined as percentage of uniquely mapped reads aligning to target region) was 73.1% and 72% for patients II-4 and II-7, respectively.

The detected variants were filtered for the alignment quality, sequence quality score, and sequencing depth of the site, to get high-confidence variants.

After filtering, more than 50.000 SNPs and 5000 Insertion/Deletion (InDels) were identified in the whole exome of each patient (Tables 3.15, 3.16).

These high-confidence SNPs and InDels were compared against those present in several databases (dbSNPs131, HapMap eight exomes, 1000 Genomes Project, YanHuang project, and two databases belonging to BGI) and the shared variants were removed, in order to reduce the pool of candidates.

Within this set of variants, a total of 141 SNPs and 246 InDels common to both family members were found.

Categories	Patient II-4	Patient II-7
Total number of SNPs	61659	54129
Missense	8423	8466
Readthrough	56	56
Nonsense	103	103
Spice site (1)	2034	2027
Synonymous-coding	7255	7248
5'-UTR	6774	6111
3'-UTR	2046	1682
Intron	33581	27326
Intergenic	1387	1110
Homozygous	26801	23910
Heterozygous	34858	30219

Table 3.15: Summary of SNPs identified in two affected subjects (II-4 and II-7) of Family #3.

(1) Intronic SNPs within10 bp of exon/intron boundary.

Categories	Patient II-4	Patient II-7
Total number of InDels	5771	4766
Frameshift	326	319
Cds-Indel	227	204
Spice site (1)	376	350
Promoter	25	19
5'-UTR	586	510
3'-UTR	234	186
Intron	3941	3130
Intergenic	56	48
Homozygous	2411	2043
Heterozygous	3360	2723
Total insertions	2632	2135
Total deletions	3139	2631
Ins-coding (2)	262	242
Del-coding (3)	291	281

Table 3.16: Summary of InDels identified in two affected subjects (II-4 and II-7) of Family #3. (1) Intronic SNPs within10 bp of exon/intron boundary; (2) Insertion in coding sequence; (3) Deletion in coding sequence

No variants shared between the two patients were found in 5 of 12 regions showing positive pLOD values.

In the remaining regions identified by linkage analysis, a total of 56 shared variants were detected. Focusing on missense, nonsense, frame-shift insertions and/or deletions, and splice-site affecting changes, that are more likely to be pathogenic mutations, 12 variants shared by the two subjects were found; 10 of them were confirmed in patient II-4 by Sanger sequencing. Screening of the other affected family members, by direct sequencing, showed that 6 of 10 variants co-segregate with the phenotype (Table 3.18).

Chromosome	Size (Mb)	Number of functionally significant variants shared between patients II-4 and II-7
2p25.3-p25.1	10.65	2
2p16.1-q23.3	98	13
2q33.1-q36.1	22.4	2
3p21.1-q27.1	129.5	14
5q33.2-q34	7.3	2
7p14.2-q22.3	70	11
7q32.3-q34	11.5	1
11p15.4-p14.3	19.25	1
12q24.22-q24.33	16	4
15q14-q23	36	4
20q13.32-q13.33	4.8	2

Table 3.17: Number of functionally significant variants located within the linkage regions and detected in both patients II-4 and II-7 of Family #3 by exome-sequencing.

Gene	Genomic Position	Nucleotide substitution	Exon	Amino acid change	Evolutionary conservation of the site	Prediction by SIFT (score)[1]
IGSF10	Chr3:151171420	c.467G>A	3	R>H	hight	Damaging (0)
PLD1	Chr3:171394591	c.2029C>T	17	P>S	hight	Damaging (0.04)
HSPB1	Chr7:75932207	c.178C>T	1	P>S	hight	Tolerated (0.78)
ACN9	Chr7:96747045	c.10C>T	1	R>W	low	Damaging (0.02)
DUOX1	Chr15:45444549	c.3259C>T	24	R>W	hight	Damaging (0)
COL20A1	Chr20:61945160	c.2275G>A	17	V>I	low	Tolerated (0.18)

Table 3.18: Functionally significant variants detected by exome-sequencing and segregating with the phenotype in Family #3. [1] Score ranges from 0 to 1; the amino acid substitution is predicted damaging if score is ≤0.05 and tolerated if score is >0.05.

The likelihood that each nucleotide substitution had a functional impact on the protein was assessed by SIFT. Moreover, one variant (c.178C>T in *HSPB1* gene) was present in NHLBI ESP Exome Variant Server (http://evs.gs.washington.edu/EVS/) with Minor allele frequency 0.0877% in European-African population.

Finally, function and expression profile of each involved gene was evaluated using bioinformatic resources, as GeneCards (http://www.genecards.org), PubMed (http://www.ncbi.nlm.nih.gov/pubmed/), and OMIM (http://www.ncbi.nlm.nih.gov/OMIM).

IGSF10 gene encodes a member of the Immunoglobulin superfamily, also known as CMF608. Expression of CMF608 is bone-specific and the main type of CMF608-positive

cells is mesenchymal osteochondroprogenitors with fibroblast-like morphology, abundant in the regions of active bone modelling and remodelling. This expression pattern suggested a functional role of CMF608 in induction, maintenance and early differentiation of the osteochondroprogenitor cells pool (Segev *et al*., 2003).

PLD1 gene encodes a phospholipase D (PLD) which is abundantly expressed in several tissues, including heart, and hydrolyzes phosphatidylcholine (PC) to generate choline and phosphatidic acid (PA). The PC-specific PLD activity was implicated in different cellular pathways, including signal transduction, membrane trafficking, and regulation of mitosis. Moreover, PLD might be involved in the development or maintenance of cardiac hypertrophy, as suggested by the broad spectrum of regulatory functions on target proteins linked to the cardiac hypertrophic signaling pathways, along with the evidence that PLD1 and PLD2 expressions were strongly enhanced in rat and human hypertrophic hearts (Peivandi *et al*., 2005).

HSBP1 gene encodes the small heat shock protein beta-1, a stress-induced chaperone ubiquitously expressed, which is able to maintain unfolded substrates in a folding-competent state (Haslbech *et al*., 2005). Besides its canonical folding properties, HSPB1 is involved in several cellular processes, such as apoptosis (Charette *et al*., 2000; Paul *et al*., 2002), cytoskeleton dynamics (Huot *et al*., 1996), and translational elongation (Cuesta *et al*., 2000). To date, defects in *HSBP1* gene were associated to Charcot-Marie-Tooth disease type 2F (CMT2F) and distal hereditary motor neuropathy (Evgrafov *et al*., 2004; Houlden *et al*., 2008).

ACN9 is the human homolog of the gene originally identified in S. cerevisiae (Dennis *et al*., 1999). Little is known about the function of this gene, data from yeast show that it is involved in gluconeogenesis and is required for assimilation of ethanol or acetate into carbohydrate (Dennis and McCammon 1999). Moreover, evidences from an association study suggested that *ACN9* may be involved in the predisposition to human alcohol dependence (Dick *et al*., 2007).

DUOX1 gene is widely expressed in several tissues, including heart, and encodes a glycoprotein which is a member of the NADPH oxidase family and participates in the synthesis of thyroid hormone, as part of a protein complex located at the apical membrane of thyroid follicular cells.

Finally, *COL20A1* gene encodes a collagen type XX alpha-1 protein, highly expressed in heart and other tissues and belonging to the FACIT (fibril-associated collagens with interrupted triple helices) subfamily (Koch *et al*., 2011).

4. DISCUSSION

Arrhythmogenic right ventricular cardiomyopathy (ARVC) is an inherited cardiac disease characterized by fibrofatty replacement of myocardial tissue, primarily affecting the right ventricle, and high incidence of serious ventricular tachyarrhythmias. It is a recognized cause of sudden cardiac death in asymptomatic young people and athletes (Marcus *et al*., 1982; Thiene *et al.*, 1988; Fontaine *et al.,* 1988; Nava *et al.*, 1988). In familial forms of ARVC, accounting for approximately 50% of cases (Hamid *et al*., 2002), autosomal dominant inheritance with reduced penetrance and variable expressivity has been reported, although recessive forms have also been described (Nava et al., 2000; McKoy et al., 2000). In the remaining sporadic cases, the etiology might be related to an acquired cause, as myocarditis (Basso *et al.*, 1996), or an unidentified inherited disorder.

Human genetic studies over the last ten years have provided insight into the potential pathogenetic mechanisms. To date, 14 different ARVC loci have been mapped and 10 genes have been associated with the disease.

The majority of causative mutations have been identified in genes encoding desmosomal proteins, as *plakoglobin* (*JUP*), *desmoplakin* (*DSP*), *plakophilin-2* (*PKP2*), *desmoglein-2* (*DSG2*), and *desmocollin-2* (*DSC2*) (McKoy et al., 2000; Asimaki et al., 2007; Rampazzo et al., 2002; Gerull et al., 2004; Pilichou et al., 2006 ; Syrris et al., 2006).

Additional mutations in non desmosomal genes, including *cardiac ryanodine receptor 2* (*RYR2*), *transforming growth factor beta 3* (*TGFβ3*), *transmembrane protein-43* (*TMEM43*), *desmin* (*DES*), and *titin* (*TTN*), have been recognized as rare causes of ARVC (Tiso *et al*., 2001; Beffagna *et al.*, 2005; Merner *et al*., 2008; Klauke *et al.*, 2010; Taylor *et al*., 2011).

The emerging genetic profile of ARVC has fostered the view that desmosomal dysfunction may be the final common pathway underlying the disease.

However, mutation screening in the desmosomal genes failed to detect causative mutations in about 50% of index cases, pointing out a greater genetic heterogeneity.

Accordingly, current genetic research aims at identifying novel disease-genes and novel mutations in the known genes.

Recognition of the primary genetic causes of ARVC provides the opportunity to investigate molecular mechanisms underlying the disease, as well as to improve the power of genetic testing. Key clinical applications of mutation screening include confirmatory testing of index cases, to facilitate interpretation of borderline cases, and cascade screening of relatives, to early identify asymptomatic mutation carriers, so-called “silent carriers”, at-risk of developing the disease. The latter is particularly relevant for prevention of juvenile sudden death, as phenotypic variability, age-related penetrance and absence of symptoms in the “concealed” phase of the disease make the timely diagnosis very difficult.

4.1 Mutations screening in desmosomal ARVC genes

Genetic screening of five desmosomal ARVC genes (*PKP2, DSP, DSG2, DSC2,* and *JUP*) in 80 Italian unrelated index cases allowed to identify mutations in 36 of them (45%), including single point mutations in 32.5% of cases (26 probands) and multiple mutations, affecting the same gene or different genes, in 12.5% (10 probands). Among single mutation carriers, 15% (9 probands) hosted mutations in *PKP2;* 7.5% (6 probands) in *DSP;* 7.5% (6 probands) in *DSG2;* 1.25% (1 proband) in *DSC2;* and 1.25% (1 proband) in *JUP.* The remaining 55% of probands (44 out of 80) resulted negative for mutations in the desmosomal genes.

Overall, 46 mutations were detected among 80 probands and in 6 cases the same variant occurred in different patients. In agreement with data reported in literature (McKoy *et al*., 2000; Rampazzo *et al*., 2002; Gerull *et al*., 2004; Pilichou *et al*., 2006; Syrris *et al*., 2006; Asimaki *et al*., 2007; Sen-Chowdhry *et al*., 2007), this study indicated a preponderance of mutations in the “big 3” ARVC genes *PKP2*, *DSP*, and *DSG2,* accounting respectively for 34.8%, 30.4%, and 26.1% of total variants identified; conversely, *DSC2* and *JUP* mutations represented 4.3%.

The occurrence of the same variant, predominantly affecting *PKP2* gene, in more than one proband could be ascribed to several factors, such as a founder effect, bias in selection of patients, or presence of mutational hotspots in some genomic regions. The latter hypothesis is suggested by the observation that several variants identified in this cohort of index cases were previously described in different populations, indicating that they are recurrent mutations among ARVC patients.

Whenever possible, the genetic analysis of family members allowed to determine the

segregation of each mutation identified in the index case, confirming the high heterogeneity in the clinical expression of ARVC mutations even among relatives.

In the respective families of two index cases (probands #2 carrying *PKP2* mutation p.T50SfsX61, and proband #4 carrying *DSP* p.R941X mutation), the phenotype of single mutation carriers ranged from a complete lack of clinical manifestations or presence of minor signs not fulfilling the diagnostic criteria, up to severe disease phenotype.

Studies on monozygotic twins indicated that environmental influences, variability in life style, and level of physical activity may contribute to the differences observed in ARVC, including age of onset, structural severity, arrhythmic risk, and clinical outcomes (Wlodarska *et al.*, 2005). However, modifier genes are likely to account for much of the broad spectrum of disease expression and await elucidation (Sen-Chowdhry *et al*., 2010).

The segregation analysis within families of index cases carrying multiple mutations highlighted a still greater genetic complexity. In the family of proband #11, only the index case and the sister, both compound heterozygotes for two novel *DSP* mutations (p.S1658F and p.I2347V) were clinically affected, while the single mutation carriers did not show evidence of disease. Similarly, in the family of proband #32, carrying three heterozygous mutations in different genes, all three mutations occurred among proband's relatives but only the sister, that was compound heterozygous for *DSP* mutations, showed a severe phenotype.

These observations raise the question of whether ARVC was inherited as a recessive trait in these family.

The frequency of compound and digenic heterozygosity observed in this study is consistent with data reported in literature (den Haan *et al*., 2009; Bauce *et al*., 2010; Xu *et al*., 2010; Fressart *et al.*, 2010) and underlines the importance of genotyping the index cases for the whole panel of genes rather than performing single-gene screening. Moreover, this relatively high incidence of multiple mutations, along with the low penetrance of some mutations, suggests that potentially pathogenic variants might recur in the general population at higher rate than hitherto supposed. Accordingly, taking into account the incomplete penetrance of the disease, the occurrence of a low-frequency mutated allele among control subjects cannot exclude its pathogenicity, as recently evidenced by Kapplinger and colleagues (Kapplinger *et al.*, 2011). This study comprehensively evaluated genetic variation in healthy individuals for ARVC genes, indicating that so-called "radical mutations", as frame-shift insertions and/or deletions,

nonsense mutations and splice-site affecting changes, are high-probability ARVC-associated mutations, while rare missense variant should be interpreted in the context of several factors, including localization of the variant in functionally critical domains, evolutionary conservation of the primary sequence, type of amino acidic substitution (conservative or non conservative with regard to phisico-chemical properties of the affected residue), co-segregation with the disease in a family, and ethinicity of the carrier.

Although these criteria represent a possible approach to infer the significance of missense variants, rare or absent among control subjects, establishing pathogenic effects of such mutations requires well-validated functional studies *in vitro* or *in vivo*, which are not widely available and are highly complex to perform. As a result, a significant proportion of genetic variants remains unclassified. This represents a gap in genotype-phenotype correlation and in risk stratification, especially for relatives, as the pathogenic role of unclassified variants is unknown and it cannot be excluded that, within families, these variants represent risk factors for disease development. Moreover, the difficulty in defining pathogenicity of some ARVC mutations and rare polymorphisms has led to a lack of uniformity in their classification by different groups. An exemplary case is *DSC2* p.A897KfsX4 frame-shift variant which was identified in the proband #3, along with *PKP2* p.F552C and *DSP* p.N375I mutations.

DSC2 p.A897KfsX4 was originally described as pathogenic mutation, since it showed co-segregation with disease in ARVC families (Syrris *et al*, 2006). However, this variation was also found in our Italian control group with minor allele frequency of 1.5% (De Bortoli *et al*., 2010) and, then, in apparently healthy subjects from other populations, with minor allele frequency ranging from 0.8% to 1.69% (Klauke *et al.*, 2010; Fressart *et al.*, 2010; Elliott *et al*., 2010; Christensen *et al*., 2010), leading to its reclassification as polymorphism.

The two base pair insertion causing p.A897KfsX4 variation involves the alternatively spliced exon 17, which is untraslated in DSC2b. Accordingly, p.A897KfsX3 variant affects only the isoform a of DSC2.

In vitro functional studies showed that, unlike wild-type protein, the DSC2a p.A897KfsX3 mutant was localised in the cytoplasm. However, in the human heart, DSC2b is the major isoform, suggesting that relative deficiency of DSC2a might be compensated by isoform b and p.A897KfsX3 may be a rare variant affecting phenotypic expression of concomitant ARVC mutations (De Bortoli et al., 2010).

Subsequently, an independent study demonstrated impaired binding of DSC2a A897fsX3 mutant to JUP and DSP. This deficiency cannot directly be compensated by DSC2b, as this isoform did not bind to JUP; however, the cytoplasmic domain of DSG2 appears to have redundant functions in binding plakoglobin (Gemlike et al., 2010).
Since the differential functions of the two DSC2 isoforms in the myocardium are not well characterized, the pathogenic potential of p.A897fsX3 cannot be excluded.
Currently, it remains unclear whether carriers of this variant exhibit subclinical disease expression, as low expression levels of DSC2a isoform in the myocardium determine lack of an overt phenotype, or if p.A897fsX3 may affect the disease expression in individuals who perform endurance training or carry other concomitant ARVC mutations.
Similarly, the pathogenic contribution of ARVC mutations located in the alternatively spliced *PKP2* exon 6, as p.R490W identified in the index case #18, is not well defined. These variants affect only the isoform b of PKP2; however, PKP2a is more expressed than PKP2b in human heart tissue (Gandjbakhch *et al*., 2011).
When properly interpreted, genetic testing may improve the distinction between familial and sporadic cases and allows the early detection of preclinical disease, affording the possibility of a timely intervention to prevent sudden cardiac death. Accordingly, in the last revision of the Task Force diagnostic criteria (Marcus *et al.*, 2011), the identification of a pathogenic mutation was included among the major criteria, highlighting the diagnostic potential of mutation analysis. However, the presence or absence of a genetic mutation alone cannot override the overall clinical assessment, as evidenced by segregation analysis in families of index cases. In the family of proband #2, two affected subjects did not carry the mutation identified in the index case. Similarly, the niece of proband #3 resulted negative for all three mutations recurring within the family, although she was clinically affected. These observations suggest the presence of additional mutations in known or not yet identified genes, underlying the disease in these subject.

According to data reported in literature, mutation screening of desmosomal genes failed to detect causative mutations in more than 50% of index cases investigated by this study, suggesting that additional and still unknown genes could be involved (Fressart et al., 2010; Bauce et al., 2010; Christensen et al., 2010; Den Haan et al., 2009). However, possibility of misdiagnosis in some cases, presence of mutations in sequences not analyzed, as promoter and UTRs regions, and/or large genomic deletions/duplications, not detectable by DHPLC and direct sequencing, cannot be excluded.

4.2 Genome-wide scan

Among the index cases investigated by this study and negative for point mutations in desmosomal genes, three belong to independent families with recurrence of ARVC.

Assuming a further genetic heterogeneity in these families, a genome-wide scan was performed in order to map novel loci and, possibly, the involved genes.

A linkage study, using high−density SNP arrays, was conducted to identify critical genomic regions segregating with the disease, in which to select candidate genes for mutation screening. Moreover, taking into account that large deletions or duplications (>1 Kb) are not detectable by DHPLC analysis and direct sequencing, the presence of genomic rearrangements, in known or yet unidentified disease-genes, was evaluated by SNP array Copy Number Variations (CNVs) analysis.

In addition, In Family #2 and in Family #3 a combined strategy of linkage analysis and exome sequencing was used to identify novel ARVC genes.

Identification of a Copy Number Variation in a desmosomal ARVC gene

In Family #1, affected-only linkage analysis gave a maximum parametric LOD score of 1.17, not statistically significant, in 11 chromosomal regions, one of them included *PKP2* locus. The subsequent CNVs analysis identified a hemizygous deletion of 122.5 Kb on chromosome 12p11.21, encompassing the entire *PKP2* gene and shared by all affected family members. It was not present in any of available public CNVs databases and was confirmed by quantitative real-time PCR. No other CNVs common to all affected family members were observed. Overall, these data support the pathogenic nature of this CNV, which is expected to determine haploinsufficiency. The occurrence of the hemizygous *PKP2* deletion also in one family member with minor signs of disease, not fulfilling the diagnostic Task Force criteria, and in three healthy relatives is consistent with the incomplete penetrance of *PKP2* mutations.

Interestingly, the telomeric end of this deletion lies less than 4 kb apart from a 2 kb low-copy repeat (LCR) (genomic position chr12:32943683-32945665) and a second LCR of similar size is located more than 26 Mb upstream (genomic position chr12:6589220-6591352). Low-copy repeats or segmental duplications are DNA fragments that range from 1 to 400 kb in length, occur at more than one site within the genome, and typically share a high level (>90%) of sequence identity (Eichler 2001). LCRs can cause genomic instability and either mediate or stimulate both recurrent and nonrecurrent CNV formation. The predominant molecular mechanism underlying recurrent genomic

rearrangements is Non Allelic Homologous Recombination (NAHR) between large directly oriented LCRs, located at a distance less than ~10 Mb from each other, which results in deletions or reciprocal duplications of the genomic segment between them (Stankiewicz and Lupski 2010). However, *PKP2* gene is located downstream from both LCRs on chromosome 12; accordingly, LCRs-based NAHR cannot account for formation of *PKP2* CNVs. It can be hypothesized that *PKP2* deletions may arise by non recurrent rearrangements due to replication-based mechanisms of DNA repair, as FoSTeS/MMBIR (fork stalling and template switching/microhomology-mediated break-induced replication), that utilize nucleotide microhomology at the rearrangement breakpoints and were recently proposed to be responsible for formation of non recurrent CNVs and complex genomic rearrangements in proximity of LCRs (Hastings *et al*., 2009).

The *PKP2* deletion described in the present study is the first case of copy number variation identified in an ARVC Italian family using high-density SNPs arrays.

Very recently, large *PKP2* deletions were detected in 3 out of 169 (2%) ARVC Dutch index cases, by Multiplex Ligation-dependent Probe Amplification (MLPA). Only one patient carried the deletion of the entire *PKP2* gene, which was also observed in four asymptomatic family members (Cox *et al*., 2011). To date, no other systematic studies on a large scale of ARVC patients or families have been performed to evaluate the contribution of copy number variation to ARVC.

The identification of a CNV segregating with the disease in this family emphasizes the importance of complementing the conventional mutation screening in ARVC genes with other approaches able to detect possible structural variations. Moreover, a genome-wide CNVs analysis, using high-resolution SNP arrays, may be useful for identifying copy number variations in novel disease genes, as well as in cardiomyopathy-related genes lying in relatively unstable genomic regions. Recent studies described the involvement of rare CNVs in the occurrence of Long QT Syndrome (Bisgaard *et al.*, 2006; Koopmann *et al*., 2006; Eddy *et al.*, 2008; Barc *et al.*, 2011) and Dilated Cardiomyopathy (Norton *et al*., 2011), suggesting than genomic structural variations may underlie inherited cardiomyopathies, although the exact contribution of CNVs to these disorders remains unknown. Estimates have indicated that CNVs could constitute 20% of mutations involved in Mendelian diseases (Botstein and Risch, 2003); this is of particular relevance to ARVC, where only approximately 50% of genetic cause has been identified.

Further large-scale studies on patients and multiplex families are required to evaluate the frequency of CNVs in ARVC genes versus point mutations and to establish a phenotype-genotype correlation.

Identification of a novel ARVC locus (ARVC15)

In Family #2, a significant evidence of linkage to a single region on chromosome 19p13.3 was obtained, with a maximum parametric LOD score of 3.85 using an affected-only approach. Non parametric Homozygosity Haplotype (HH) analysis confirmed linkage results. Analysis of haplotype segregation on chromosome 19p13.3 showed a common region shared by all affected subjects and recombination events in two of them refined a critical interval about ~2 Mb in size, in which 44 known genes and two ORFs are currently mapped.

These results present evidence for the existence of a novel ARVC locus on chromosome 19p13.3, providing the basis for the identification of a novel disease-gene. Since this locus is the fifteenth reported so far, it should be named ARVC15.

Among genes mapped on 19p13.3 critical region, *Protein Tyrosine Phosphatase Receptor-type Sigma (PTPRS)* was selected as candidate gene for mutation screening on the basis of its role in cell to cell adhesion. Direct sequencing of coding and untraslated regions (UTRs) of *PTPRS* in the probands's DNA did not identify any causative mutation, making it unlikely that defects in this gene underlie the disease in this family. However, the possibility of mutations in promoter or intronic regions, cannot be ruled out. Moreover, genome-wide CNVs analysis excluded the presence of rare genomic rearrangements shared by all affected subjects. Considering the large number of genes mapped on ARVC15 locus, the identification of the causative mutation in this family was attempted by exome-sequencing in two affected family members. After filtering, a total of 147 novel variants shared by both subjects were identified; however, none of these involved genes mapped on 19p13.3 critical interval. The subsequent evaluation of sequence coverage depth in this region revealed a poor uniformity and a low read depth (mean coverage <15X) for 67 exons of different genes, indicating that not all genes on ARVC15 locus were sufficiently covered.

The inadequate coverage of some genes within the critical region may, in part, underlie the failure of this approach in identifying the causative variant in this family.

A low coverage can be due to several factors, including poor capture or sequencing and errors in alignment. Moreover, not all sequences obtained from the analyzed samples

were aligned to the reference genome and to the regions covered by capture probes, so as to allow base calling; the capture specificity (defined as percentage of uniquely mapped reads aligning to target region) for each sample resulted approximately 73%, indicating that the remaining 27% of reads were not aligned. On the other hand, the causal variant may have been covered but not accurately called, for example in the presence of a complex indel.

Also the analytical approach applied to exome data has some limitations.

Considering that more than ten thousand functional variants were identified in each sample, a first filtering step against data from several databases (dbSNPs131, HapMap eight exomes, 1000 Genomes Project, YanHuang project, and two databases belonging to BGI) was required to reduce the pool of candidate variants. However, due to the high number of sequenced exomes and genomes, filtering of variants in a manner that is independent of the minor allele frequency (MAF) may remove pathogenic alleles occurring in the general population at low frequency. This risk is especially relevant for ARVC, as a non penetrant pathogenic allele does not result in a phenotype that might otherwise exclude an individual from a control population.

In general, the estimated probability of identifying a single causal gene by exome-sequencing of few samples is higher for recessive disorders compared to dominant diseases, as supported by simulation studies and by the greater number of successful reports in the literature (Bamshad *et al*., 2011).

Nevertheless, since the knowledge of all protein-coding exons in the genome is still incomplete, the disease gene could be yet unknown or not annotated and, therefore, not included in the exome target.

Finally, it cannot be ruled out that the pathogenic mutation involves an intronic or regulatory sequence.

Although exome-sequencing failed to detect the causal variant underlying the pathogenic phenotype in this family, genome-wide linkage results provided strong evidence for a novel ARVC locus on chromosome 19p13.3, highlighting the soundness of this strategy for identifying susceptibility regions in large and highly informative families.

Sanger sequencing of the exons on 19p13.3 locus that were insufficiently covered by exome-sequencing and/or re-examination of the filtered-out variants detected in this region, including those in intronic and UTRs sequences, could allow the identification of a novel disease-gene.

In addition, exome data obtained in the present study allow for storing of the complete library of novel coding variants detected in these patients for potential future in silico identification of mutations in newly discovered genes. This is particularly attractive for ARVC, due to the relative high incidence of multiple mutations. Moreover, a large number of common polymorphisms were identified in both subjects; such changes could contribute to modulating the phenotypic expression of the disease, in terms of age of onset, severity, and clinical outcome. Although these data does not allow, at present, to perform a genotype-phenotype correlation, whole-genome and whole-exome sequencing approaches are starting to replace traditional genetic testing of several inherited cardiomyopathies (Meder *et al.*, 2011), providing the possibility of sistematically investigating the role of genetic modifiers in determining the high clinical variability observed in and across families.

Identification of a putative ARVC candidate gene

In Family #3, affected-only linkage analysis gave a maximum parametric LOD score of 0.90, not statistically significant, in 17 chromosomal regions. The subsequent CNVs analysis did not detect any structural variation shared by all affected family members.

On the basis of these results, the identification of the causative mutation in this family was attempted by exome-sequencing in two affected family members.

After filtering, a total of 387 novel variants shared by both subjects were found and 56 of them were located in 11 regions previously identified by linkage analysis.

Focusing on missense, nonsense, frame-shift insertions and/or deletions, and splice-site affecting changes, that are more likely to be pathogenic mutations, 12 variants common to both subjects were found, two of them were not confirmed by Sanger sequencing. Among the remaining 10 variants, six co-segregated with the pathogenic phenotype within the family. Considering the function and expression profile of each involved gene and the current knowledge about the disease, a more likely pathogenetic role may be supposed for the missense variant identified in *COL20A1* gene.

COL20A1 gene encodes a collagen type XX alpha-1 protein, highly expressed in heart and belonging to the FACIT (fibril-associated collagens with interrupted triple helices) subfamily.

Collagen is an extra-cellular matrix component that contributes to passive tension in stretched muscle, thereby influencing the end-diastolic volume of the heart.

It is known that myocardial passive tension includes contributions from cardiomyocytes,

through titin-dependent force, and from collagen in the extracellular matrix. Titin's contribution is larger than collagen's at shorter sarcomer lengths, while at longer sarcomer lengths collagen fibrils straighten and their stiffness increases (Xu *et al.,* 2000).

How an alteration in a collagen protein can result in ARVC remains, at present, largely elusive and requires further investigation. Genetic screening of *COL20A1* in a large cohort of ARVC patients, negative for mutation in the known genes, could elucidate the effective involvement of this gene in the genetic determination of the disease. Moreover, future studies are needed to determine the pathogenic contribution of the other novel variants identified by exome-sequencing and co-segregating with the phenotype in this family.

5. CONCLUSIONS

Genetic screening of five desmosomal ARVC genes in 80 Italian probands identified causative mutations in 45% of cases.

The genes most frequently involved were *PKP2*, *DSP* and *DSG2,* accounting respectively for 34.8%, 30.4%, and 26.1% of the total mutations. The relatively high incidence of multiple mutations, identified in 12.5% of index cases, indicated that this condition is quite frequent among ARVC patients. Genetic analysis extended to available family members confirmed the high heterogeneity in the clinical expression of ARVC mutations even among relatives, whose phenotype ranged from a complete lack of symptoms and/or clinical manifestations to a severe form of disease.

Lack of pathogenic mutations in the remaining 55% of index cases suggested that additional and still unknown genes could be involved in the genetic determination of ARVC. In this perspective, a genome-wide scan was performed in three large ARVC families, showing no mutations in any of the desmosomal genes.

In Family #1, a heterozygous *PKP2* deletion segregating with the pathogenic phenotype was identified by CNVs analysis, highlighting the importance of complementing the conventional mutation screening in ARVC genes with other approaches able to detect possible structural variations. Moreover, a genome-wide CNV analysis of multiplex families could be useful for identifying large deletions/duplications in novel disease genes.

In Family #2, a novel ARVC locus (ARVC15) was mapped on chromosome 19p13.3 by linkage analysis, providing the basis for the identification of a novel disease-gene.

This result supports the continued search for novel disease-genes through genome-wide approaches based on ascertainment and collection of large, informative families.

Finally, in Family #3, exome-sequencing identified *COL20A1* gene as putative candidate gene for ARVC. Genetic screening of *COL20A1* in a large cohort of ARVC patients, negative for mutation in the known genes, could elucidate its effective involvement in the genetic determination of the disease.

APPENDIX A

Amplicon	bp	Forward 5'-3'	Reverse 5'-3'	PCR T_{ann}°C	T°C DHPLC
1	414	ACTCGAGCGGGGCGGGGCTCG	ACTCCCAGCACGCGGGGTGAG	68	Direct sequencing
2	329	ACTTGTTCTTGGCCTTCATT	TTGGGAAAAGTAAACACTCAAA	TD70>60	53.0 / 55.6 / 58.0
3	971	GGGGCAAACTTCTCGTCATC	GCAGCTGCCTGAAAAGTCATT	TD70>60	Direct sequencing
4	310	TGCTTCCCAGTATTCGCTGA	GGTTTCAGTGTGCAAAGTCACC	TD70>60	61.0
5a	273	GCCTCAGTTGTGCTACACATAG	CAGCCACCTCCAATTTGTTG	TD70>60	56.0 / 60.0
5b	304	CGTGGCATCCTCAAGCTTCT	TGAGCCCATCAATCATTTGC	TD70>60	58.1 / 59.1
6	308	TTCAGGGGAGGTGATGTTTG	GGATTACAGGCGCAGACC	TD70>60	Direct sequencing
7	333	GGAGTTGATGGCCTTGACTG	TCCTGACTTCCTTGGGGCTA	TD70>60	58.5
8	307	TGCCAGTTTCCAAACACCTG	AAACCTAAAACCAAGCGGCTA	TD70>60	55.2 / 56.5 / 58.7
9	291	TGATATCACACCTGCAAGGA	CACAAACACACACTCTCTCTCAT	TD70>60	56.9 / 58.7
10	330	CTGGTCTCCTGGTTTGAGTG	TTTCATCTCTGAATTGAATGTAG	TD70>60	57.8 / 60.8
11	330	AAACATCTTCATCAACCTCTGGT	CGGGAGGTGATACAGACAACA	TD70>60	55.3 / 57.1 / 61.2
12a	231	GAAAAAGAATGTTCTTCACCCA	TCGCGTGCATTCTGGTAACT	TD70>60	Direct sequencing
12b	278	TTCCTGACACAGTCCCGAGT	CATCCTGTTTGCTGCCATGT	TD70>60	Direct sequencing
13	307	ACCGAGTGGCCTGACTTCAT	CGATTTCTTCCCAGGGTCAA	TD70>60	58.5 / 59.9 / 61.0
14a	284	TTGACCCTGGGAAGAAATCG	CAGGGGACCACGGAAATAGA	TD70>60	58.2

Table 1. Primers sequences, amplification and analysis conditions for PKP2 gene (Taq Gold DNA Polymerase)

Amplicon	bp	Forward 5'-3'	Reverse 5'-3'	PCR T_{ann}°C	T°C DHPLC
1	422	GGTAGCGAGCAGCGACCTC	AAAACCTTTCCACCTTCGGG	65	65.9 / 66.5
2	365	GATTCCGGGTAAAGGGTCTC	TCTGTTCTGAAAAAGCGTGTCT	62	60.5 / 62.6
3	433	TGGTTCATGAATCTCCGTCTGT	GGGAACATTTGTGCTGCCTT	62	57.2 / 59.2
4	471	TTAAGTCCTGGGGTAAAGAAAA	GGAGGAAAATCCTGCAAACAG	55	58.6 / 61.3
5	443	GCATTAGCCATTTGGGAACC	TTCCCCATTTAAGAAGTGGGATT	62	56.4 / 59.7 / 61.8
6	262	GGGATCTGAGGCCAGTATCTGA	ATCGATGAACAGGTGCCTCC	62	58.0
7	309	ACCTGCAGAGAACACCAGTCA	AGACCAATCATTCCCCGAGA	62	61.1 / 62.1
8	382	AACAGCGTGATTCTTTGGCA	CCAACCCCTGGTGTAGGGTA	55	Direct sequencing
9	312	AGCTTTCATGCAGGCTCACC	GCACTCAAAATCAATGAAGAGG	62	53.7 / 56.8 / 58.7
10	414	ATAGTTTCCCGCTGCCACAT	AAATGCTTGCTTGGCTCTGG	65	57.6 / 60.4
11	442	TGCCGACGAATTTGTGATTT	TTGTTCCATAGCTGCTGATTTC	60	55.7 / 56.4
12	394	TCAGCTTCATTTGAGGGGAAA	GGCAAGGCATCGTGTGTCTA	62	59.3 / 61.8
13	359	GGTTTTTGTGCAGTGGTGTGA	AGGAGGGCTGAGCTGACTTG	62	60.3
14	372	CCCATCTAGTGGGTGGCATT	CCAGTTTTATGCAAACTCCCTT	62	58.9 / 59.6
15	505	TTCTTCGTGCACTAAATTTTCA	AATCCTGCCAGAAGCCTGTT	62	56.6 / 58.0
16	480	CCATGGAAGTTGACTGATGTG	ATGCGAGGCTAGCGGAATTA	62	55.9
17	370	TCTGCTTTGACGTTGTTCCC	AACCTGTGTGGCCACTGAAA	62	57.6 / 58.2
18	437	TTTTATAAACTTTGCCGCCCA	GGCAGTCCATGAAAAGAGCAT	62	Direct sequencing
19	382	TCAAGTGAATTTCTGGGTGA	AAGCCTTCACAAAATGGGTT	58	57.0
20	323	TGCTCATCTCCTAAGCTGTAAC	CGCTTTACAACAAATCAGCA	62	53.6 / 55.3

21	312	TAGACGTGCAGCCCAATGAT	AAGACAGGCAGGAGACAGGG	65	57.0 / 58.8
22	489	TAGGGGAAACAGCCTGGAGA	CAGCGTATTGGAGCATGGAA	TD72>62	Direct sequencing
23a	455	GAATGCACATTGGTCTGGGA	CACATTGCCTTGCTTTCTGC	62	56.9 / 58.5
23b	477	TACCAGGCAGAGTGTTCCCA	CTCCTTGATGGTGGTCTTCG	62	58.0
23c	471	AGGCACCCGGAAGAGAGAAT	GCCTCCTCCTGAAACTCAGC	62	56.0 / 57.0 / 60.7
23d	461	ACTGAAGCAGGTCATGCAGC	CCAGCTGCTGTTTCCTCTGA	62	56.7 / 59.0
23eBg	326	TCACCCGAGAAAACAGGAGC	TCTCGCGTTTTCATCTTCCA	62	57.4 / 59.6
23eEnd	271	TTGATGATGCTGCCAAAACC	AACCGCGTGATATCCTGGTC	62	57.0 / 59.4
23f	503	GCAAACAGTAGTGCGACGGA	TGCTCATTCCTCAAGTGAGCTT	62	60.6 / 61.6
23g	407	CGGAACCTGAGGCTGGAGTA	AAAGAACAGCAGGGCACACA	TD72>62	54.8 / 56.2 / 59.8
24a	488	CAAGCTCACAGTGTATCCAGGG	TGCTTGGAGTCTTTCGATCTCA	62	Direct sequencing
24b	471	GGAAGACTCAATATTCCCGCA	AAGCAGATGCTCCAGCGATA	62	57.8 / 59.3 / 59.8
24c	476	GAAGGTGACAGCAATGCAGC	CTGAAGCAATCTGGGCTTCC	62	57.8 / 58.7
24d	490	TTGATGATCCATTTTCAGGCA	CAGCTTGAACCCTGGAGGAA	62	58.0 / 59.1 / 59.7
24e	472	CCTTCCAAGGAATCAGACAACC	CGAATACCGTGGCCCTTTT	65	58.3 / 59.3
24f	502	CAGAACGAGCTGTCACTGGG	TGCTCACACAGTTCTTTGAAGG	62	Direct sequencing
24g	493	CCTCAGGAAGCGTAGAGTGG	GTCAAAGATGGCTGCAATGG	TD72>62	57.2 / 58.5 / 59.3
24h	500	TTAGCAGCTCCCGACATGAA	TTCGGTGCTTATCCTCCCAT	62	58.8 / 61.2 / 62.0
24i	467	CATAGGCTTCGAGGGTGTGA	GTGGCGTCAAAGCTTCCTCT	65	Direct sequencing
24l	479	GGATGCCATAAATCGCTCCA	GACGCACTGCATCCAAGTGTA	65	55.3 / 56.8

Table 2. Primers sequences, amplification and analysis conditions for DSP gene (Taq Gold DNA Polymerase)

Amplicon	bp	Forward 5'-3'	Reverse 5'-3'	PCR T_{ann}°C	T°C DHPLC
1	314	CCAGGGAGGAGCCGAGTG	GATTTTCCGAAGCCCCAGGT	TD70>60	67.0 / 69,1
2	391	AGATTTCTCCTCGGGCACTT	TGCACTGAATACCCCTGGAT	TD70>60	54.8 / 55.1 / 57.5
3	463	GCCTCATAGGAAATACGAAGCA	CCGGAATGGGAAAGAGAATC	TD70>60	Direct sequencing
4	393	GGCTTTTGGCTAAGATCAAATC	GCATCCAAAGCGTAACCTGT	TD70>60	53.1 / 55.0
5	491	TCTTGATCGAGAAGAAACACCA	AAGCAATGGCATGTAAAGTCC	TD70>60	Direct sequencing
6	490	CCCATTCACGCTTATGTCCT	TGGACAGCACATCCCTAAAA	TD70>60	53.8 / 55.0 / 55.8
7+8	700	TCTGCAAAAGCTCTGACTGC	TTTTAAGTGTTCAGGGCTCAAA	TD70>60	Direct sequencing
9a	343	TGCTGCTATATTTCCTGTGCAT	TCCAATTATTTGGCCTTTGC	TD70>60	54.7 / 55.7 / 56.5
9b	355	CCTACACCCATTCCCATCAA	GGTGAAAATTCCCCCTCATC	TD70>60	54.8 / 56.9
10	373	AGAGGTTTCCAATTCATGCAG	CTTGACCTCGTGATCCACCT	TD70>60	52.3 / 53.7 / 54.3
11	421	TCTGTTGTCAGCAATAGGAACA	GGTTCAGGACCTCATTTCATAA	TD68>58	55.4 / 56.8 / 59.0
12	455	GCAATGAAAGAACATTTGTGGA	TTGTTTCCCTATTCACCCTCA	TD70>60	Direct sequencing
13	289	GACAAGTCCAGGAAGGGACA	CACTTCCCTAGGCCCCTTTA	TD70>60	55.0 / 57.5 / 59.5
14a	292	CTGGCCTCAGTGGAAATAGC	GCAGGCTTCTGTGTTCTTCC	TD70>60	58.9 / 60.1
14b	299	TCATTTCTGCCAGTGGATCA	TCTTCGTTCAGTGCAACAGC	TD70>60	60.6
14c	225	GATGGAAGGTGGGAAGAACA	CCCCCACCACCAATACATAA	TD70>60	61.0 / 62.8
14d	286	TGACCACTGAAACCACGAAG	GGGTCCCATTTCTCTTTCCT	TD70>60	Direct sequencing
15a	273	TTTCCCTGATGGTTCCTTGT	GCGGTCATCTAGCTCTCCTT	TD70>60	53.8 / 54.5 / 57.5
15b	331	CGGCCTCTTACACTGAGGAA	ACTGGGAAGCTACTGCCAGA	TD70>60	57
15c	377	TCGCTGAATGCTTCTATTGG	CTAGAAGCCATTGGGTCAGG	TD70>60	56.5 / 57.9
15d	263	TCTGGCAGTAGCTTCCCAGT	GCTGGAGCATACACCCTCTC	TD70>60	60.1
15e	261	CACCTCTTCCTGACCCAATG	GAAGATGCTGAGTGCCTTCC	TD70>60	59.8
15f	412	CCTTGGTAGATCAGCCTTATGC	TGCTTGGTAACTCTGGTGGA	TD70>60	58.0 / 59.0 / 60.0
15g	305	ACGGTGTCTGGAGCTGGA	GGAAGCAGAGACAGTGTGGTC	TD70>60	57.2 / 58.5

Table 3. Primers sequences, amplification and analysis conditions for DSG2 gene (Taq Gold DNA Polymerase)

Amplicon	bp	Forward 5'-3'	Reverse 5'-3'	PCR T_{ann}°C	T°C DHPLC
1	708	TCAGACCTCGCTCTGTAATTGA	TATCCCCGTTCCCCTAGTTT	58	Direct sequencing
2	199	ACACATTAAAGTTTTCTTTTTAT	GGCGTATATGTACCACAGCA	62	Direct sequencing
3	400	CCCCACGTGCATACATTACT	TGGTTTTCATTCGTCTTTAAGC	58	54.8 / 55.4
4	269	CCCCTACCCAGCTAATCCTC	GGAAACTATAGACTCCCACAGCA	58	55.6 / 58.5
5	332	TGAAAGCTCTGCTGAAATAAAGA	GGAGTAGCCAGAGCATTGGT	58	56.5 / 57.2
6	266	GCCAAAATGAATTTGAAGCATAC	TTGAAACACAGTTAATTTGCCATA	60	54.7
7	384	CATAGAACATGTGAATGTTTTGGA	CAAAACCAGCATACTCCAAGG	58	55.0 / 58.0 / 59.5
8	252	GTTGGTGCTTTCCCCCAATA	AGGCCAGAGATGTGCATATTA	58	54.3 / 55.6
9	324	CATCGTGTTCAATTTTTGTGA	CCTTTCTTTCCATTAAATTCTAGC	60	52.2 / 53.5 / 55.3
10	374	ACTCGTTAGCATTGCCAAAT	TAACGTAACAAAATAAGCTA	58	56.5 / 57.9
11	375	CAAGAAGTAGCAGTGGCATAAGG	AACAGAGTGCATGTATCCAGCTT	60	51.7 / 56.0
12	345	GTGTTCAGTGCATACTTTTGTGG	GCAGACATCCTGATGTTGAAAA	58	57.0 / 58.0 / 59.0
13	356	tgttcagaagaaatcagtgaca	GTGTCTTGAAAGTTACTTTAAAGG	58	57.2 / 58.0
14	263	GATTTATGTGTGTATTAACCATTG	CGCATTATAAGCGAATTCATCC	58	57.7
15a	194	CATAATTTTGTGTTCCTCTCTGT	AGGATTCCGAGGTCTGGTGT	58	56.2 / 60.6 / 61.8
15b	332	GGCTTCACAACCCAAACTGT	TGAAAATTATAGTCAGAATCCAGT	58	61.0 / 61.4 / 62.2
15'	226	GCCACATGCGTGACTTTTAG	ACTTTCTGCCAAGGGGAAAA	58	53.7 / 55.2
16	397	CAATGAAAGGTAAATCAAAGCAA	AAAAACCCCCACAAATAGCA	58	56.3 / 56.8

Table 4. Primers sequences, amplification and analysis conditions for DSC2 gene (Taq Gold DNA Polymerase)

Amplicon	bp	Forward 5'-3'	Reverse 5'-3'	PCR T_{ann}°C	T°C DHPLC
1	474	GGACAGTCAGGCGAGATAGC	GCCTTGCTCAGATCTCTGGT	60	Direct sequencing
2	399	GCCAGGTGACTTCCTGCT	GTGGGCCCCTAGTTAGCAT	62	61.3 / 62.5+1 / 63+1.5
3	390	CTGCTCCCCAGTGTCTGC	CTCCCCTGAGGACATCTGC	62	63.4 / 64.3+0.5 / 64.8+1
4	427	GACTCTCCCGTGTGTGATGA	TTATGGAAGCTCAGGGAAGG	62	63.6+0.5 / 64.1+1 / 65+1
5	395	ATATTTCCAGAGGGGCGTCA	CCAAGGCTGTGCAGGATAGA	62	63.7
6_7	580	CGAACTATTCGTGCTTTAGCTG	GGACTGGGGGCTCTAAATCT	62	60.2+0.5 / 62.6+1 / 63.6+1.5
8	517	CCCCTTTAGGTCATCCCACT	CTTTGCTACAGCGGCTTTG	62	62.3+0.5 / 62.7+1
9	300	GAGGGAAGGGATACTTGAAGC	CCACAGAGGACACCCTGAC	65	61.8+0.5 / 63.9+1
10	276	CTGTCATGGGGAGGAGTTGT	GTCCAGGCCTCCCAAATC	65	63.2
11_12	550	ATTGCTACAGGGTGGAGGTG	AGGAGACCCCCAAAAGTGTT	65	Direct sequencing
13	250	GCCCCCTCTTTTAGAAGCAT	GCAGTTGCCACTGGTCCT	62	61.2
14'UTR	487	GTAGAGGAGGCAGCTGAAGG	AAGCCACTCCGTGTCACC	65	62.4
14A	477	TGTCTTTGGTGGGGATGGGG	CAGACCCAGAGAAGGAACCA	TD 65-75	Direct sequencing
14B	482	TGGCCACTAAAGCTTCAGACT	GGGGTCTGAAACAGGAAGG	65	61.4
14C	290	CCTGTCCCACCCACACAGCT	CTAGGGAAGCCCCTCAACTTT	65	Direct sequencing
1	474	GGACAGTCAGGCGAGATAGC	GCCTTGCTCAGATCTCTGGT	60	Direct sequencing
2	399	GCCAGGTGACTTCCTGCT	GTGGGCCCCTAGTTAGCAT	62	61.3 / 62.5+1 / 63+1.5
3	390	CTGCTCCCCAGTGTCTGC	CTCCCCTGAGGACATCTGC	62	63.4 / 64.3+0.5 / 64.8+1

Table 5. Primers sequences, amplification and analysis conditions for JUP gene (GoTaq DNA Polymerase)

Gene	Exon	Amplicon size (bp)	Forward 5'-3'	Reverse 5'-3'	Primer Concentration
PKP2	2	127	tttaatatttgcttgattgcag	TGTCATAGGTTTTAGGAACAGG	500 nM
PKP2	7	140	ttttcagcggtcattttggt	TCTCCGTCAGCGTAAGCAAT	500 nM
PKP2	13	113	agcagttgaggagcgaagag	TTGTTGGAGGCATAGctgaa	550 nM
ACTB	4	59	CGAGCGCGGCTACAGCTT	CCTTAATGTCACGCACGATT	500 nM
TBP	2	106	CTGTTTCTTGGCGTGTGAAG	CGCTGGAACTCGTCTCACTA	350 nM

Table 6. Primers sequences and amplification conditions for quantitative real-time PCR (DyNAmo™ HS SYBR® Green qPCR Kit, Finnzymes)

Amplicon	bp	Forward 5'-3'	Reverse 5'-3'	PCR T_{ann}°C	DNA Polimerase
1	595	GGAGCCGTGGCACAGTTTAG	CTTGGAGCGCCTGCATTT	TD 68-58	Taq Gold
2	387	CATGATCCTTCCCCATTGTC	CAGCCATAAATGCACACAGG	TD 72-62	Taq Gold
3	369	CCTTGCTTTCCTCCTCCTCT	AAGTCCACTGTGGCTGAGGT	TD 72-62	Taq Gold
4	377	CTGCAGCAATTCTCCCAGTC	CAGGAGGGTTTGGGGTAACT	TD 72-62	Taq Gold
5	417	TGTGCAGTGCTCAGAACCAT	TATCCTCAGTGTGCGGCTTT	65	Taq Gold
6	287	TGAACATAAGCCACTTTAGGAA	TGGGTCACAGTTACCATCAC	TD 70-60	GoTaq
7	374	GCTTTGACAAGCCCTCAGAC	AACACTGGGTGGAACAAAGG	TD 75-65	Taq Gold
8	450	TTTGCTGGGGAATCTGGTGT	TTCCTGCTTGGGTGTGCAG	TD 75-65	Go Taq
9	352	GCCTTGGGAAGTCCTCTTTT	CGGCTGAGATTTTCGTGTCT	65	Taq Gold
10	490	TCTTCCCCTCCCAACCTCA	AGAACAACCGTCCCCTTCCT	TD 75-65	Go Taq
11A	359	GACCCTGGGCCATAGTTTGT	CGATGCTGTAACGTGTGGTG	65	Taq Gold
11B	645	GACTGAGAACACAGCCACCA	CATAACCCACAAACCGCTCT	TD 75-65	Taq Gold
12	397	cagaggtggacaggtgacaa	TAGGGACAAAGAGGGGGAAG	65	Taq Gold
13	576	CTCTCCGTACCCTCTTTTTCTG	GCTGTGCTGATGGGGATACT	60	Taq Gold
14A	446	CTGGTGAGCACAGGGTTCTT	AGCAGGATCTGAGTGGTGGT	TD 75-65	Go Taq
14B	435	CACGGCCATTTTGGTAAGTT	GCCAATTCCAAAGTCAAGGA	TD 75-65	Go Taq
15+16	567	AAGAGCGCCCAGTTATTCAC	CAGGAGTCACAGCACAGCA	TD 72-62	Go Taq
17	353	CCTCCTTGCTTGTTCTCAGC	cagccctcacacctttgtct	TD 75-65	Go Taq
18A	296	ATACAACCCCACCTTGTGC	GCAAGCCGGAACACATAC	TD 70-60	Taq Gold
18B	631	CAGTTTGGCCGTGAGGACT	ggacttgccttgagtgacca	TD 75-65	Go Taq
19	388	AAGCAGGGACTTGGGACAG	tgatccctcacttcacacca	TD 75-65	Taq Gold
20	592	CAGGATTCAGTGGGATCAGG	ggcatatggggtatcaggaa	TD 72-62	Go Taq
21+22	614	GAAGGGAAGACTCAGAGAAACG	gcctgtgactgaccacagag	65	GoTaq
23	469	AAAGACCCATCTGGCCACTA	cccaaatcttgctgagttgaa	65	GoTaq
24+25	699	GGGCTGAGATAAGCCTCCTT	gtggctgcaccaagcatag	65	GoTaq
26	347	GCTATCGTGAGTCCTCAGGTG	cacaagacaggtgggcaaa	65	Taq Gold
27+28	543	CATGAGCCACCCTGAGTCTT	gggagacatgggatctagca	65	GoTaq
29+30	633	ATCTGGGAGCGGTCAGAGT	gaagtgggttccatgagaatg	65	Taq Gold
31	303	GACAGGTGACATCCTTGTGGT	TGACGATAAAGCAGCCTGTG	TD 75-65	Go Taq
32	472	AGGTACGTCCACCCCACTCT	caccaccttctagtccccatt	65	GoTaq
33	451	TGCCCCTACCTACCTATCCA	cacacacccaaagattcacg	65	Taq Gold
34+35	530	TGTAGCTGTCACTGGCTTGG	ccttggcctttgtatccatc	65	Taq Gold
36	347	GGGGTGAAGATAGGGAGGAT	ttccccgaggactctaacag	65	Taq Gold
37	374	CAAGCTTAGGCTGTCCCATC	accgtctacccacagtgacc	TD 72-62	Taq Gold
38A	441	CTGCAAGAGACACGCACAAG	TGGTTTTGGAATTGGAAGGA	TD 70-60	Go Taq
38B	466	AGCTGTGTTTCTGCACCA	GCCAAAGTTAGTTCTCTTTGAA	60	Go Taq
38C	485	ATCCCGTGACATTTCATTTTT	GCTCTCAGAGGAGGACCACT	62	Taq Gold
38D	534	CAGTTCTGAGGGTAAGGTCA	gttcacacaaggaaacgaga	62	Taq Gold

Table 7. Primers sequences and amplification conditions for PTPRS gene

APPENDIX B

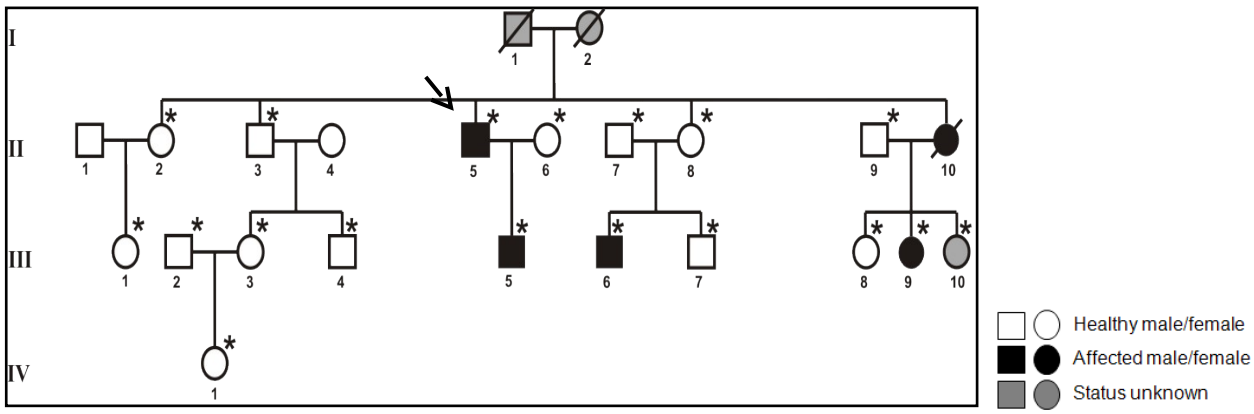

Figure 1: Pedigree of Family #1. Asterisks denote genotyped subjects. The proband is indicated by the arrow.

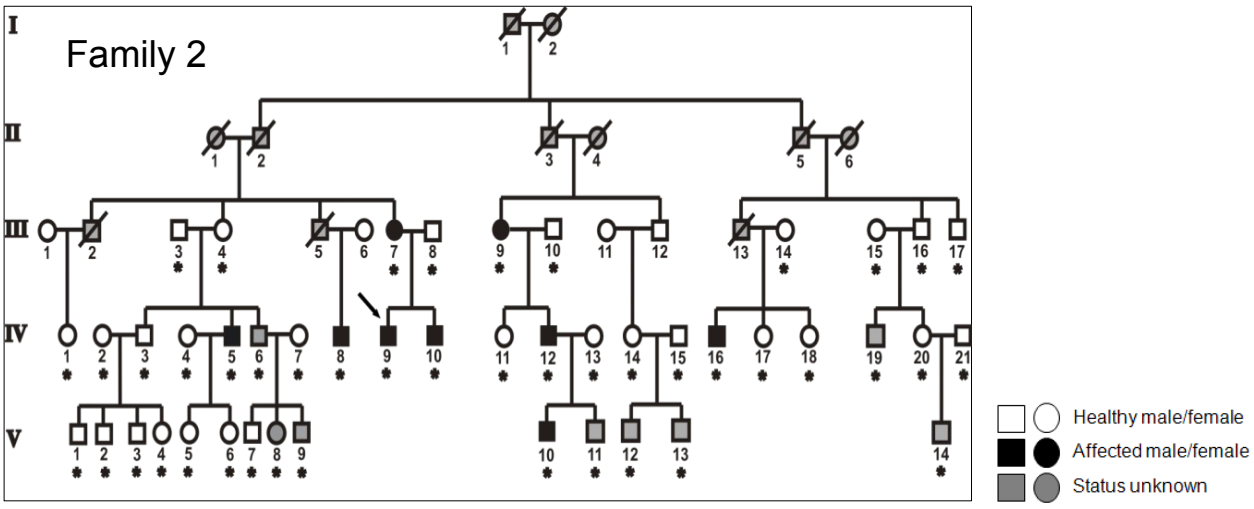

Figure 2: Pedigree of Family #2. Asterisks denote genotyped subjects. The proband is indicated by the arrow.

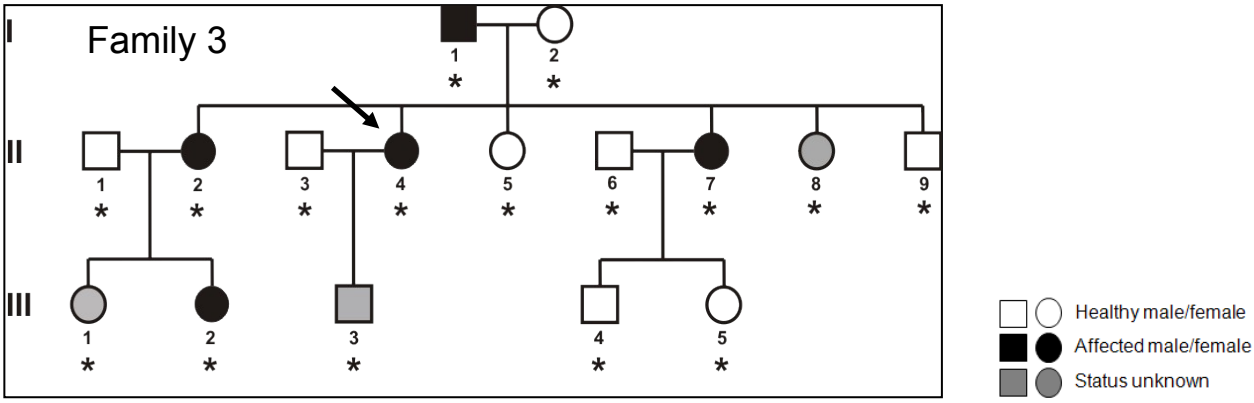

Figure 3: Pedigree of Family #2. Asterisks denote genotyped subjects. The proband is indicated by the arrow.

REFERENCES

-Angelini A, Basso C, Nava A, Thiene G. Endomyocardial biopsy in arrhythmogenic right ventricular cardiomyopathy. Am heart 1996;132:203-6.

-Armstrong DK, McKenna KE, Purkis PE, Green KJ, Eady RA, Leigh IM, Hughes AE. Haploinsufficiency of desmoplakin causes a striate subtype of palmoplantar keratoderma. Hum Mol Genet. 1999;8:143-8.

-Asimaki A, Syrris P, Wichter T, Matthias P, Saffitz JE, McKenna WJ. A novel dominant mutation in plakoglobin causes arrhythmogenic right ventricular cardiomyopathy. Am J Hum Genet. 2007;81:964-73.

-Asimaki A, Syrris P, Wichter T, Matthias P, Saffitz JE, McKenna WJ. A novel dominant mutation in plakoglobin causes arrhythmogenic right ventricular cardiomyopathy. Am J Hum Genet. 2007;81:964-73.

-Asimaki A, Tandri H, Huang H, Halushka MK, Gautam S, Basso C, Thiene G, Tsatsopoulou A, Protonotarios N, McKenna WJ, Calkins H, Saffitz JE. A new diagnostic test for arrhythmogenic right ventricular cardiomyopathy. N Engl J Med. 2009;360:1075-84.

-Awad MM, Calkins H, Judge DP; Medscape. Mechanisms of disease: molecular genetics of arrhythmogenic right ventricular dysplasia/cardiomyopathy. Nat Clin Pract Cardiovasc Med. 2008;5:258-67.

-Awad MM, Dalal D, Tichnell C, James C, Tucker A, Abraham T, Spevak PJ, Calkins H, Judge DP. Recessive arrhythmogenic right ventricular dysplasia due to novel cryptic splice mutation in PKP2. Hum Mutat. 2006 ;27:1157.

-Bamshad MJ, Ng SB, Bigham AW, Tabor HK, Emond MJ, Nickerson DA, Shendure J. Exome sequencing as a tool for Mendelian disease gene discovery. Nature Reviews 2011; 12: 745-755.

-Barc J, Briec F, Schmitt S, Kyndt F, Le Cunff M, Baron E, Vieyres C, Sacher F, Redon R, Le Caignec C, Le Marec H, Probst V, Schott JJ. Screening for Copy Number Variation in Genes Associated With the Long QT Syndrome. J Am Coll Cardiol 2011; 57 (1): 40-7.

-Basso C, Corrado D, Marcus FI, Nava A, Thiene G. Arrhythmogenic right ventricular cardiomyopathy. Lancet 2009: 373: 1289-1300.

-Basso C, Thiene G, Corrado D, Angelini A, Nava A, Valente M. Arrhythmogenic right ventricular cardiomyopathy. Dysplasia, dystrophy, or myocarditis? Circulation 1996; 94: 983-91.

-Bauce B, Basso C, Rampazzo A, Beffagna G, Daliento L, Frigo G, Malacrida S, Settimo L, Danieli G, Thiene G, Nava A. Clinical profile of four families with

arrhythmogenic right ventricular cardiomyopathy caused by dominant desmoplakin mutations. Eur Heart J 2005; 26:1666-75.

-Bauce B, Frigo G, Marcus FI, Basso C, Rampazzo A, Maddalena F, Corrado D, Winnicki M, Daliento L, Rigato I, Steriotis A, Mazzotti E, Thiene G, Nava A. Comparison of clinical features of arrhythmogenic right ventricular cardiomyopathy in men versus women. Am J Cardiol. 2008;102:1252-7.

-Bauce B, Nava A, Beffagna G, Basso C, Lorenzon A, Smaniotto G, De Bortoli M, Rigato I, Mazzotti E, Steriotis A, Marra MP, Towbin JA, Thiene G, Danieli GA, Rampazzo A. Multiple mutations in desmosomal proteins encoding genes in arrhythmogenic right ventricular cardiomyopathy/dysplasia. Heart Rhythm. 2010;7:22-9.

-Bauce B, Rampazzo A, Basso C, Mazzotti E, Rigato I, Steriotis A, Beffagna G, Lorenzon A, De Bortoli M, Pilichou K, Marra MP, Corbetti F, Daliento L, Iliceto S, Corrado D, Thiene G, Nava A. Clinical phenotype and diagnosis of arrhythmogenic right ventricular cardiomyopathy in pediatric patients carrying desmosomal gene mutations. Heart Rhythm. 2011;8:1686-95.

-Beffagna G, De Bortoli M, Nava A, Salamon M, Lorenzon A, Zaccolo M, Mancuso L, Sigalotti L, Bauce B, Occhi G, Basso C, Lanfranchi G, Towbin JA, Thiene G, Danieli GA, Rampazzo A. Missense mutations in desmocollin-2 N-terminus, associated with arrhythmogenic right ventricular cardiomyopathy, affect intracellular localization of desmocollin-2 in vitro. BMC Med Genet. 2007;8:65.

-Beffagna G, Occhi G, Nava A, Vitiello L, Ditadi A, Basso C, Bauce B, Carraro G, Thiene G, Towbin JA, Danieli GA, Rampazzo A. Regulatory mutations in transforming growth factor-beta3 gene cause arrhythmogenic right ventricular cardiomyopathy type 1. Cardiovasc Res. 2005; 65: 366-73.

-Bentley et al. Accurate whole human genome sequencing using reversible terminator chemistry. Nature 2008; 456: 53-59.

-Bisgaard AM, Rackauskaite G, Thelle T, Kirchhoff M, Bryndorf T. Twins with mental retardation and an interstitial deletion 7q34q36.2 leading to the diagnosis of long QT syndrome. Am J Med Genet A 2006; 140: 644 – 8.

-Borrmann CM, Grund C, Kuhn C, Hofmann I, Pieperhoff S, Franke WW. The area composita of adhering junctions connecting heart muscle cells of vertebrates. II. Colocalizations of desmosomal and fascia adhaerens molecules in the intercalated disk. Eur J Cell Biol 2006; 85:469-485.

-Botstein D and Risch N. Discovering genotypes underlying human phenotypes: past successes for mendelian disease, future approaches for complex disease. Nat Genet 2003;33(Suppl.):228-237.

-Charette SJ, Lavoie JN, Lambert H, and Landry J. Inhibition of Daxx-mediated apoptosis by heat shock protein 27. Mol Cell Biol 2000;20: 7602–7612.

-Choi HJ, Park-Snyder S, Pascoe LT, Green KJ, Weis WI. Structures of two

intermediate filament-binding fragments of desmoplakin reveal a unique repeat motif structure. Nat Struct Biol. 2002; 9:612-20.

-Choi HJ, Weis WI. Structure of the armadillo repeat domain of plakophilin 1. J Mol Biol 2005; 346: 367-376.

-Christensen AH, Andersen CB, Tybjaerg-Hansen A, Haunso S, Svendsen JH. Mutation analysis and evaluation of the cardiac localization of TMEM43 in arrhythmogenic right ventricular cardiomyopathy. Clin Genet. 2011;80:256-64.

-Christensen AH, Benn M, Tybjaerg-Hansen A, Haunso S, Svendsen JH. Missense variants in plakophilin-2 in arrhythmogenic right ventricular cardiomyopathy patients, disease-causing or innocent bystanders? Cardiology. 2010;115:148-54.

-Coonar AS, Protonotarios N, Tsatsopoulou A, Needham EW, Houlston RS, Cliff S, Otter MI, Murday VA, Mattu RK, McKenna WJ Gene for arrhythmogenic right ventricular cardiomyopathy with diffuse nonepidermolytic palmoplantar keratoderma and woolly hair (Naxos desease) maps to 17q21. Circulation 1998; 97: 2049-2058.

-Corrado D and Thiene G. Arrhythmogenic right ventricular cardiomyopathy/dysplasia: clinical impact of molecular genetic studies. Circulation 2006;113:1634-7.

-Corrado D, Basso C, Leoni L, Tokajuk B, Bauce B, Frigo G, Tarantini G, Napodano M, Turrini P, Ramondo A, Daliento L, Nava A, Buja G, Iliceto S, Thiene G. Three-dimensional electroanatomic voltage mapping increases accuracy of diagnosing arrhythmogenic right ventricular cardiomyopathy/dysplasia. Circulation. 2005;111:3042-50.

-Corrado D, Leoni L, Link MS, Della Bella P, Gaita F, Curnis A, Salerno JU, Igidbashian D, Raviele A, Disertori M, Zanotto G, Verlato R, Vergara G, Delise P, Turrini P, Basso C, Naccarella F, Maddalena F, Estes NA 3rd, Buja G, Thiene G. Implantable cardioverter-defibrillator therapy for prevention of sudden death in patients with arrhythmogenic right ventricular cardiomyopathy/dysplasia. Circulation. 2003;108:3084-91.

-Cox MG, van der Zwaag PA, van der Werf C, van der Smagt JJ, Noorman M, Bhuiyan ZA, Wiesfeld AC, Volders PG, van Langen IM, Atsma DE, Dooijes D, van den Wijngaard A, Houweling AC, Jongbloed JD, Jordaens L, Cramer MJ, Doevendans PA, de Bakker JM, Wilde AA, van Tintelen JP, Hauer RN. Arrhythmogenic right ventricular dysplasia/cardiomyopathy: pathogenic desmosome mutations in index-patients predict outcome of family screening: Dutch arrhythmogenic right ventricular dysplasia/cardiomyopathy genotype-phenotype follow-up study. Circulation. 2011;123: 2690-700.

-Cuesta R, Laroia G, and Schneider RJ. Chaperone hsp27 inhibits translation during heat shock by binding eIF4G and facilitating dissociation of cap-initiation complexes. Genes Dev. 2000; 14: 1460 –1470.

-d'Amati G, di Gioia CR, Giordano C, Gallo P. Myocyte transdifferentiation: a possible pathogenetic mechanism for arrhythmogenic right ventricular cardiomyopathy. Arch Pathol Lab Med. 2000;124:287-90.

-Dalal D, Jain R, Tandri H, Dong J, Eid SM, Prakasa K, Tichnell C, James C, Abraham T, Russel SD, Sinha S, Judge DP, Bluemke DA, Marine JE, Calkins H. Long-term efficacy of catheter ablation of ventricular tachycardia in patients with arrhythmogenic right ventricular dysplasia/cardiomyopathy. J Am Coll Cardiol 2007; 50 (5): 432-440.

-Daliento L, Turrini P, Nava A, Rizzoli G, Angelini A, Buja G, Scogmaniglio R, Thiene G. Arrhythmogenic right ventricular cardiomyopathy in young versus adult patients: similarities and differences. J Am Coll Cardiol 1995,25:655-64.

-De Bortoli M, Beffagna G, Bauce B, Lorenzon A, Smaniotto G, Rigato I, Calore M, **Li Mura IE**, Basso C, Thiene G, Lanfranchi G, Danieli GA, Nava A, Rampazzo A. The p.A897KfsX4 frameshift variation in desmocollin-2 is not a causative mutation in arrhythmogenic right ventricular cardiomyopathy. Eur J Hum Genet. 2010;18:776-82.

-Delmar M. The intercalated disk as a single functional unit. Heart Rhythm. 2004;1:12-3.

-Delva E, Tucker DK, Kowalczyk AP The desmosome. Cold Spring Harb Perspect Biol. 2009;1:a002543.

-den Haan AD, Tan BY, Zikusoka MN, Lladó LI, Jain R, Daly A, Tichnell C, James C, Amat-Alarcon N, Abraham T, Russell SD, Bluemke DA, Calkins H, Dalal D, Judge DP. Comprehensive desmosome mutation analysis in north americans with arrhythmogenic right ventricular dysplasia/cardiomyopathy. Circ Cardiovasc Genet. 2009;2:428-35.

-Dennis RA, McCammon MT. Acn9 is a novel protein of gluconeogenesis that is located in the mitochondrial intermembrane space. Eur J Biochem 1999; 261:236 –243.

-Dennis RA, Rhodey M, McCammon MT. Yeast mutants of glucose metabolism with defects in the coordinate regulation of carbon assimilation. Arch Biochem Biophys 1999; 365: 279 –288.

-Dick D, Aliev F, Wang JC, Saccone S, Hinrichs A, Bertelsen S, Budde J, Saccone N, Foroud T, Nurnberger Jjr., Xuei X, Conneally PM, Schuckit M, Almasy L, Crowe R, Kuperman S, Kramer J, Tischfield JA, Hesselbrock V, Edenberg HJ, Porjesz B, Rice JP, Bierut L, Goate A. A Systematic Single Nucleotide Polymorphism Screen to Fine-Map Alcohol Dependence Genes on Chromosome 7 Identifies Association With a Novel Susceptibility Gene *ACN9.* Biol Psychiatry 2008; 63: 1047–1053.

-Dusek RL, Godsel LM, Green KJ. Discriminating roles of desmosomal cadherins: Beyond desmosomal adhesion. J Derm Science 2007; 45: 7-21.

-Eddy CA, MacCormick JM, Chung SK, et al. Identification of large gene deletions and duplications in KCNQ1 and KCNH2 in patients with long QT syndrome. Heart Rhythm 2008;5:1275–81.

-Eichler EE. Recent duplication, domain accretion and the dynamic mutation of the human genome. Trends Genet. 2001 Nov;17(11):661-9.

-Elliott P, O'Mahony C, Syrris P, Evans A, Rivera Sorensen C, Sheppard MN, Carr-White

G, Pantazis A and McKenna WJ. Prevalence of Desmosomal Protein Gene Mutations in Patients With Dilated Cardiomyopathy. Circ Cardiovasc Genet 2010;3;314-322.

-Evgrafov OV, Mersiyanova I, Irobi J, Van Den Bosch L, Dierick I, Leung CL, Schagina O, Verpoorten N, Van Impe K, Fedotov V, Dadali E, Auer-Grumbach M, Windpassinger C, Wagner K, Mitrovic Z, Hilton-Jones D, Talbot K, Martin JJ, Vasserman N, Tverskaya S, Polyakov A, Liem RK, Gettemans J, Robberecht W, De Jonghe P, and Timmerman V. Mutant small heat-shock protein 27 causes axonal Charcot-Marie-Tooth disease and distal hereditary motor neuropathy. Nat. Genet. 2004; 36: 602– 606.

-Fixman M and Freire JJ. Theory of DNA melting curves. Biopolymers. 1977, Dec; 16:2693-2704.

-Fontaine G, Fontaliran F, Guiraudon G, Frank R, Laurenceau JL, Malergue C, Grosgogeat Y. The arrhythmogenic right ventricle. In : Iwa T, Fontaine G (eds) Cardiac arrhythmias. Recent progress in investigation and management. Amsterdam: Elsevier Science BV 1988;189-202.

-Forbes MS, Sperelakis N, 1985. Intercalated discs of mammalian heart: a review of structure and function. Tissue Cell 1985; 17: 605-648.

-Franke WW, Borrmann CM, Grund C, Pieperhoff S. The area compisita of adhering junctions connecting heart muscle cells of vertebrates. I. Molecular definition in intercalated disks of cardiomyocites by immunoelectron microscopy of desmosomal proteins. Eur J Cell Biol 2006; 85: 69-82.

-Fressart V, Duthoit G, Donal E, Probst V, Deharo JC, Chevalier P, Klug D, Dubourg O, Delacretaz E, Cosnay P, Scanu P, Extramiana F, Keller D, Hidden-Lucet F, Simon F, Bessirard V, Roux-Buisson N, Hebert JL, Azarine A, Casset-Senon D, Rouzet F, Lecarpentier Y, Fontaine G, Coirault C, Frank R, Hainque B, Charron P. Desmosomal gene analysis in arrhythmogenic right ventricular dysplasia/cardiomyopathy: spectrum of mutations and clinical impact in practice. Europace. 2010;12:861-8.

-Gandjbakhch E, Charron P, Fressart V, Lorin de la Grandmaison G, Simon F, Gary F, Vite A, Hainque B, Hidden-Lucet F, Komajda M, Villard E. Plakophilin 2A is the dominant isoform in human heart tissue: consequences for the genetic screening of arrhythmogenic right ventricular cardiomyopathy. Heart 2011; 97(10):844-9.

-Garcia-Gras E, Lombardi R, Giocondo MJ, Willerson JT, Schneider MD, Khoury DS, Marian AJ. Suppression of canonical Wnt/beta-catenin signaling by nuclear plakoglobin recapitulates phenotype of arrhythmogenic right ventricular cardiomyopathy. J Clin Invest. 2006;116:2012-21.

-Garcia-Pavia P, Syrris P, Salas C, Evans A, Mirelis JG, Cobo-Marcos M, Vilches C, Bornstein B, Segovia J, Alonso-Pulpon L, Elliott PM. Desmosomal protein gene mutations in patients with idiopathic dilated cardiomyopathy undergoing cardiac transplantation: a clinicopathological study. Heart 2011; 97(21):1744-52.

-Garrod DR, Chidgey M. Desmosome structure, composition and function Biochim. Biophys Acta 2007.

-Garrod DR, Chidgey M. Desmosome structure, composition and function. Biochim Biophys Acta. 2008;1778:572-87.

-Gehmlich K, Syrris P, Peskett E, Evans A, Ehler E, Asimaki A, Anastasakis A, Tsatsopoulou A, Vouliotis AI, Stefanadis C, Saffitz JE, Protonotarios N, and McKenna WJ. Mechanistic insights into arrhythmogenic right ventricular cardiomyopathy caused by desmocollin-2 mutations. Cardiovascular res 2011; 90:77-87.

-Gerlis LM, Schmidt-Ott SC, Ho SY. Anderson RH. Dysplastic conditions of the right ventricular myocardium: Uhl's anomaly vs arrhythmogenic right ventricular dysplasia. Br Heart J 1993; 69: 142-50.

-Gerull B, Heuser A, Wichter T, Paul M, Basson CT, McDermott DA, Lerman BB, Markowitz SM, Ellinor PT, MacRae CA, Peters S, Grossmann KS, Drenckhahn J, Michely B, Sasse-Klaassen S, Birchmeier W, Dietz R, Breithardt G, Schulze-Bahr E, Thierfelder L. Mutations in the desmosomal protein plakophilin-2 are common in arrhythmogenic right ventricular cardiomyopathy. Nat Genet. 2004;36:1162-4.

-Goossens S, Janssens B, Bonné S, De Rycke R, Braet F, van Hengel J, van Roy F. A unique and specific interaction between alphaT-catenin and plakophilin-2 in the area composita, the mixed-type junctional structure of cardiac intercalated discs. J Cell Sci. 2007;120:2126-36.

-Green KJ and Simpson CL. Desmosomes: new perspectives on a classic. J Invest Dermatol 2007,127:2499-515. Review.

-Grossmann KS, Grund C, Huelsken J, Behrend M, Erdmann B, Franke WW, Birchmeier W. Requirement of plakophilin 2 for heart morphogenesis and cardiac junction formation. J Cell Biol 2004, 67: 149-60.

-Hamid MS, Norman M, Quraishi A, Firoozi S, Thaman R, Gimeno JR, Sachdev B, Rowland E, Elliott PM, McKenna WJ. Prospective evaluation of relatives for familial arrhythmogenic right ventricular cardiomyopathy/dysplasia reveals a need to broaden diagnostic criteria. J Am Coll Cardiol. 2002;40:1445-50.

-Haslbeck M, Franzmann T, Weinfurtner D, and Buchner. Some like it hot: the structure and function of small heat-shock proteins. Nat. Struct. Mol. Biol 2005; 12: 842– 846.

-Hastings PJ, Lupski JR, Rosenberg SM, Ira G. Mechanisms of change in gene copy number. Nat. Rev. Genet. 2009; 10:551–64.

-Hatzfeld M Plakophilins: Multifunctional proteins or just regulators of desmosomal adhesion? Biocm.Biophys Acta 2006; 1773: 69-77.

-Houlden H, Laura M, Wavrant-De Vrie`ze F, Blake J, Wood N, and Reilly MM. Mutations in the HSP27 (HSPB1) gene cause dominant, recessive, and sporadic distal HMN/CMT type 2. Neurology 2008; 71:1660 –1668.

-Huber AH, Nelson WJ, Weis WI. Three-dimensional structure of the armadillo repeat

region of beta-catenin. Cell. 1997;90:871-82.

-Huot J, Houle F, Spitz DR, and Landry J. HSP27 phosphorylation-mediated resistance against actin fragmentation and cell death induced by oxidative stress. Cancer Res. 1996; 56: 273–279.

-Indik JH and Marcus FI. Arrhythmogenic Right Ventricular Dysplasia/Cardiomyopathy. Indian Pacing and Electrophysiology J 2003 3(3):148-156.

-Janssens B, Goossens S, Staes K, Gilbert B, van Hengel J, Colpaert C, Bruyneel E, Mareel M, van Roy F. AlphaT-catenin: a novel tissue-specific beta-catenin-binding protein mediating strong cell-cell adhesion. J Cell Sci. 2001;114:3177-88.

-Kapplinger JD, Landstrom AP, Salisbury BA, Callis TE, Pollevick GD, Tester DJ, Cox MG, Bhuiyan Z, Bikker H, Wiesfeld AC, Hauer RN, van Tintelen JP, Jongbloed JD, Calkins H, Judge DP, Wilde AA, Ackerman MJ. Distinguishing arrhythmogenic right ventricular cardiomyopathy/dysplasia-associated mutations from background genetic noise. J Am Coll Cardiol. 2011;57:2317-27.

-Kircher M and Kelso J. High-throughput DNA sequencing-concepts and limitations. Bioessays 2010; 32: 524–536.

-Klauke B, Kossmann S, Gaertner A, Brand K, Stork I, Brodehl A, Dieding M, Walhorn V, Anselmetti D, Gerdes D, Bohms B, Schulz U, Zu Knyphausen E, Vorgerd M, Gummert J, Milting H. De novo desmin-mutation N116S is associated with arrhythmogenic right ventricular cardiomyopathy. Hum Mol Genet. 2010;19:4595-607.

-Koch M, Foley JE, Hahn R, Zhou P, Burgeson RE, Gerecke DR, Gordon MK. α1(XX) Collagen, a New Member of the Collagen Subfamily, Fibril-associated Collagens with Interrupted Triple Helices. J Biol Chem 2001; 276 (25): 23120–23126.

-Kong A, Gudbjartsson DF, Sainz J, Jonsdottir GM, Gudjonsson SA, Richardsson B, Sigurdardottir S, Barnard J, Hallbeck B, Masson G, Shlien A, Palsson ST, Frigge ML, Thorgeirsson TE, Gulcher JR, Stefansson K. A high-resolution recombination map of the human genome. Nat Genet. 2002 Jul;31(3):241-7. Epub 2002 Jun 10.

-Koopmann TT, Alders M, Jongbloed RJ, et al. Long QT syndrome caused by a large duplication in the KCNH2 (HERG) gene undetectable by current polymerase chain reaction-based exon-scanning methodologies. Heart Rhythm 2006; 3: 52–5.

-Kostin S., Hein S, Bauer EP, *et al*. Spatiotemporal development and distribution of intercellular junctions in adult rat cardiomyocytes in culture. Circ. Res. 1999 85**:** 154–167.

-Kypta RM, Su H, Reichardt LF. Association between a Transmembrane Protein Tyrosine Phosphatase and the Cadherin-Catenin Complex. J Cell Biol 1996; 134: 1519-1529.

-Lacroix D, Lions C, Klug D, Prat A. Arrhythmogenic right ventricular dysplasia: catheter ablation, MRI, and heart transplantation. J Cardiovasc Electrophysiol. 2005;16:235-6.

-Lahtinen AM, Lehtonen A, Kaartinen M, Toivonen L, Swan H, Widén E, Lehtonen E, Lehto VP, Kontula K. Plakophilin-2 missense mutations in arrhythmogenic right ventricular cardiomyopathy. Int J Cardiol. 2008;126:92-100.

-Leask A and Abraham DJ. TGF-beta signaling and the fibrotic response. FASEB J. 2004;18:816-27.

-Li D, Liu Y, Maruyama M, Zhu W, Chen H, Zhang W, Reuter S, Lin SF, Haneline LS, Field LJ, Chen PS, Shou W. Restrictive loss of plakoglobin in cardiomyocytes leads to arrhythmogenic cardiomyopathy. Hum Mol Genet. 2011;20:4582-96.

-Li J, Levin MD, Xiong Y, Petrenko N, Patel VV, Radice GL. N-cadherin haploinsufficiency affects cardiac gap junctions and arrhythmic susceptibility. J Mol Cell Cardiol. 2008;44:597-606.

-Li J, Swope D, Raess N, Cheng L, Muller EJ, Radice GL. Cardiac tissue-restricted deletion of plakoglobin results in progressive cardiomyopathy and activation of {beta}-catenin signaling. Mol Cell Biol. 2011;31:1134-44.

-Li R, Li Y, Fang X, Yang H, Wang J, Kristiansen K, Wang J. SNP detection for massively parallel whole-genome resequencing Genome Res. 2009; 19: 1-9.

-Lilien J and Balsamo J. The regulation of cadherin-mediated adhesion by tyrosine phosphorylation/dephosphorylation of β-catenin. Current Opinion in Cell Biology 2005, 17:459–465.

-Lombardi R, Dong J, Rodriguez G, Bell A, Leung TK, Schwartz RJ, Willerson JT, Brugada R, Marian AJ. Genetic fate mapping identifies second heart field progenitor cells as a source of adipocytes in arrhythmogenic right ventricular cardiomyopathy. Circ Res. 2009;104:1076-84.

-Marcus FI, Fontaine GH, Guiraudon G, Frank R, Laurenceau JL, Malergue C, Grosgogeat Y. Right ventricular dysplasia: a report of 24 adult cases. Circulation 1982; 65:384-98.

-Marcus FI, McKenna WJ, Sherrill D, Basso C, Bauce B, Bluemke DA, Calkins H, Corrado D, Cox MG, Daubert JP, Fontaine G, Gear K, Hauer R, Nava A, Picard MH, Protonotarios N, Saffitz JE, Sanborn DM, Steinberg JS, Tandri H, Thiene G, Towbin JA, Tsatsopoulou A, Wichter T, Zareba W. Diagnosis of arrhythmogenic right ventricular cardiomyopathy/dysplasia: proposed modification of the Task Force Criteria. Eur Heart J. 2010 ;31:806-14.

-Marcus FI, Nava A, Thiene G. Arrhythmogenic right ventricular cardiomyopathy/dysplasia: recent advances. Milan: Springer Verlag, 2007: 147-58.

-McKenna WJ, Thiene G, Nava A, Fontaliran F, Blomstrom-Lundqvist C, Fontaine G, Camerini F. Diagnosis of arrhythmogenic right ventricular dysplasia/cardiomyopathy. Task Force of the Working Group Myocardial and Pericardial Disease of the European Society of Cardiology and of the Scientific Council on Cardiomyopathies of the

International Society and Federation of Cardiology. Br Heart J 1994, 71:215-8.

-McKoy G, Protonotarios N, Crosby A, Tsatsopoulou A, Anastasakis A, Coonar A, Norman M, Baboonian C, Jeffery S, McKenna WJ. Identification of a deletion in plakoglobin in arrhythmogenic right ventricular cardiomyopathy with palmoplantar keratoderma and woolly hair (Naxos disease). Lancet. 2000; 17;355:2119-24.

-Meadows LS, Isom LL. Sodium channels as macromolecular complexes: Implications for inherited arrhythmia syndromes. Cardiovasc. Res 2005; 67:448-458.

-Meder B, Haas J, Keller A, Heid C, Just S, Borries A, Boisguerin V, Scharfenberger-Schmeer M, Stahler P, Beier M, Weichenhan D, Strom TM, Pfeufer A, Korn B, Katus HA, Rottbauer W. Targeted Next-Generation Sequencing for the Molecular Genetic Diagnostics of Cardiomyopathies. Circ Cardiovasc Genet 2011;4;110-122.

-Merner ND, Hodgkinson KA, Haywood AF, Connors S, French VM, Drenckhahn JD, Kupprion C, Ramadanova K, Thierfelder L, McKenna W, Gallagher B, Morris-Larkin L, Bassett AS, Parfrey PS, Young TL. Arrhythmogenic right ventricular cardiomyopathy type 5 is a fully penetrant, lethal arrhythmic disorder caused by a missense mutation in the TMEM43 gene. Am J Hum Genet. 2008 ;82:809-21.

-Mertens C, Hofmann I, Wang Z, Teichmann M, Sepehri Chong S, Schnölzer M, Franke WW. Nuclear particles containing RNA polymerase III complexes associated with the junctional plaque protein plakophilin 2. Proc Natl Acad Sci U S A. 2001;98:7795-800.

-Mertens C, Kuhn C, Franke WW: Plakophilins 2a and 2b: constitutive proteins of dual location in the karyoplasm and the desmosomal plaque. J Cell Biol 1996; 135: 1009-1025.

-Miravet S, Piedra J, Castano J, Raurell I, Francí C, Dunach M, and Antonio García de Herreros. Tyrosine Phosphorylation of Plakoglobin Causes Contrary Effects on Its Association with Desmosomes and Adherens Junction Components and Modulates β-Catenin-Mediated Transcription. Molecular and Cellular Biology 2003; 23 (20):7391–7402.

-Miyazawa H, Kato M, Awata T, Kohda M, Iwasa H, Koyama N, Tanaka T, Huqun, Kyo S, Okazaky Y, Hagiwara K. Homozygosity Haplotype allows a genomewide search for the autosomal segments shared among patients. Am J Hum Genet 2007; 80 :1090-1102.

-Morton NE. Sequential tests for the detection of linkage. Am J Hum Genet. 1955 Sep;7(3):277-318.

-Muller J, Ritt DA, Copeland TD, Morrison DK. Functional analysis of C-TAK1 substrates binding and identification of PKP2 as a new C-TAK1 substrate. EMBO J 2003; 22: 2633-2640.

-Muller T, Choidas A, Reichmann E, Ullrich A. Phosphorylation and Free Pool of β-Catenin Are Regulated by Tyrosine Kinases and Tyrosine Phosphatases during Epithelial Cell Migration. J Biol Chem 1999; 274 (15): 10173–10183.

-Nava A., Bauce B., Basso C., Muriago M., Rampazzo A., Villanova C., Daliento L., Buja G., Corrado D., Danieli G.A., Thiene G. Clinical profile and long-term follow-up of 37 families with arrhythmogenic right ventricular cardiomyopathy. J Am Coll Cardiol. 2000; 36:2226-33.

-Nava A., Thiene G., Canciani B., Scognamiglio R., Daliento L., Buja G., Martini B., Stritoni P., Fasoli G. Familial occurrence of right ventricular dysplasia: a study involving nine families. J Am Coll Cardiol. 1988;12:1222-8.

-Norgett EE, Hatsell SJ, Carvajal-Huerta L, Cabezas JC, Common J, Purkis PE, Whittock N, Leigh IM, Stevens HP, Kelsell DP. Recessive mutation in desmoplakin disrupts desmoplakin-intermediate filament interactions and causes dilated cardiomyopathy, woolly hair and keratoderma. Hum Mol Genet. 2000;9:2761-6.

-Norton N, Li D, Rieder MJ, Siegfried JD, Rampersaud E, Zuchner S, Mangos S, Gonzalez-Quintana J, Wang L, McGee S, Reiser J, Martin E, Nickerson DA, Hershberger RE. Genome-wide Studies of Copy Number Variation and Exome Sequencing Identify Rare Variants in BAG3 as a Cause of Dilated Cardiomyopathy. Am J Hum Genet 2011; 88: 273–282.

-Ott J, Donis-Keller H. Statistical methods in genetic mapping. Genomics. 1994 Jul 15;22(2):496-7.

-Paul C, Manero F, Gonin S, Kretz-Remy C, Virot S, and Arrigo AP. Hsp27 as a negative regulator of cytochrome C release. Mol. Cell. Biol 2002; 22: 816 – 834.

-Peivandi AA, Huhn A, Lehr HA, Jin S, Troost J, Salha S, Weismüller T, and Löffelholz K. Upregulation of Phospholipase D Expression and Activation in Ventricular Pressure-Overload Hypertrophy. J Pharmacol Sci 2005; 98: 244 – 254.

-Pilichou K, Nava A, Basso C, Beffagna G, Bauce B, Lorenzon A, Frigo G, Vettori A, Valente M, Towbin J, Thiene G, Danieli GA, Rampazzo A. Mutations in desmoglein-2 gene are associated with arrhythmogenic right ventricular cardiomyopathy.Circulation.2006;113:1171-9.

-Pilichou K, Remme CA, Basso C, Campian ME, Rizzo S, Barnett P, Scicluna BP, Bauce B, van den Hoff MJ, de Bakker JM, Tan HL, Valente M, Nava A, Wilde AA, Moorman AF, Thiene G, Bezzina CR. Myocyte necrosis underlies progressive myocardial dystrophy in mouse dsg2-related arrhythmogenic right ventricular cardiomyopathy. J Exp Med. 2009;206:1787-802.

-Priori SG, Napolitano C, Tiso N, Memmi M, Vignati G, Bloise R, Sorrentino V, Danieli GA. Mutations in the cardiac ryanodine receptor gene (hRyR2) underlie catecholaminergic polymorphic ventricular tachycardia. Circulation. 2001;103:196-200.

-Protonotarios N, Tsatsopoulou A, Patsourakos P, Alexopoulos D, Gezerlis P, Simitsis S, Scampardonis G. Cardiac abnormalities in familial palmoplantar keratosis. Br Heart J 1986; 56: 321-326.

-Rampazzo A, Nava A, Danieli GA, Buja G, Daliento L, Fasoli G, Scognamiglio R, Corrado D, Thiene G. The gene for arrhythmogenic right ventricular cardiomyopathy maps to chromosome 14q23-q24. Hum Mol Genet 1994,3:959-62.

-Rampazzo A, Nava A, Malacrida S, Beffagna G, Bauce B, Rossi V, Zimbello R, Simionati B, Basso C, Thiene G, Towbin JA, Danieli GA. Mutation in human desmoplakin domain binding to plakoglobin causes a dominant form of arrhythmogenic right ventricular cardiomyopathy. Am J Hum Genet. 2002;71:1200-6.

-Saffitz J.E., D.L. Lerner & K.A. Yamada. Gap junction distribution and regu- lation in the heart. *In* Cardiac Electrophysiology: From Cell-to-Bedside. D.P. Zipes & J. Jalife, Eds. 2004: 181–191. 4th ed. Saunders. Philadelphia.

-Saffitz JE, Asimaki A, Huang H. Arrhythmogenic right ventricular cardiomyopathy: new insights into disease mechanisms and diagnosis. J Investig Med. 2009;57:861-4. Review.

-Sallee JL, Wittchen ES, Burridge K. Regulation of Cell Adhesion by Protein-tyrosine Phosphatases II. Cell-Cell Adhesion. J Biol Chem 2006; 281: 16189-16192.

-Sato PY, Musa H, Coombs W, Guerrero Serna G, Patino GA, Taffet SM, Isom LL, Delmar M. Loss of plakophilin-2 expression leads to decreased sodium current and slower conduction velocity in cultured cardiac myocytes. Circ res 2009, 105: 523-526.

-Segev O, Samach A, Faerman A, Kalinski H, Beiman M, Gelfand A, Turam H, Boguslavsky S, Moshayov A, Gottlieb H, Kazanov E, Nevo Z, Robinson D, Skaliter R, Einat P, Binderman I, and Feinsteina E. CMF608 a novel mechanical strain-induced bone-specific protein expressed in early osteochondroprogenitor cells. Bone 2004; 34: 246–260.

-Sen-Chowdhry S, Syrris P, Pantazis A, Quarta G, McKenna WJ and Chambers JC. Mutational Heterogeneity, Modifier Genes, and Environmental Influences Contribute to Phenotypic Diversity of Arrhythmogenic Cardiomyopathy. Circ Cardiovasc Genet 2010; 3: 323-330.

-Sen-Chowdhry S, Syrris P, Prasad SK, Hughes SE, Merrifield R, Ward D, Pennell DJ, McKenna WJ. Left-dominant arrhythmogenic cardiomyopathy: an under-recognized clinical entity J Am Coll Cardiol. 2008;52:2175-87.

-Sen-Chowdhry S, Syrris P, Ward D, Asimaki A, Sevdalis E, McKenna WJ. Clinical and genetic characterization of families with Arrhythmogenic Right Ventricular Dysplasia/Cardiomyopathy provides Novel Insights into patterns of disease expression. Circulation 2007; 115; 1710-1720.

-Stankiewicz P and Lupski JR. Structural Variation in the Human Genome and its Role in Disease. Annu. Rev. Med. 2010;61:437–55.

-Stappenbeck TS, Bornslaeger EA, Corcoran CM, Luu HH, Virata ML, Green KJ. Functional analysis of desmoplakin domains: specification of the interaction with keratin versus vimentin intermediate filament networks. J Cell Biol. 1993;123:691-705.

-Stokes DL and Wagenknecht T. Calcium transport across the sarcoplasmic reticulum: structure and function of Ca2+-ATPase and the ryanodine receptor. Eur J Biochem 2000, 267:5274-9. Review.

-Syrris P, Ward D, Evans A, Asimaki A, Gandjbakhch E, Sen-Chowdhry S, McKenna WJ. Arrhythmogenic right ventricular dysplasia/cardiomyopathy associated with mutations in the desmosomal gene desmocollin-2. Am J Hum Genet. 2006;79:978-84.

-Tandri H, Saranathan M, Rodriguez ER, et al. Non invasive detection of myocardial fibrosis in arrhythmogenic right ventricular cardiomyopathy using delayed-enhancement magnetic resonance imaging. J Am Coll Cardiol 2005; 45: 98-103.

-Taylor M, Graw S, Sinagra G, Barnes C, Slavov D, Brun F, Pinamonti B, Salcedo EE, Sauer W, Pyxaras S, Anderson B, Simon B, Bogomolovas J, Labeit S, Granzier H, Mestroni L. Genetic variation in titin in arrhythmogenic right ventricular cardiomyopathy-overlap syndromes. Circulation. 2011;124:876-85.

-Thiene G and Basso C. Arrhythmogenic right ventricular cadiomyopathy. An Update. Cardiovasc Pathol. 2001; 10:109-11.

-Thiene G, Corrado D, Basso C. Arrhythmogenic right ventricular cardiomyopathy/dysplasia. Orphanet J Rare Dis. 2007;14;2:45.

-Thiene G, Nava A, Angelini A, Daliento L, Scognamiglio R, Corrado D. Anatomoclinical aspects of arrhythmogenic right ventricular cardiomyopathy. In Advances in cardiomyopathies. Edited by Baroldi G, Camerini F, Goodwin JF. Milano: Springer Verlag, 1990:397-408.

-Thiene G, Nava A, Corrado D, Rossi L, Pennelli N. Right ventricular cardiomyopathy and sudden death in young people. N Engl J Med. 1988;318:129-33.

-Tiso N, Stephan DA, Nava A, Bagattin A, Devaney JM, Stanchi F, Larderet G, Brahmbhatt B, Brown K, Bauce B, Muriago M, Basso C, Thiene G, Danieli GA, Rampazzo A. Identification of mutations in the cardiac ryanodine receptor gene in families affected with arrhythmogenic right ventricular cardiomyopathy type 2 (ARVD2). Hum Mol Genet. 2001;10:189-94.

-Van Tintelen JP, Entius MM, Bhuiyan ZA, Jongbloed R, Wiesfeld AC, Wilde AA, van der Smagt J, Boven LG, Mannens MM, van Langen IM, Hofstra RM, Otterspoor LC, Doevendans PA, Rodriguez LM, van Gelder IC, Hauer RN: Plakophilin-2 mutations are the major determinant of familial arrhythmogenic right ventricular dysplasia/cardiomyopathy. Circulation 2006, 113:1650-8.

-Van Tintelen JP, Van Gelder IC, Asimaki A, Suurmeijer AJ, Wiesfeld AC, Jongbloed JD, van den Wijngaard A, Kuks JB, van Spaendonck-Zwarts KY, Notermans N, Boven L, van den Heuvel F, Veenstra-Knol HE, Saffitz JE, Hofstra RM, van den Berg MP. Severe cardiac phenotype with right ventricular predominance in a large cohort of patients with a single missense mutation in the DES gene. Heart Rhythm. 2009;6:1574-83.

-Wang K, Li M, Hadley D, Liu R, Glessner J, Grant SFA, Hakonarson H, Bucan M. PennCNV: An Integrated hidden Markov model designed for high-resolution copy number variation detection in whole-genome SNP genotyping data. Genome Res 2007; 17: 1665-1674.

-Wichter T, Borggrefe M, Haverkamp W, Chen X, Breithardt G. Efficacy of antiarrhythmic drugs in patients with arrhythmogenic right ventricular disease. Results in patients with inducible and noninducible ventricular tachycardia. Circulation 1992, 86: 29-37.

-Wichter T, Paul M, Eckardt L et al. Arrhythmogenic right ventricular cardiomyopathy. Antiarrhythmic drugs, catheter ablation, or ICD? Herz 2005, 30: 91-101.

-Wlodarska EK, Konka M, Zaleska T, Ploski R, Cedro K, Pucilowska B, Bekiesinska-Figatowska M, Rydlewska-Sadowska W, Ruzyllo W, Hoffman P. Arrhythmogenic right ventricular cardiomyopathy in two pairs of monozygotic twins. Int. J. Cardiol 2005; 105:126–33.

-Wu Y, Cazorla O, Labeit D, Labeit S, Granzier H. Changes in Titin and Collagen Underlie Diastolic Stiffness Diversity of Cardiac Muscle. J Mol Cell Cardiol 2000; 32:2151–2161.

-Xiao W, Oefner PJ. Denaturing high-performance liquid chromatography: A review Hum Mut 2001; 17: 439-474.

-Xu T, Yang Z, Vatta M, Rampazzo A, Beffagna G, Pilichou K, Scherer SE, Saffitz J, Kravitz J, Zareba W, Danieli GA, Lorenzon A, Nava A, Bauce B, Thiene G, Basso C, Calkins H, Gear K, Marcus F, Towbin JA; Multidisciplinary Study of Right Ventricular Dysplasia Investigators. Compound and digenic heterozygosity contributes to arrhythmogenic right ventricular cardiomyopathy. J Am Coll Cardiol. 2010;55:587-97.

-Yamada S, Pokutta S, Drees F, Weis WI, Nelson WJ. Deconstructing the cadherin-catenin-actin complex. Cell. 2005;123:889-901.

-Yang Z, Bowles NE, Scherer SE, Taylor MD, Kearney DL, Ge S, Nadvoretskiy VV, DeFreitas G, Carabello B, Brandon LI, Godsel LM, Green KJ, Saffitz JE, Li H, Danieli GA, Calkins H, Marcus F, Towbin JA. Desmosomal dysfunction due to mutations in desmoplakin causes arrhythmogenic right ventricular dysplasia/cardiomyopathy. Circ Res 2006, 99:646-55.

-Yoerger DM, Marcus F, Sherrill D et al., Multidisciplinaty study of right ventricular dysplasia investigators. Echocardiographic findings in patients meeting task force criteria for arrhythmogenic right ventricular dysplasia: new insights from the multidisciplinary study of right ventricular dysplasia. J Am Coll Cardiol 2005; 45: 860-65.

-Zhurinsky J, Shtutman M and Avri Ben-Ze'ev. Plakoglobin and β-catenin: protein interactions, regulation and biological roles. Journal of Cell Science 2000; 113, 3127-3139 .